FORMATION DAMAGE QUANTIFICATION BY NUCLEAR MAGNETIC RESONANCE

BY

MOHAMED ABDALSALAM HANFI JAD

A Thesis Presented to the
DEANSHIP OF GRADUATE STUDIES

KING FAHD UNIVERSITY OF PETROLEUM & MINERALS

DHAHRAN, SAUDI ARABIA

In Partial Fulfillment of the
Requirements for the Degree of

MASTER OF SCIENCE

In

PETROLEUM ENGINEERING

May 2016

KING FAHD UNIVERSITY OF PETROLEUM & MINERALS

DHAHRAN- 31261, SAUDI ARABIA

DEANSHIP OF GRADUATE STUDIES

This thesis, written by **MOHAMED ABDALSALAM HANFI JAD** under the direction his thesis advisor and approved by his thesis committee, has been presented and accepted by the Dean of Graduate Studies, in partial fulfillment of the requirements for the degree of **MASTER OF SCIENCE IN PETROLEUM ENGINEERING.**

Mohamed Mahmoud

Dr. Mohamed A. Mahmoud
(Advisor)

Dr. Abdulla S. Sultan
Department Chairman

Dr. Abdulla S. Sultan
(Member)

Dr. Salam A. Zummo
Dean of Graduate Studies

Dr. Abdulazeez Abdulraheem
(Member)

14/11/16

Date

© Mohamed Abdalsalam Hanfi Jad

2016

I dedicate my thesis work to my parents, family and all my friends.

ACKNOWLEDGMENTS

All praise is due to Allah, who gave me the power and patience during my life to reach this stage and complete this work, and To Him is due to all praise in the first life and the Hereafter.

I would like to thank King Fahd University of Petroleum & Minerals for providing me the scholarship to pursue my master degree in petroleum engineering. Thanks are extended to the Department of petroleum engineering Faculty and students, to my advisor Dr. Mohamed A. Mahmoud for his recommendation, patience, and guidance during my thesis work and to Dr. Abdulazeez Abdulraheem and to the chairman of the department Dr. Abdullah S. Sultan for their valuable time and comments.

Also, I would like to thank Research Institute for allowing me to conduct all experiments using NMR instrument and thanks for all those who help me there especially Mr. Hatim, Mr.Syed.

I will not forget to thank Mr. Abdulrahim Muhammadain who help me a lot in operating the instruments and also special thanks to Mr. Abdul Samad and Mr. Moussa.

I am thankful to my uncles, Dr. Adel and Dr. Saad to their support and valuable advice. Thanks are also due to Mr. sayed omer for his continuous support.

Finally, I would like to thank all my friends and all who help me to accomplish this work.

TABLE OF CONTENTS

LIST OF TABLES

LIST OF FIGURES

ABSTRACT

Full Name : Mohamed Abdalsalam Hanfi Jad

Thesis Title : Formation Damage Quantification by Nuclear Magnetic Resonance

Major Field : Petroleum Engineering

Date of Degree : May 2016

Formation damage can be defined as any reduction in the reservoir permeability in the near-wellbore area. Well intervention such as drilling, completion, matrix stimulation, and EOR operations cause permeability reduction in sandstone and carbonate formations. The invasion of fresh water and HCl into sandstone formation causes the clays to migrate and swell leading to permeability reduction. Also, viscoelastic surfactant (VES) adsorption during acid stimulation and EOR processes on the carbonate rock surface may cause permeability reduction.

In this study, NMR technique, coreflooding, and SEM analysis were used to quantify the formation damage in both carbonate and sandstone outcrop core samples and the possible damaging mechanisms responsible of formation damage. These mechanisms are fines migration and precipitation of reaction product in sandstone cores of high clay content, and viscoelastic surfactant (VES) adsorption on carbonate cores that are used in matrix stimulation and EOR process. In addition we located the adsorption damage in carbonate cores due to the VES during EOR processes and it was in the micro, meso, or macro pores. NMR profiles show the region of damage and those impacted by the adsorption.

Coreflooding experiments results showed a clear damage in sandstone rocks after flooding the core by de-ionized water (DIW) and HCl. Permeability reduction of 84% and 7.9% was

reported for samples flooded by DIW and HCl, respectively. NMR results showed a clear change in the pore size distribution after the injection of HCl. In addition, the SEM images showed the migration of the clay minerals in sandstone rocks. The high viscosity VES system adsorbed more than the low viscosity system on the carbonate rocks.

ملخص الرسالة

الاسم الكامل : محمد عبدالسلام حنفى جاد

عنوان الرسالة : تقدير الاضرار في المنطقة المحيطة بالبئر عن طريق الرنين النووى المغنطيسى

التخصص : هندسة البترول

تاريخ الدرجة العلمية : مايو 2016

يعرف التلف بالمنطقة المحيطة بالبئر باى انخفاض فى نفاذية الزيت الخام من المنطقة المحيطة بالبئر. عمليات التدخل في الآبار مثل الحفر، الاستكمال ، تحسين النفاذية باستخدام الأحماض و عمليات تحسين النفط المستخلص تؤدى الى انخفاض النفاذية فى الصخور الرملية والكربونية. يسبب دخول بعض السوائل كالماء وحمض الهيدروكلوريك المستخدمة في عمليات الحفر وغيرها الى انتفاخ المعادن الطينية وهجرتها مما يؤدى الى انخفاض النفاذية. اما بالنسبة للصخور الكربونية ، فقد وجد ان مسببات توتر الأسطح اللزجة المطاطية المستخدمة فى عمليات تحسين النفط المستخلص وعمليات تحفيز النفاذية تلتصق باسطح الصخور الكربونية.

في هذه الدراسة ، تم استخدام تقنية الرنين النووي المغناطيسي ، نظام الحقن و مجهر المسح الالكترونى لحساب الضرر على الطبقة في الصخور الرملية و الكربونية و تحديد الآلية المسؤولة عن إحداث الضرر. هذه الآليات هي تحرك الجزيئات الصغيرة و انتفاخ المعادن الصلصالية في الصخور الرملية التي تحتوي على نسبة كبيرة منها. بالاضافة إلى امتصاص السطحية ذات المرونة اللزجة في الصخور الكربونية و التي تستخدم في عمليات التحفيز الحمضي للصخور. بالإضافة إلى ذلك ، تم تحديد موقع الضرر الناتج عن امتصاص السطحية ذات المرونة اللزجة خلال عمليات حقن الأحماض او عمليات تعزيز النفط المستخلص و الذي يمكن ان يحدث في المسامات ذات الحجم الكبير والمتوسط والصغير. استخدمت الرسومات البيانية للرنين النووي المغناطيسي لتوضيح نطاق الضرر على المسامات و تحديد حجم المسامات الأكثر تضررا بالامتصاص.

أبانت نتائج نظام الحقن الضرر بشكل واضح بعد حقن العينات الرملية بالماء وحمض الهيدروكلوريك. قلل حقن الماء النفاذية بنسبة 84 % بينما كانت النسبة 7.9 % عند استخدام حمض الهيدروكلوريك. وأظهرت نتائج الرنين المغناطيسي النووي تغير في التوزيع الحجمى للمسامات نتيجة لضخ محلول حامض الهيدروكلوريك. كما وضحت

الصور المأخوذة بإستخدام مجهر المسح الالكترونى هجرة المعادن الصلصالية فى الصخور الرماية. ايضا ، وجد ان المحلول عالى اللزوجة يؤدى الى امتصاص اعلى من المحلول منخفض اللزوجة فى الصخور الكربونية.

CHAPTER 1

INTRODUCTION

1.1 Formation Damage

Formation damage can be defined as any impairment in the permeability around the wellbore area. The damage may extend few feet from the wellbore which could impact the productivity of the reservoir significantly. The damage around the wellbore is attributed to many processes such as drilling, completion, acidizing, and EOR.

Recently, nuclear magnetic resonance (NMR) relaxation time (T_2) measurement assisted with core flooding system and supported with the SEM to study fines deposition (Byrne et al. 2000, Green et al. 2013) were used to characterize Formation damage. Types of formation damage is discussed below.

1.1.1 Damage by Drilling Mud Particles

The damage caused by drilling solids depends mainly on the distribution of the pore size, wellbore overpressure and how particle size is distributed in the drilling fluid. The experimental results showed that the damage from drilling particles to the well productivity ranging from 1 to 10% depending on the invasion depth. However, practically in the field the situation may differ from the lab tests in term of penetration of mud particles which may be due to very porous zones or ‘’micro fracturing’’ during drilling pressure surges.

1.1.2 Damage by Cement Filtrates

Kruger (1988) reported two ways through which cement filtrate may damage formation permeability. Firstly, settle of cement in the pore spaces as crystals after hydrate with lime.

Secondly, reaction of the silica in the formation with lime in filtrate which result of calcium silicate hydrate.

1.1.3 Damage by Perforation

Studies on perforation damage showed that the shot that made in fluid containing solids or in a case which the formation pressure is lower than the wellbore pressure affect adversely the productivity of the well (Alle and Morzel 1956, Krueger 1956). There are three factors that contribute to the flow impediment by solids which are the drilling damage outside the perforation, perforating fluid and the perforating process.

1.1.4 Damage by Plugging

Asphalts, formation fines, inorganic scales and waxes are the main source of plugging. The plugging problem has a major effect on rapid declining of natural depletion of a field. During the production operation, the precipitation of organic and inorganic materials may lead to either restrict production or in worst case plugging the well. Inorganic scale such as $CaCO_3$, $CaSO_4$ is one of the most common well plugging conditions which occurs within the tubing string. Organic scale materials such as crude oil and broadly called “paraffins” precipitate near the well or inside the wellbore.

1.1.5 Damage by VES

Adsorption and retention of VES on formation rocks make the EOR and stimulation processes economically unfeasible. Loss of VES was observed by several studies (Patzkó et al. 1993, Paria et al. 2004, Curbelo et al. 2007, Liu et al. 2010, Yu et al. 2010 and ShamsiJazeyi et al. 2014).

1.2 Nuclear Magnetic Resonance

In 1946 a group of researchers at “Stanford and MIT”, in the United States developed NMR. It became a valuable and reliable technique in many applications such as physics, chemistry, and medicine. Later in 1960, researchers used NMR in the oil industry.

The NMR is associated with the interaction of the electromagnetic radiation with matter. It implies to be observed by irradiating a sample and observing the response of the system to the radiation as the frequency is varied. Since the frequency of the electromagnetic radiation distinguish between the different types of interaction (e.g. X-ray frequency = 1018 Hz, Microwave cookers frequency = 109 Hz).

The use of NMR method in the oil-field applications is not common comparing with the chemical and the medical applications. Brown and Gamson (1960) used the earth magnetic field to perform his first NMR measurements in a borehole.

Many of the important concepts arise as a consequence of the down-hole NMR concept such as the quantification of the movable fluid fraction and the interpretation of the measured NMR response in terms of rock permeability (Timur 1969).

The strength of the magnetic field used in the NMR varies from application to another. For example the oil-field applications require a low magnetic field strength in contrast to chemical applications that require high magnetic field strength.

The NMR has a radical power to quantify the amount of matter that participates to the NMR signal. The signal magnitude is directly proportional to the number of magnetic moments that create the signal. Thus, it can be assumed that the pore fluids and the fluids that bound to the clays are the creators of the signal measured by the NMR tools.

1.2.1 Nuclear Magnetism

NMR corresponds to the hydrogen nuclei behavior when an external magnetic fields applied (Coates et al., 1999). By applying a magnetic field that induced by an external permanent magnet the spinning protons align with or opposite to the external magnetic field. Since tenuous preponderance of nuclei stratify analogues to the magnetic field increase the net magnetization (M_0) analogues to the applied magnetic field.

1.2.2 Radio frequency and their associated process

Consider a protons spinning of ^1H nucleus in a sample influenced by external magnetic field. Part of these protons will be aligned with the magnetic field and the others will be opposing so they will cancel each other. The remaining protons might be with or opposite to the magnetic field which represent the net magnetization vector (M_o).

The resonance in the NMR can be defined as the net magnetization vector (M_o) precessing at Larmor frequency around the applied field. The challenge is to utilize the radio frequency pulse to perturb the net magnetization away from their alignment with the applied magnetization field.

1.2.3 Relaxation

Edwards (2003) found out that the nuclei relax which means it returned back to the ground state. An important question in this experiment is how long the relaxation process takes because the duration will affect the success of the experiment. The relaxation precessing in NMR experiment takes place by two ways: spin-lattice relaxation (T_1) and spin-spin relaxation (T_2). Figure 1 shows the precessing motion of the spinning protons (Edwards 2003).

In longitudinal relaxation, the nucleus loses its energy as a vibrational or translational energy. This energy will be transferred to the lattice. The half-life for this process is called

the spin-lattice relaxation time (T_1). Temperature, solution viscosity, structure and molecular size are the main factors that affect the T_1- time.

In transverse relaxation, the nucleus loses its energy by exchange its spin with another nucleus whereas the energy transferred to the neighboring nucleus through this process. The half-time for this process is called the spin-spin relaxation time (T2).

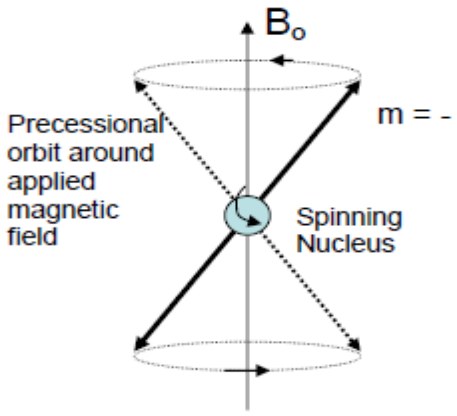

Figure 1: the precessing motion of the spinning protons (Edwards 2003).

The target of the NMR logging tools is the hydrogen which exists amply in the water and hydrocarbons that fills the pores and can be detected by tuning the tools frequency to the magnetic resonant frequency of the hydrogen. The porosity can be given by the number of hydrogen atoms that given by NMR signal amplitude.

The decay of the NMR amplitude during each measurement signal called the relaxation time. The pore sizes is representing by the relaxation time. Small relaxation times mean small pores that correspond to the clay-bound and capillary bound water. In contrast, the long relaxation times reflect the large pores that correspond to the easily producible fluids. The long relaxation time (T_2) with 3700 sec at 40̊ C was recorded for water in a test tube which might be the case for the vuggy carbonate. While the short relaxation time was

noticed for the water in rock pore space. The relaxation time for a sandstone is 10 msec for the micro pores and 500 msec for the macro pores (Kenyon et al., 1995).

1.2.4 **Longitudinal relaxation**

The longitudinal magnetization which stratify analogous to the external applied field lose energy and relax as exponential in simplest cases. The time required to the excited magnetic moments to return back to the z-axis is defined as longitudinal relaxation (T_1). Which can be described as

$$\frac{dM_z}{dt} = -\frac{[M_z - M_0]}{T_1} \tag{1.1}$$

Where M_0 represents magnetization at thermal equilibrium state and M_z represents z-axis magnetization. The Inversion-Recovery (IR) pulse sequence is used to measure longitudinal relaxation time. By applying sequences of pluses start from 180^o pulse that tilts the net magnetization in the negative z-axis. After waiting time t, a 90^o pulse causes the net magnetization to return back to the x-y plane. In the x-y plane the receiver coil detects the decaying signal. The value of the net magnetization in the positive z-axis is given after the 90^o pulse immediately after the wait time *t* by the amplitude of the FID. The longitudinal relaxation time given as

$$M_z(t) = M_0\left(1 - 2\exp\left(\frac{-t}{T_1}\right)\right) \tag{1.2}$$

1.2.5 **Transverse relaxation**

The transverse or spin-spin relaxation can be described as the process of relaxation of the transverse components of the magnetization to the equilibrium value of zero. Bloch (1946) showed that basically, the transverse components of magnetization (M_x and M_y) have

exponential relaxation with T_2 called the transverse relaxation time. It can be described by the following equation:

$$\frac{dM_{x,y}}{dt} = -\frac{M_{x,y}}{T_2} \quad (1.3)$$

This transverse relaxation rate in inhomogeneous magnetic field is denoted by $\frac{1}{T_{2*}}$ and is given as:

$$\frac{1}{T_2} = \frac{t}{T_{2*}} + \gamma \Delta B_0 \quad (1.4)$$

Where ΔB_0 represents inhomogeneity of the applied field. The pulse sequence designed by Carr-Purcell-Meiboom-Gill (CPMG) recompense this effect of the inhomogeneous field partially. These pulse sequence starts with a 90^o radio frequency pulse applied in the x-axis to tilt the net magnetization onto the y-axis.

1.2.6 **Free Induction Decay**

Since there is no any disturb been caused M will be in equilibrium in the z-axis. When a RF applied in the x-y plane which is perpendicular to that of the static field plane, the net magnetization tips up z-plane to the x-y plane, and the angle of tipping θ is:

$$\theta = \gamma B_1 t_p \quad (1.5)$$

Where t_p represents time of which vibrating field applied and B_1 represent amplitude of applied field. In NMR measurements, usually the applied Radio frequency (RF) pulse of ($\theta = 180^o$) or ($\theta = 90^o$). The relaxation takes place once the RF pulse removed which return the net magnetization to the steady state. A free induction decay is the sinusoidal current in the coil that place in the x-y plane.

1.2.7 **NMR Logging Applications**

The NMR principle used to analyze the pore-fluids in the rock is resemble to that used in the medical field to portray the tissues inside the human body. In 1991, Numar introduced the magnetic resonance imaging logging (MRIL) by taking the laboratory NMR equipment and turns it inside-out.

The MRIL tool comprises of a permanent magnet at the center of the device which magnetizes the formation material. Framing this magnet, an antenna relocates pulses of radio frequency energy into the formation as an oscillating magnetic field. Between these pulses the antenna recorded the decaying "echo" signal from those hydrogen protons that are in resonance with the permanent magnetic field.

As advantage of the MRIL tool that only fluids are visible to the device. This is different from all the traditional logging tools that consider sensitive to both fluids and rocks components such as bulk-density, neutron, and acoustic-travel-time logging tool (Coates et al., 1999). MRIL has the ability to provide three types of information: fluids quantity in the rock, properties of the fluids and the pore sizes which accommodate the fluids.

1.3 Matrix Acidizing

Matrix acidizing is used to improve well productivity by removing damage near the wellbore and increasing the permeability. The acid creates channels through dissolution when react with the rock material. Productivity impairment can be caused by many factors such as pseudo-skin factors, partial completion and formation damage. However, matrix acidizing can be used only when the impairments caused by formation damage.

In acidizing process, Acids are injected into the reservoir to dissolve material that caused the damage in sandstone and carbonate rocks. The selection of the treating fluid is governed

by the type of the damage and the formation. Carbonates rocks composed mainly from calcite ($CaCO_3$) and dolomite ($MgCO_3$). Usually, carbonate reservoirs were stimulated using HCl. The following equations show the reactions of HCl with the carbonates:

$$CaCO_3 + 2\ HCl \rightarrow CaCl_2 + H_2O + CO_2 \quad (1.6)$$

$$CaMg(CO_3)_2 + 4HCl \rightarrow CaCl_2 + MgCl_2 + H_2O + CO_2 \quad (1.7)$$

Permeability contrasts in the reservoir may result from reservoir heterogeneity and different depths of damage. Thus, diversion is needed to avoid injecting more acid into the permeable zones and those zones nearer to the injection point.

Successful of acid treatments depend on the acid placement. Improper acid placement means that more acid will be consumed to have the same amount of simulation (Economides and Nolte, 2000). Also, improper acid placement will result in ineffective damage removal. Furthermore, non-uniform stimulation could cause high drawdown that may result in early water and gas production (Al-Anzi et al., 2004). Placement can be achieved mechanically (combination of coiled tubing and packers) and chemically (foams, emulsified acid, polymers and VES).

1.4 Enhanced Oil Recovery

It is known also as tertiary recovery, enhanced oil recovery (EOR) is performed by injecting a substance into the reservoir to recover the oil that could not recovered by water flooding. EOR can be classified to three main methods: thermal, gas and chemical. The thermal methods performed by introducing heat to the reservoir. Thermal methods focus mainly on reducing the crude oil viscosity by heating. Gas methods performed by injecting carbon dioxide (CO_2) into the reservoir to recover the oil. Chemical methods include alkali,

polymers and/or surfactant flooding. These chemicals substance were used to reduce interfacial tension, change wettability and control mobility to increase the oil recovery.

1.5 Thesis Objectives

- Identify the damage location in sandstone cores using NMR technique.
- Compare the NMR results with the pressure drop and permeability measurement from core flooding system.
- Investigate the damage caused by fresh water and HCl on the sandstone cores.
- Identification of damage caused by VES in carbonate rocks using NMR.
- Compare the pressure drop results and permeability measurement with NMR results.
- Identify the adsorption location in carbonate rocks from NMR-T2 distribution.
- Investigate the effect of viscosity on adsorption in carbonate rock using permeability measurement.
- Study the effect of $CaCl_2$ and NaCl and shear rate on VES Viscosity.

CHAPTER 2

LITERATURE REVIEW

2.1 Damage by Clay Swelling

Neasham (1977) studied the dispersed clay morphology of sandstone reservoirs and the common geological–petrophysical properties that are used in evaluating hydrocarbon bearing reservoirs. The author defined the dispersed clay as silicate clay minerals that attached to the rock mineral surfaces and those minerals are: kaolinite, illite, smectite and generally attached to rock mineral surfaces. They define the three different types of dispersed clay based on the clay crystal structure and location on pore walls or within inter-granular pores and pore throats and divided it as flows:

1. Discrete particle: It usually developed as pseudo-hexagonal, crystals like plates attached as detached particles to pore walls or occupying inter-granular pores as shown in Figure 2.

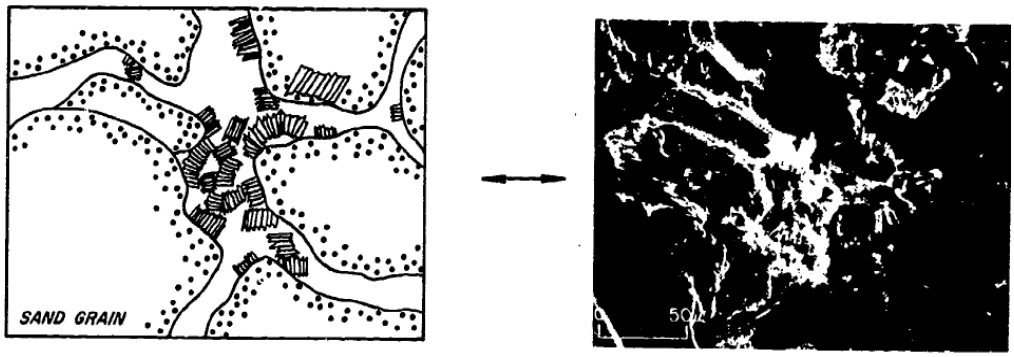

Figure 2: Discrete particles Kaolinite (Neasham, 1977)

2. Pore-lining**:** can be defined as those clays attached to pore walls which appear as long and thin clay coating as portrayed in Figure 3. Illite, chlorite, and montmorillonite were observed with pore-lining crystal morphologies (Figure 3).

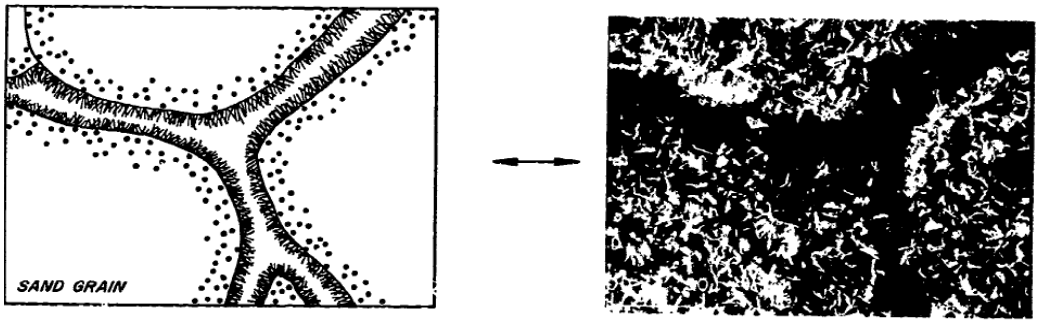

Figure 3: Pore-lining Chlorite (Neasham, 1977)

3. Pore bridging**:** It also attached to the pore walls. This type of clays include illite, chlorite, and montmorillonite extent into or completely across a pores to create bridging effect (Figure 4).

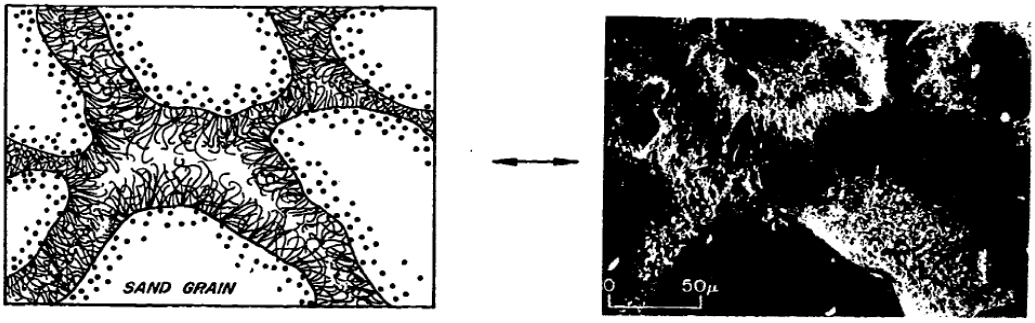

Figure 4: Pore bridging illite (Neasham, 1977)

The porosity/air permeability test showed that the clay morphology of the highest permeability sands show that the discrete particle type is the dominant type affecting the permeability. Whereas the intermediate air permeability sands is affected mostly by the pore-lining variety. In the other hand, the low permeability sand contains pore bridging

clay types. The median pore diameter (M_{dp}) and pore sorting coefficient (S_{op}) which are obtained from the capillary pressure curve and initial-residual saturation data are distinctly different for the three sandstone groups. However, it is minimal in the pore-lining and pore-bridging type. The clay content that found in the pore-lining and pore-bridging types (7 to 20 %) is relatively greater than that of the discrete particle group (5%). The significant differences in textural properties also can contribute strongly in controlling the rock pore space and permeability. Rocks in moderate and poorly sorted types must be evaluated based on the texture and clay morphology.

Priisholm et al., (1987) conducted core experiments on samples from the Gassum and Haldager formations to determine whether the reservoir damage caused by swelling clays or blocking clays. Based on the core analysis results they observed that both porosity and permeability significantly with small changes caused by lithofacies variations. An air permeability increased about 3% when the plugs cleaned with methanol to remove precipitated salts from pores. They proposed three different filtered brines to be used: the synthetic formation brine should not form any damage, the KCl solution should not cause clay swelling and a deionized water should damage the clays exist. The results obtained from the SEM and X-ray diffraction technique showed that the tested samples contain 3 to 12 % clay minerals. Clays found to be critical to both particle migration and rock/fluid interactions. The kaolinite is the only clay mineral present in the Haldager formation, whereas the Gassum formation contains authigenic kaolinite, chlorite, illite, and mixed layer clays.

Porosity and permeability may change significantly within small distances in the reservoir. The adsorbed water in clay mineral decreases the density of the grain. Also they

demonstrate through the flow experiments that both Haldager and the Gassum formations are sensitive to change in differential pressure, flow direction and brine composition. Both of the formations produced fines that are mainly produced when pumping is stopped and restarted and at major changes in flow rates. The diagram of fines production related to porosity shows inversely relationship. The permeability decreased when the plugs flushed by deionized water and the permeability could not be restored by flow reversals in the plugs with swelling clays.

Monaghan, et al., (1959) investigated the effect of interaction of fresh water with clays on oil permeability of water-sensitive formations through a laboratory experiments. A mixture of crushed quartz with 5% of one of kaolinite, illite or montmorillonite was blended for two hours and packed in a Lucite column and then sequential flooded with a sodium chloride solution, Kerosene and fresh water to see their effect in the permeability. The study concluded that oil permeability of a sand contains fresh water is appreciably less than that of the same sand contains salt water if an expanding-type clay such as montmorillonite is present and such damage can be only partially improved not completely.

Al-Aboudi, et al., (1995) studied the formation damage caused by clay-free inhibitive fluids and clay-based in a two sandstone rocks with different permeabilites. In addition they investigated the effect of varying the differential pressure and temperature.They used a closed loop circulating system consists of filtration autoclave with Hassler Cell and a filtrate collector under the following conditions: circulating temperature of up to 90ºC, circulating pressure of up to 10 MPa, Sleeve pressure of up to 15 MPa and fluid velocity along the core face of up to 3 m/s. The fluid system that used to damage the cores has

different polymers and formation pore bridging material. Bentonite was used as clay and chalk as formation pore bridging material. Many polymers were used such as Hydroxyethyl cellulose (HEC), xanthan gum (XC polymer), a low viscosity and high viscosity polyanionic cellulose (PAC) and a starch derivative. Gypsum, magnesium oxide and potassium acetate were used as a source of Ca^{2+}, Mg^{2+} and K^{+} cations.

As a results of these experiments several observations could be concluded as follow:

1. The main factor influencing the extent and value of damage in high permeable sandstone is the presence of clay and pore bridging materials.
2. In low permeable sandstone the damage is mainly caused by polymer molecules blocking the comparatively narrow pore channels.
3. The chalk influence the filtration properties that appear in different fluids. Fluid 5 showed a high API filtrate loss but a low dynamic filtrate loss because of its MgO content.
4. The damage caused in the low permeable sandstone (Obernkirehner sandstone) by clay free fluids is higher than that caused by clay-based fluids at 90ºC and that due the ability of polymers to block the pore openings so a higher damage ratio results.
5. In contrast, the damage caused in the high permeable sandstone (Bentheimer sandstone) by clay-based fluids is higher than one caused by clay-free fluids at 90ºC and that because of wide pores blocked by laminated particles of bentonite.
6. The amount and the distribution of the particle sizes of pore bridging materials should be selected with respect to the distribution of the pore sizes of the formation rock.

Table 1 Properties of the used fluids

Properties	Fluid Number					
Specific gravity (g/cm^3)	1	2	4	5	6	7
pH	7.8	7.6	8	9.2	8.6	8.3
API fluid loss	1.02	1.15	1.15	1.03	1.01	1.13
Plastic viscosity mPas	15/4	25/16	34/9	20/13	37/19	32/18
Yield Point dPa	9.6/4.8	43/4.8	106/9.6	48/9.6	446/120	533/144
Gel (10^{11}) dPa	4.8/9.6	9.6/4.8	9.6/4.8	14.4/14.4	86/9.6	77/4.8
Gel (10^{1}) dPa	9.6/9.6	14.4/9.6	9.6/4.8	39/29	91/14.4	82/14.4

Hayatdavoudi, et al., (1998) conducted several experiments on a core plugs prepared from Tuscaloosa sand from central Louisiana at room temperature, pH of 12 raised using caustic soda, the total injected volume was 500 cm^3, the differential pressure was 500 psi, the overburden pressure was 1000 psi and flow rate of 11.1 cm^3/min. The fluid contacted for 45 min and zero shut-in time (retrieving the sample immediately by the end of the experiment). In order to understand the kaolinite damage mechanism, Hayatdavoudi focus

in his second hypothesis because it required fewer amounts of energy and pressure than his first hypothesis, that content is to study the modification of kaolinite to dickite, nacrite, and halloysite with sodium reach condition and a reasonable pressure, flow rate and temperature gradient. He also proposed several probable chemical reactions in support of the second hypothesis. As a consequence of these experiments, analysis of permeability before and after flow showed that the loss in permeability percentage is 55.99 % and 66.2 % for core 1 and core 2, respectively. The analysis of SEM/EDX/XRD data support the second hypothesis since the presence of fragmentation and break-down process of the kaolinite plates as indication of the alteration to other minerals such as hallyosite and dickite as shown in Figure 5 and 6. They concluded that:

- It is very much possible to cause formation damage in a short time (45 minutes) at low temperature and a high pH = 12.
- In this work, kaolinite did not alter to smectite, therefore, they rejected the hypothesis relating the conditions of change between the two types of clays. i.e. conversion of kaolinite to smectite (1:1 clay to 2:1 clay) under our experimental conditions.
- The kaolinite clay mineral undergoing a highly oxidative process by Sodium peroxide, could partially alter to dickite and halloysite.
- The formation damage, in this study, is not caused by migration of kaolinite plates mentioned previously, it is rather caused by an oxidation process resulting in disintegration of kaolinite booklets and appearance of many other mineral fragments within the same pore space. i.e. kaolinite multiplied many times within the same volume of pore by altering to dickite and halloysite even without migration.

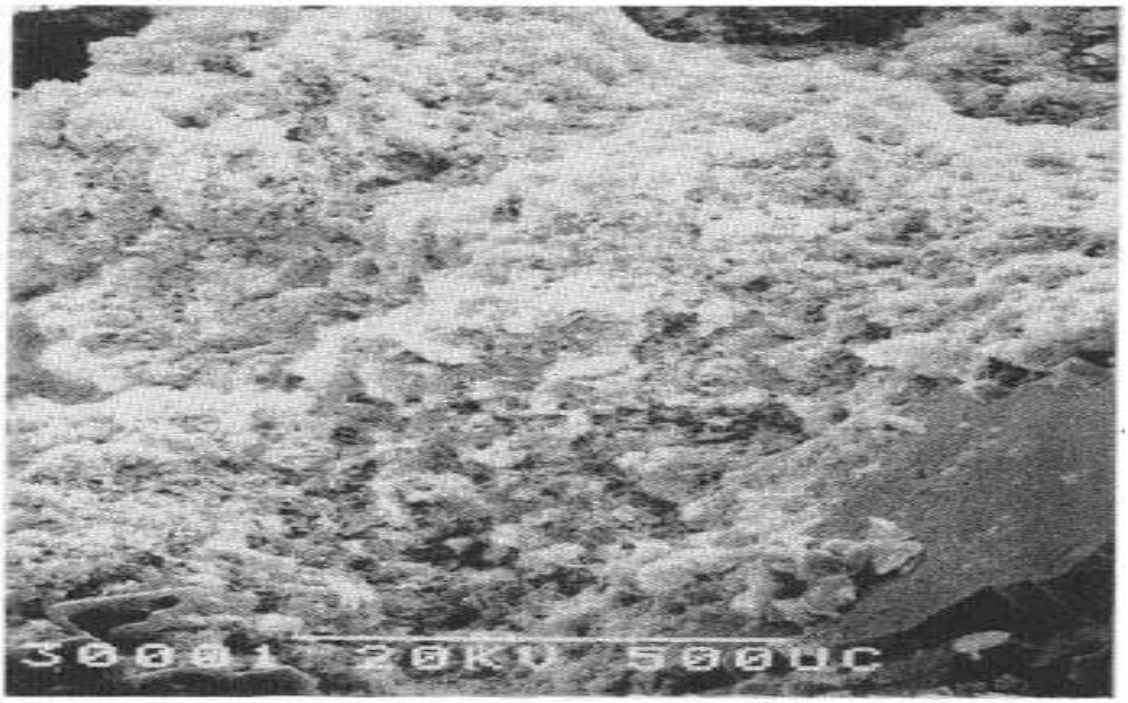

Figure 5: Break down of kaolinite plates to many altered fragments

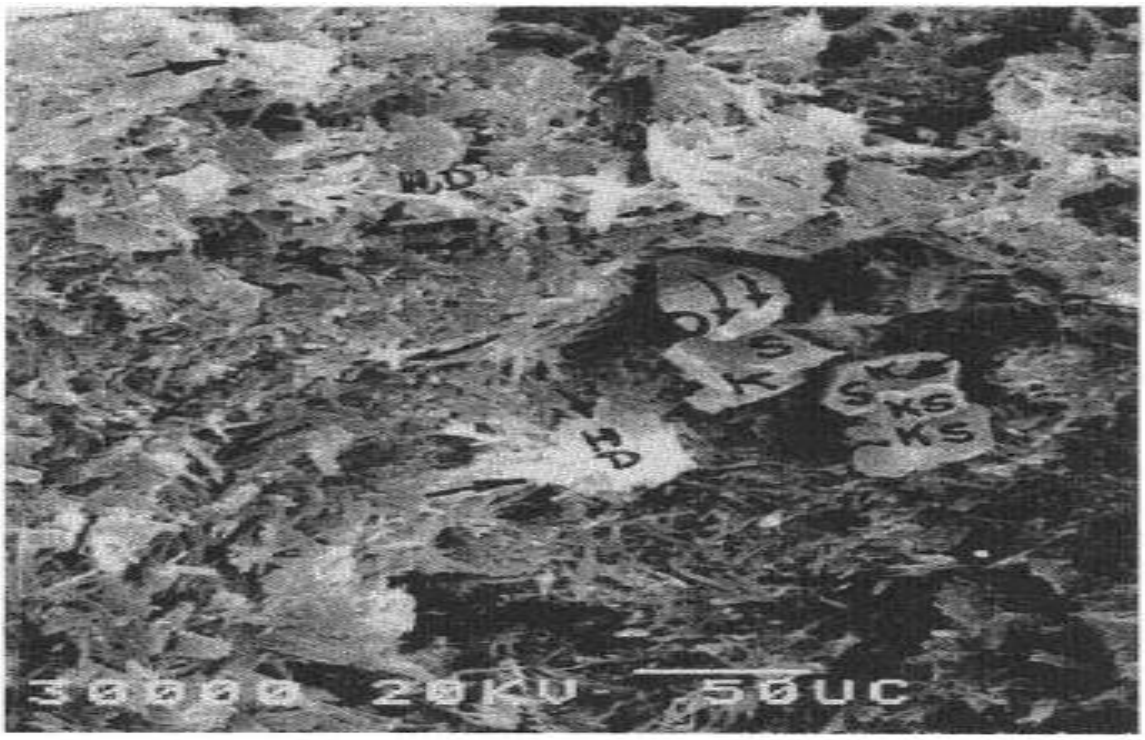

Figure 6: the sheared planes of kaolinite plates (KS), the oxidation sites of kaolinite (O) and hair like tubes of dcikite and halloysite (DH).

Audibert, et al., (1999) studied the influence of polymers on formation damage. In these experiments different polymer additives of a KCL/polymer mud were used as a fluid loss reducers with the Clashach sandstone cores that composed of 95 % quartz and less than 1 % illite. The cores pore diameter within the range of 20 μm to 30 μm and the average permeability measured using brine was 600 mD. 20 gm/L Nacl was used to saturate the core. The residual water saturation (S_{wi}) obtained by flowing kerosene in the obverse direction to the filtration which measured using various flow rates. The core was flooded with polymer solutions to observe the effect of invasion and back production on the core permeability under two saturation conditions: residual water saturation and100 % brine saturation. The measured permeability to brine at the end of the test reduced sharply while the decrease in kerosene permeability was not that much. To sum up, for these polymers the reduction in permeability is attributed to both change of water saturation and polymer plugging. A considerable decrease in permeability was caused by starch and it was approximately due to cell debris in the unpurified solution. Xanthan also shows that permeability was reduced significantly which could be due to the rigidity of the polymer and the high molecular weight.

Audibert, et al., (1999) studied the role of polymers in damaging Clashach sandstone cores that has small amount of clay (< 1 % illite). A blender of KCl and polymer mud with various polymer additives were used during the experiments. The starch induced strong particle flocculation during the adsorption test. They observed that the fluid loss that characterize the polymer stabilize at low temperature. Whereas, at 110˚C and above there was noticeable decay of fluid loss control due to degradation of some of the polymer. They

that the polymer plugging and a change the water saturation which cause a permeability reduction.

Bishop (1977) Studied the role of the very high salinity brine on causing the flocculation on the pore lining clays by the clay particles such as smectite, kaolinite and fine quartz particles that lead to pore throat bridging and plugging. Experiments were conducted to investigate the formation damage caused by saturated salt water based mud in a sandstone field in South America. The return permeability testing (Figure 7) can evaluate the effect of permeability reduction on the well performance and emphasize the formation damage was induced by the flocculation. The results showed that the permeability reduced by 74 % of the initial permeability due to the invasion of the representative volume of mud filtrate (damage take place after injection of around 1-2 pore volumes of saturated KCl mud filtrate). Many analyses were conducted to figure out the damage mechanisms.

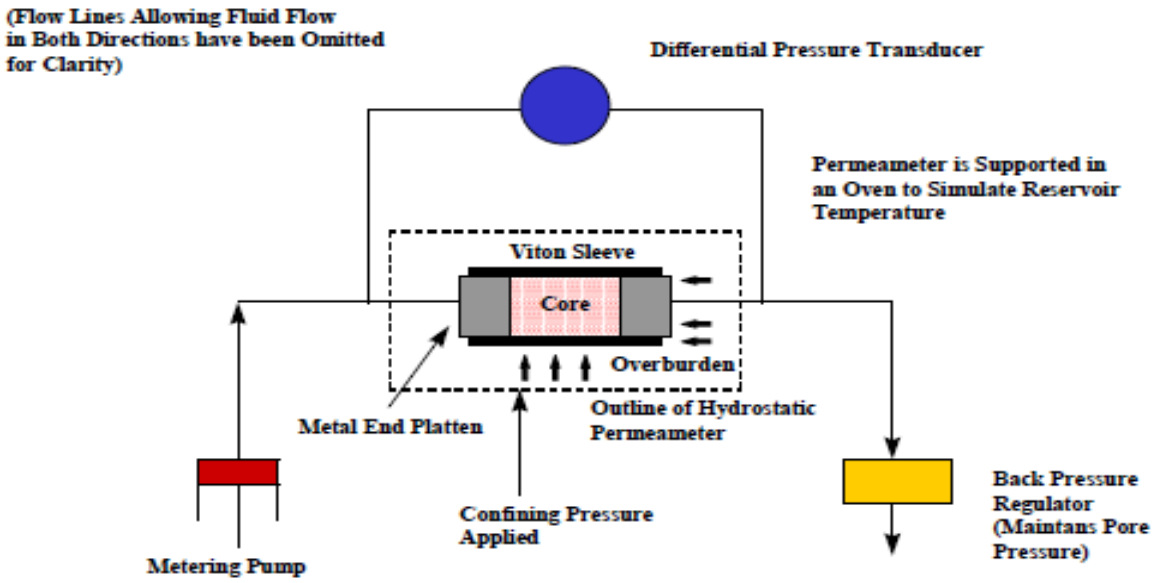

Figure 7: Schematic of Return Permeability Test Apparatus

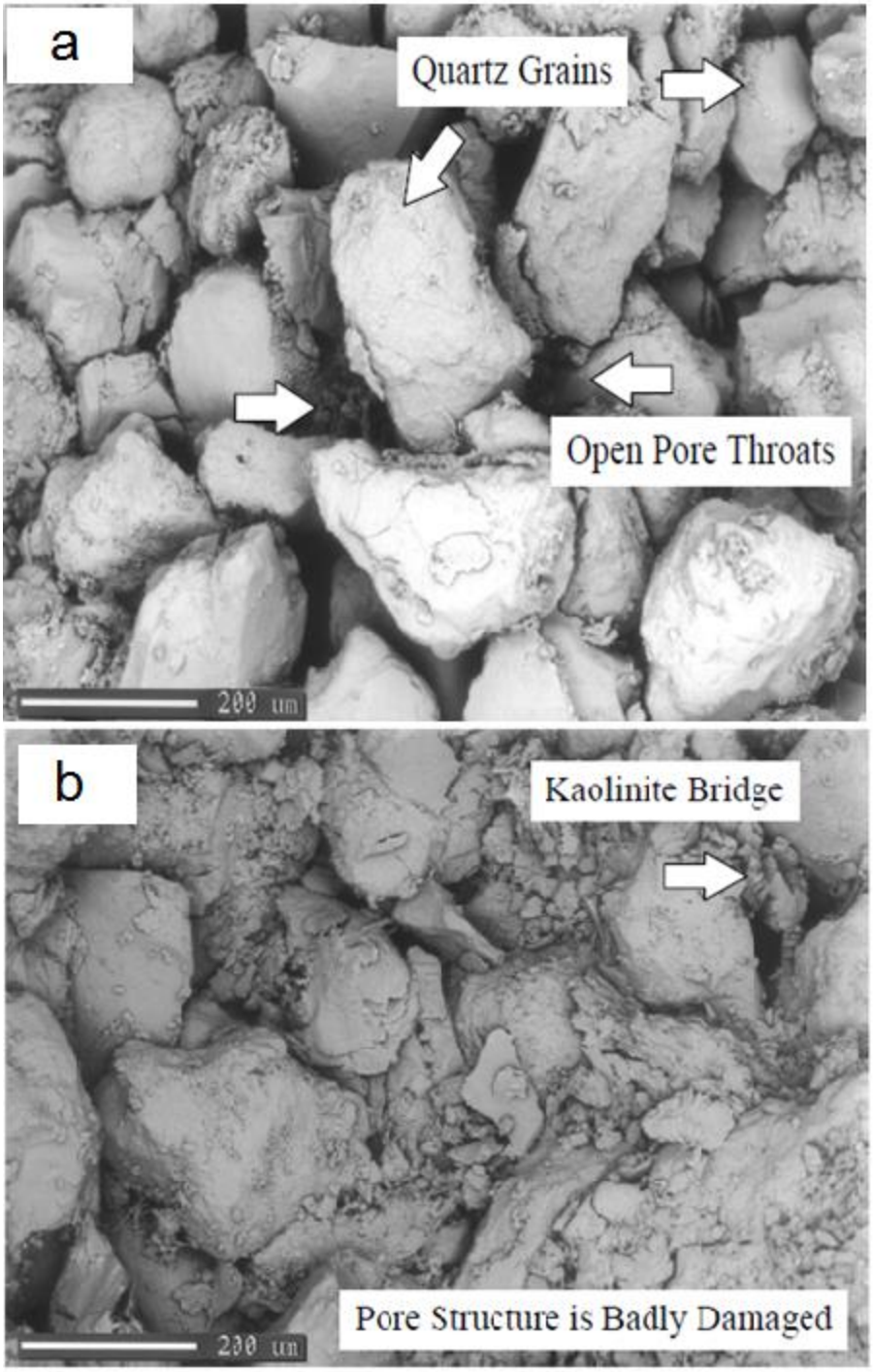

Figure 8: SEM image for core before (a) and after (b) damage

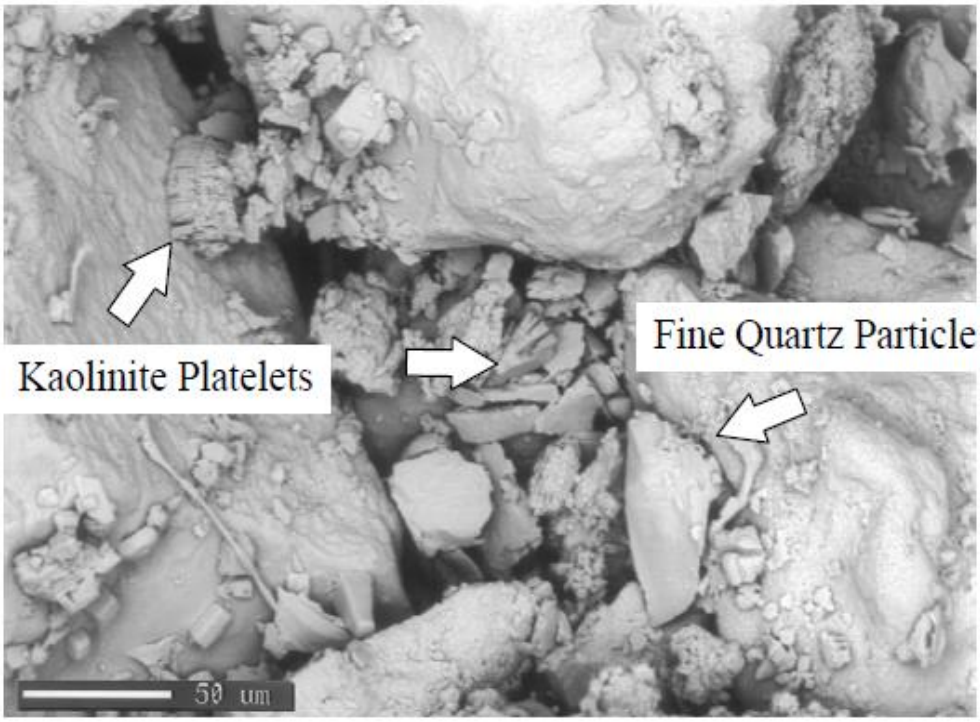

Figure 9: Bridged and Plugged Throat

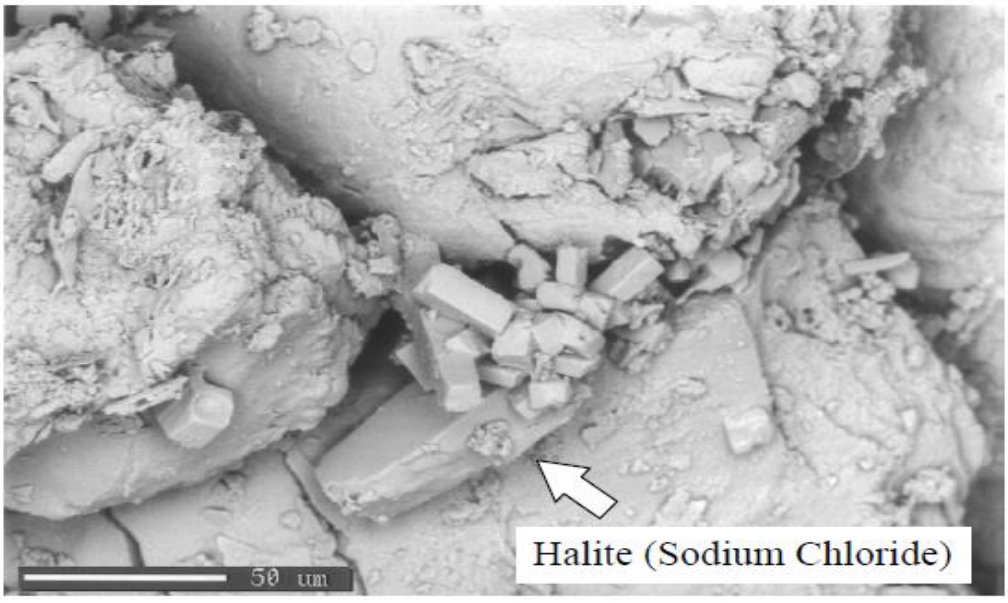

Figure 10: Halite Crystals Occluding a Pore Throat

The SEM results showed that the formation damage happened due to plugging and bridging of pore throats. Figure 8 show the SEM images for the core before (a) and after (b) damage. Figures 9 and 10 illustrates the core after invaded by the saturated salt mud filtrate. Maximizing the images of the individual pore throats clarifies the bridging material which appears to be fine quartz grains and kaolinite clusters. In Figure 11, The EDS identifies the sodium chloride crystals which can be clearly seen at the pore throats.

Wilson et al., (2014) studied North Sea sandstone reservoir in term of clay mineralogy and their effect on the formation damage. The North Sea reservoir has Kaolin mineral (highly crystalline) and has sand size 60 µm. The depth of burial increases the morphology of kaolinite aggregate changes and the illite occurred as pore-filling networks of extended particles. Kaolinite tends to block the pores. Many samples was taken at different depths from North Sea reservoirs show the predominance of kaolinite and illitic minerals. They found that kaolinite was formed early at low temperatures then converted to dickite as the depth of burial and temperature increased. On other hand, illite was formed at later stages and at temperature more than 100˚C. Before the flow test, SEM analysis showed that kaolinite appeared in Vermiform and book-like aggregates composed of euhedral hexagonal particles. While illitic clay was made in pore-filling and pore-bridging modes. Furthermore, chlorite creates different edges around quartz grains made up of interlocking bladed crystals. After the flow tests, SEM observations suggested the removal of the fine lath-like illitic particles that bridged and lined pores as well as disruption of the kaolinite aggregates.

Nadeau (1998) studied the effect of the diagentic clay on the sandstone reservoir. The experiment conducted using three minerals dolomite, kaolinite and quartz to form the

synthetic sandstone since it requires low temperature and short run times. The reaction performed at temperatures of 200˚C for 19 to 45 days and can be written as:

$$\text{Dolomite} + \text{kaolinite} + \text{quartz} \rightarrow \text{smectite} + \text{calcite} + Co_2 \quad (2.1)$$

The nominal reaction mix consists of 90 wt. % quartz, 5 wt. % dolomite and 5 wt. % kaolinite. The mix was stirred with 4 ml of brine. The sample were vacuum-saturated using 1000 ppm NaCl brine for one hour then saturated under high pressure (2000 psi) overnight. Several analytical methods were used to characterize the sample such as XRD and SEM. The results showed that the most of the dolomite in the reacted sample was dissolved to produce calcite and barely smectite detected. The SEM analysis illustrated that the smectite exsist as a very fine and pervasive micro-porous cement that bridging the pore space. Figure 11a shows a sample of 100% quartz in which no clay was formed. The morphology of the clay formed during the early stages of the reaction (Figure 11b). Note the extremely small and thin individual clay particles growing out into the pore space. Figure 11c and 11d show extensive clay formation, often bridging the entire pore space.

The experimental work in this study show that:

- When smectite was grew to 5 wt. % the brine permeability reduced to 98 %.
- The pore bridging texture of the clay was responsible for the permeability reduction.
- The clay morphology collapse on air-drying.
- Commonly observed pore-lining smectite morphology in reservoir sandstone may be an artifact of conventional sample preparation method.

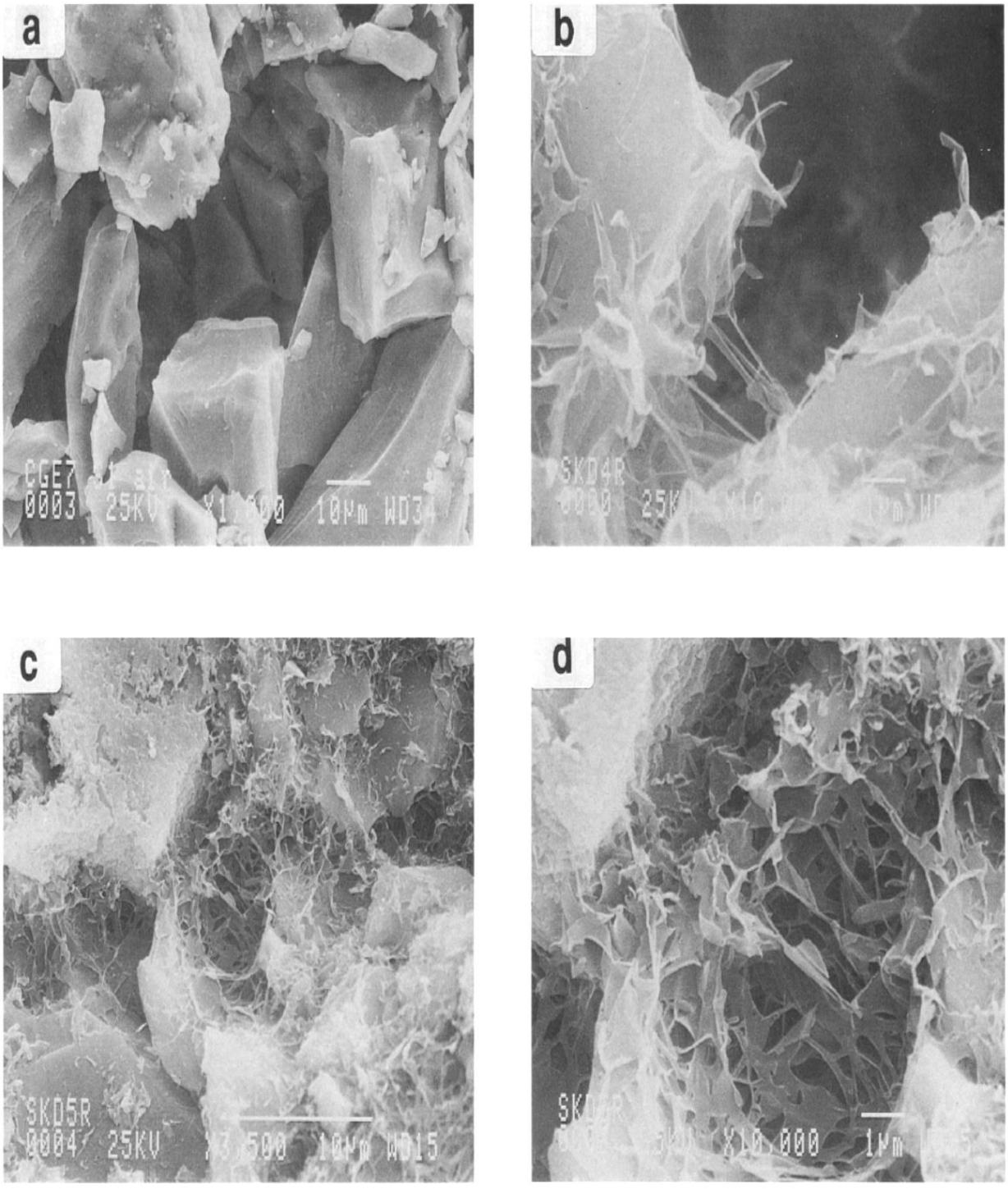

Figure 11: SEM of 100% quartz (Figure 11a). Figure 11b shows incipiently formed smectite clay. Note the delicate, microporous, pore-bridging smectite morphology occluding most of the available pore space in Figure 11c and 11d

2.2 Damage by Fine Migration

Mahmoud et al., (2015) study the influence of HCl on the illitic sandstone. 1.5 inches diameter and 6 inches length Bandera, Berea, Kentucky and Scioto sandstone cores were used. Bandera sandstone was flooded initially by 5 wt. % NaCl to measure initial permeability then flooded by 15 wt. % HCl at 80°F and rate of 5 cm^3/min and finally flooded by 5 wt. % NaCl in the reverse flow direction to measure the final permeability. The initial permeability was 4.1 mD. After injection of 15 wt. % HCl the permeability reduced significantly to 0.85 mD. Figure 12 depict that pressure drop was increased sharply from 400 to 1500 psi after injecting 15 wt. % HCl. The gradual increase in the pressure drop was due to fine migration and blocking the pore throats subsequently the permeability was lost.

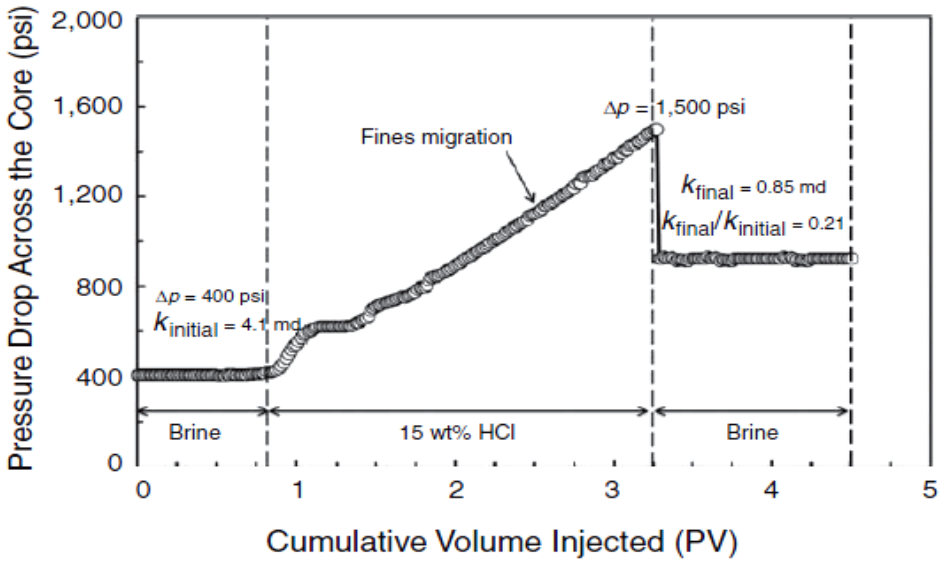

Figure 12: Pressure drop across Bandera sandstone during injecting 15 wt. % HCl at 80°F and 5 cm^3/min

2.3 Damage by VES Adsorption

Curbelo et al., (2007) studied the adsorption of VES from aqueous solution on the reservoir rocks. An Açu sandstone core plugs of 3.8 cm diameter, 8.7 cm length and porosity of 24% were used in this experiments. The cores were roasted at 700^{o}C for 18 hours. Then they were coated with resin. The flooding experiments were performed into two steps:

1. Flooding of two nonionic surfactant (ENP95 and ENP150) at a constant pressure of 30 psi.
2. The losses of surfactant measured by collecting the effluent. The surfactant solutions were injected into the core until the surfactant concentration in the effluent equaled to that in the injected surfactant.

The results showed that ENP95 was adsorbed at higher extent than ENP150 because the previous surfactant has a smaller ethoxylation degree, that is, a smaller polar part.

Yu et al., (2011) conducted a core flooding experiments on a pink desert limestone cores using surfactant based acid as injection fluid. The core were injected with a blended of 15 wt% HCl, 7 vol% VES, 0.3 vol% corrosion inhibitor at a constant flow rate ranging from 1.5 to 40 cm^3/min. they found that amount of retained surfactant is a function of the acid injection rate. Only 20% of the injected surfactant removed by the mutual solvent.

2.4 Quantification of Formation Damage

Van Everdingen and Hurst (1949) introduced the concept of the skin effect using Laplace transform to quantifying the region near the wellbore. The dimensionless quantity S, the skin factor, was used to estimate the additional pressure drop within the wellbore. The skin effect causes additional steady-state pressure drop. Skin can be estimated using the following equation:

$$S = \left(\frac{K_e}{K_a} - 1\right) \ln\left(\frac{r_a}{r_w}\right) \quad (2.2)$$

Where K_e is the external permeability, K_a is the altered permeability in the damage zone, r_a is the radius of the damage and r_w is the radius of the wellbore.

Muskat (1981) developed the following relationship:

$$\frac{Q_d}{Q} = \frac{\ln\frac{r_e}{r_w}}{\frac{K}{K_d}.\ln\frac{r_d}{r_w} + \ln\frac{r_e}{r_d}} \quad (2.3)$$

The permeability of the damage zone K_d and the radius of the damage zone r_d have major effect on the productivity of the damaged formation. Muskat defined the damage ratio as:

$$DR = \left(1-\frac{K_d}{K}\right) . 100 \quad (2.4)$$

Ghofrani et al., (1996) defined a new damage ratio (DR) to evaluate the core formation damage ratio with different fluids. The cores were divided into segments with permeability K_i for each segment. The permeability was measured before and after contamination. Then the average permeability of a series of layers was calculated by Monicard equation (Monicard 1980):

$$K_{av} = \frac{l}{\sum_{i=1}^{n}\frac{l_i}{K_i}} \quad (2.5)$$

While the sectional damage ratio (SDR) for each segment is given by:

$$SDR = \left(1-\frac{K_{di}}{K}\right) . 100 \quad (2.6)$$

The new defined damage ratio allows the determination of the reliable extent of the damaged zone of the tested core.

Basan (1985) studied the potential for formation damage using the Formation Damage Index (FDI). FDI is a number determined by petrographic techniques used for classification of the potential for formation damage in shaly sandstones. the numbers, which indicate

increasing tendency toward damage, represent a formation condition modal that is based on ten generic reservoir lithologies. Basan presented FDI numbers that reflect the formation condition based on 10 generic reservoir lithology's (FDI 1-10) as shown in (Table 2).

Rock-related damage, sa opposed to other types of wellbore damage, is best understood where the potential triggering mechanism can be identified. Although, there are a few minor mechanisms that contribute to damage, the important ones are:

- Dispersion/migration.
- Particle migration.
- Mineral precipitation.
- Lattice expansion or unconsolidation.

Each number in the FDI model has an increasing potential to one or more of these mechanics.

The most fluid sensitive rocks are those that have small amount of clay (less than 10%) that occurs in a form that produces a high surface area to pore volume. Where clay is responsible for formation integrity, there is a high potential for formation unconsolidation. They conclude that formation damage conditions can be identified and classified by their tendency toward wellbore damage.

Table 2 Classification the potential formation damage in shaly sandstone using FDI technique

FDI number	Reservoir condition
1	Indurated sandstone with low clay content, ranging near 5%, clay is distributed in the matrix
2	Indurated sandstone with a high clay content, averaging over 15%, clay is distributed in rock clasts
3	Indurated sandstone with a moderate clay content, averaging 10% or less, authigenic clay occurs as pore-fill
4	Indurated sandstone containing organic particles of immobile hydrocarbon
5	Indurated sandstone with a moderate to high clay content (10 – 15+ %), occurring as dispersed matrix and bound by a soluble cement
6	Indurated sandstone with low clay content, normally less than 10%, but is occurring as a grain attachment in pore spaces
7	Indurated sandstone with a moderate to high clay content (10 – 15 %) and occurring as biogenically mixed matrix
8	Indurated sandstone with less than 10% authigenic clay occurring as grain lining
9	Sandstones that have clay as primary binder. Clay content rarely exceeds 10%
10	Unconsolidated or semi-consolidated sandstones that have weak clay content, Normally, clay content is less than 10% and commonly less than 5%

Al-Yaseri et al., (2015) studied the formation damage in sandstone in-situ at micrometer pore scale caused by fines movement and the associated mechanism. They used NMR technique and high resolution x-ray micro-computed tomography. A brine (5 wt. % NaCl + 1% KCl in deionized water) contained suspended barite particles was used to simulate the fines in the subsurface. As a result of that, reduction in permeability was observed. Figure 13 shows that the permeability decreased as the barite concentration increased. They found that the permeability follows the power law as following:

Sample 1: $k = 3.94t^{-0.343}$ (2.7)

Sample 2: $k = 2.701t^{-0.403}$ (2.8)

The accumulated weight of produced fluid versus time for different barite concentration (Figure 14).

Figure 15 and 16 show the NMR T_2 curves of the undamaged and damaged core samples for different barite concentrations. The T_2 is related to the surface to volume ratio with the following equation:

$$\frac{1}{T_1} = \frac{\rho S}{V} \quad (2.9)$$

Where, ρ is the surface relativity (assumed constant in this study).

The average time (T_2) for different concentration were decreased from 0.72 s to 0.31 s and from 0.86 s to 0.25 s for the concentration 0f 10 gm/L and 20 gm/L respectively. Shrinking of pore size is clearly from the shifting of the curves toward smaller time (T_2). In addition, the reduction of the longest peak of T_2 in both cases clarify that the barite particles plugged the larger pores and split into smaller pores.

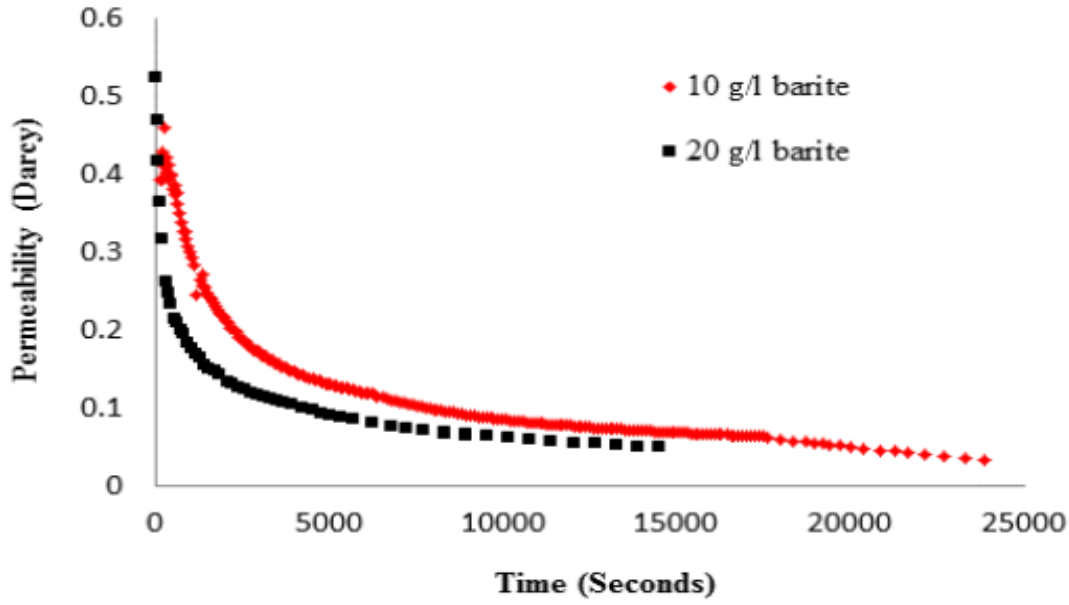

Figure 13: Permeability versus time at different barite concentrations

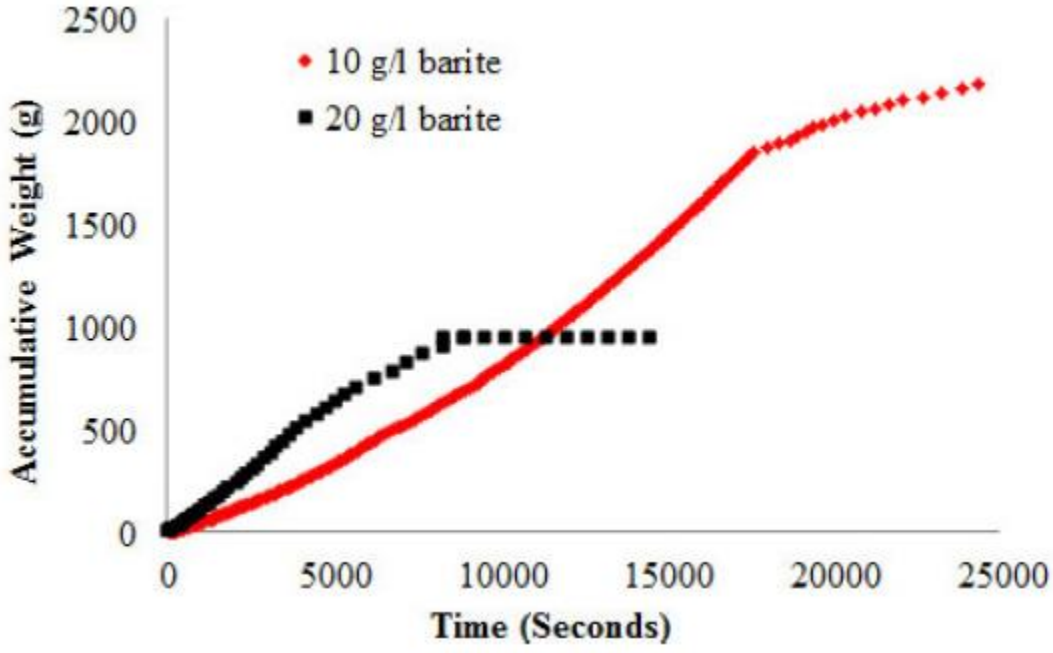

Figure 14: Accumulated weight of produced fluid versus time for different barite concentration

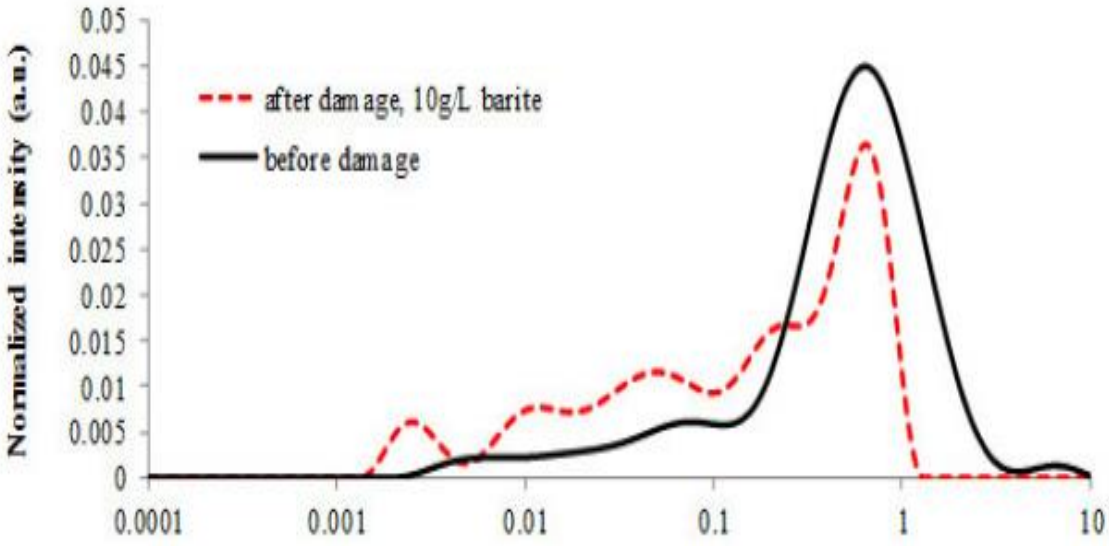

Figure 15: NMR T2 response before and after injection damage

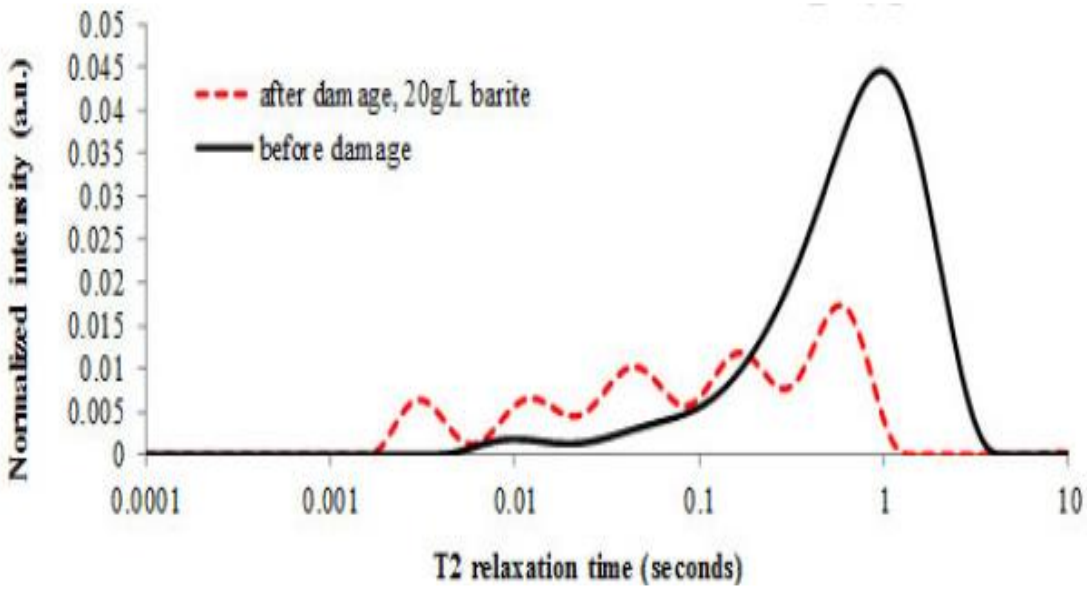

Figure 16: NMR T2 response before and after damage

2.5 Nuclear Magnetic Resonance

Brown and Gamson (1960) conducted the first NMR measurement in a borehole using the earth magnetic field. They found that NML can be used in all formations since they are not highly magnetic. Also they showed that the free fluid index delineates the fluid-containing zones and may be used as a minimum effective porosity index. As mentioned that NML could estimate a permeability index, distinguish oil zone from water zone, and water and oil saturation in the immediate vicinity of the borehole.

Seevers (1966) proposed a model to estimate the specific permeability of sandstone using the fluid content (FFI) and the thermal relaxation time (T_1). The model is a combination of the Kozeny-Carman equation and the equation of the relaxation of nuclear spin polarization of liquids in porous media.

$$K = A * FFI \left[\frac{T_1 T_B}{T_B - T_1}\right]^2 \quad (2.10)$$

The model is assumed to be valid if the relevant part of the pore size distribution can be described precisely and the FFI and T_1 are descriptive of this part. The tests were performed on a cores with permeability range from 0.01 to 8000 millidarcys. The parameter A varied between 0.23 to 11 darcy/sec^2. The deviation factor between the measured and the calculated permeabilities was less than 0.5.

Timur (1969) estimate the producible porosity ($\emptyset_p$) and permeability (K) by performing a laboratory experiments on more than 150 sandstone samples. They used the (FFI) parameter which obtained from the nuclear magnetism log (NML) within 2.9 porosity units to estimate $\emptyset_p$ through the correlation:

$$\emptyset_p = 1.4\, FFI - 3.2 \quad (2.11)$$

Also the permeability can be estimated either by α which can be obtained with NML as:

$$\alpha = FFI\ [\frac{T_1\ T_B}{T_B - T_1}]^2 \quad (2.12)$$

Or β which can be obtained with both NML and porosity log as:

$$\beta = \frac{\emptyset^{4.4}}{10^4\ [1-\frac{1.4FFI-3.2}{\emptyset}]^2} \quad (2.13)$$

Where α is a parameter need NML and β is a parameter need NML and porosity log for estimating K.

Saraf et al., (1967) used the NMR technique to estimate fluid saturation on Boise sandstone and measure the two- and three phase relative permeabilites. They applied the Darcy's law which concluded that the relative permeability to different fluid can be determined from the saturation alone. The experiments were conducted using three fluids kerosene, Heavy water (deuterium oxide) and nitrogen to represent the hydrogen-containing fluid phase, the aqueous phase and the gas phase respectively. The average porosity of the sandstone was 26 % and the air permeability of the cores was in the range from 1.6 to 1.7 darcies. Single-phase water permeability varied from 1.4 to 1.5 darcies. They found that the three phase water permeability depends only on the water saturation while the three phase oil permeability depends on the water and oil saturation. Moreover, the relative permeability to gas found to be dependent on the total liquid saturation.

CHAPTER 3

METHODOLOGY AND EXPERIMENTAL PROCEDURE

This study was performed on both limestone and sandstone core plugs.

3.1 Experiment procedure

The procedures followed to perform these experiments divided into section based on the rock type. The samples were prepared to be compatible with the apparatus used for the tests. In addition, the brine fluids used in all experiments were prepared using deionized water.

3.1.1 Sandstone sample

- Drying the sample at 60˚C for 24 hrs.
- Weight the sample after drying to measure the dry weight.
- Saturate the sample with brine (KCl) under pressure for 24 hours.
- Weight the saturated sample to measure the porosity of the sample.
- Measure the density of the brine (KCl).
- Measure the viscosity of the brine (KCl).
- Perform NMR measurement for the saturated sample with brine (KCl).
- Measure the initial permeability with brine (KCl).
- Flood the sample with DIW/ HCl.
- Measure the final permeability using (KCl).
- Perform NMR measurement for the sample.

3.1.2 Carbonate sample

- Drying the sample at 100˚C for 24 hrs.
- Weight the sample after drying to measure the dry weight.
- Saturate the sample with DIW under pressure for 24 hours.
- Weight the saturated sample to measure the porosity of the sample.
- Perform NMR measurement for the saturated sample with DIW.
- Measure the initial permeability with DIW.
- Inject 7 vol. % VES into the core.
- Perform NMR measurement for the saturated sample after VES flooding.
- Measure the final permeability with DIW.

3.2 Apparatus

3.2.1 Kinematic Viscosity Bath

The viscosity of the fluid was measured at different temperatures based on the kinematic viscosity using Oswald viscometer (Figure 17).

3.2.2 Hydrometer

The specific gravity of the fluid is measured using the hydrometer (Figure 18) based on the principle of buoyancy. The apparatus is sink in the fluid to a level correspond to the liquid's relative density.

Figure 17: Kinematic Viscosity Bath.

Figure 18: Hydrometer

3.2.3 Core flood system

A high pressure and high temperature core flooding system (Figure 19) was used to flood the core samples. It consists of:

- Two Isco Syringe pumps have a maximum injection pressure of 7500 psi.
- Hassler-sleeve core holder.
- Back pressure regulator up to 1000 psi.
- Data acquisition system which has the capability to record pressures every one second.

3.2.4 NMR Rock Core Analyzer

NMR signals generated from liquids (oil or brine) when the sample is placed in a magnetic field and then excited with a brief pulse of radio frequency energy. Immediately, after the pulse, an NMR signal appears, which then dies away with a characteristic relaxation time or decay rate known as T_2.

The NMR apparatus (Figure 20) consists of four main elements:

- Electrons cabinet which comprising the primary electronic components of the NMR instrument.
- Magnet unit which comprising the magnet unit and the RF probe.
- Chiller recirculating unit.
- Desktop computer.

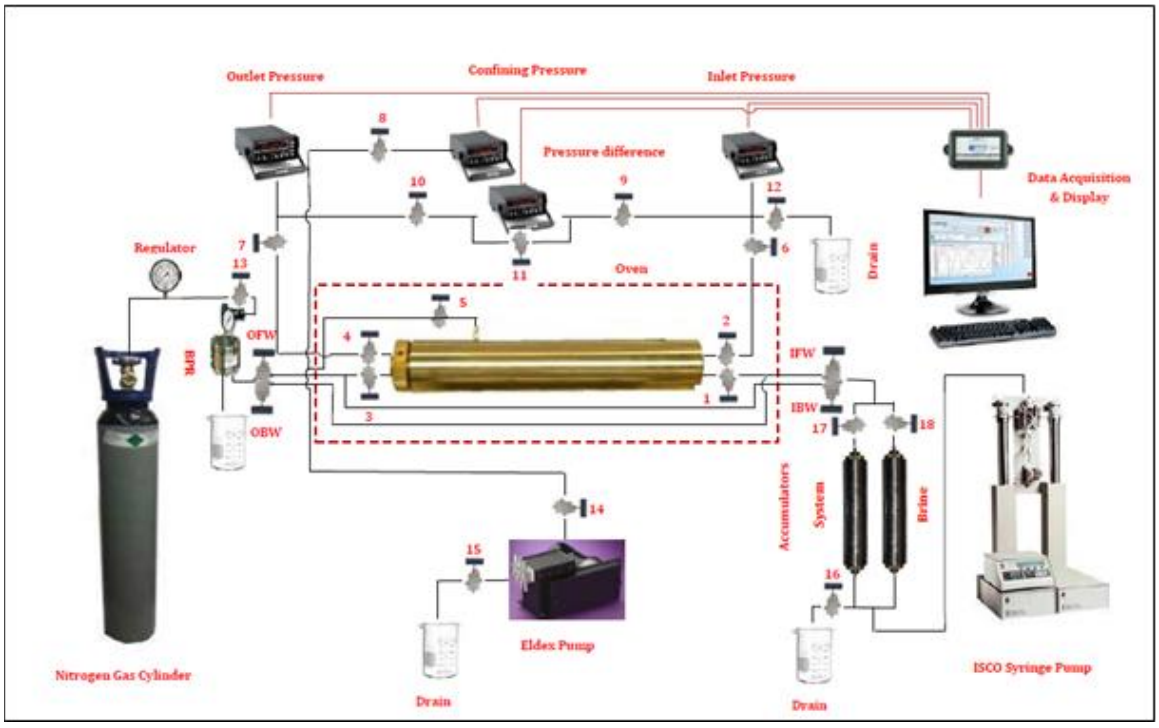

Figure 19: Core flood system

Figure 20: NMR Rock Core Analyzer

CHAPTER 4

RHEOLOGICAL STUDY OF VES

4.1 Introduction

In 1997, VES (viscoelastic surfactant) system was introduced as a new fracturing and acidizing fluid instead of the conventional polymer. It provides sufficient viscosity and viscoelasticity to create a fracture. The fluids can be easily prepared simply by mixing a desired amount of VES with brine. VES was used in many applications in the petroleum industry such as matrix stimulation and EOR.

4.2 Viscoelastic Fluids

Viscoelastic fluids are those fluids that have viscos and plastic properties. The relationship between the stress and strain in Hookean elastic solid is independent of time. Whereas in viscoelastic fluids the stress will gradually dissipate. The deformation will be recovered gradually by these materials upon removal of stress.

4.3 Chemistry of Surfactants

Surfactants play a key role in many well treatments because of their unique properties. Surfactants are used to reduce surface tension, change wettability, mobilize residual oil, and disperse corrosion inhibitors. Surfactants are chemical agents which composed of a polar head group (hydrophilic part) and a tail group (hydrophobic part). Figure 21 shows the typical structure of surfactants.

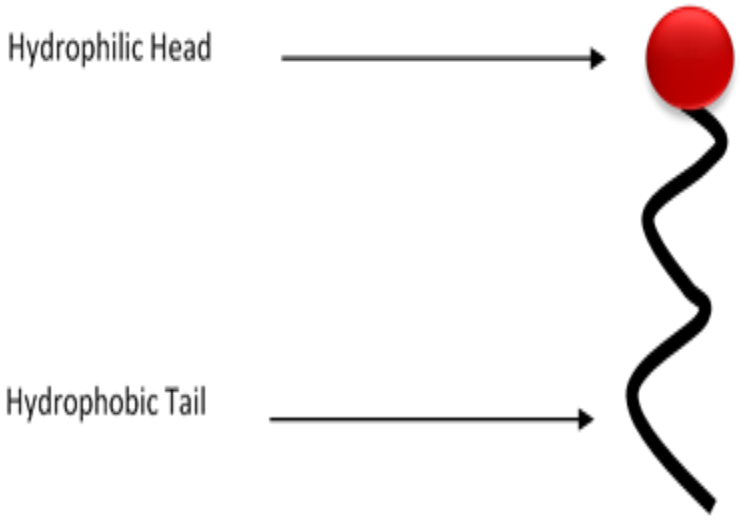

Figure 21: Schematic of surfactant structure

Frequently, the hydrophobic tail consists of around 10-20 carbon atoms which form a long hydrocarbon chain and this chain may contain oxygen atoms, amide groups, ester groups and double bonds or benzene ring.

4.4 Classification of Surfactants

Generally, the hydrophobic group consists of hydrocarbon chain with 10-20 carbon atoms. The chain may include oxygen atoms, benzene ring, amide groups, ester groups, or double bonds.

Surfactants can be classified based on the ionic nature of the head group to nonionic, cationic, anionic or zwitterionic. Each of them has its own characteristics based on how it ionizes in aqueous solution. Table 3 shows some of the common used surfactants.

Table 3 List of surfactant and their structure based on the head group charge

Surfactant		Chemical Structure
Anionic	Sodium dodecyl sulfate	$CH_3\ (CH_2)_{11}\ SO_4^-Na^+$
	Sodium dodecyl benzene sulfonate	$CH_3\ (CH_2)_{11}\ C_6H_4\ SO_3^-Na^+$
Cationic	Cetyltrimethylammonium bromide	$CH_3\ (CH_2)_{15}\ N(CH_3)_3^+Br^-$
	Dodecylamine hydrochloride	$CH_3\ (CH_2)_{11}\ NH_3^+Cl^-$
Non-ionic	Polyethylene oxides	$CH_3\ (CH_2)_7\ (O.\ CH_2\ CH_2)_8\ OH$

4.4.1 Anionic surfactants

Anionic surfactants possess a negative charge when they ionize in aqueous solution. The hydrophilic head compromises carboxylates, sulfates, phosphates and sulfonates. Anionic surfactants is the most commonly used in EOR. They have good properties such as creation of self-assembled structure, lowering IFT, stable and has low adsorption on reservoir rock (Green and Wilhite, 1998). They dissociate in water to produce an amphiphilic anion and a cation.

4.4.2 Nonionic surfactants

Nonionic surfactants have non charged head group. They were used in EOR (Gupta and Mohanty, 2007). Nonionic surfactants are more preferable for acids. Their molecules dissolve in the aqueous phase by hydrogen bonds via a chain ethylene oxide or propylene oxide groups. When they are used in non-acidic medium it may cause formation damage because they separate and lose their characteristics.

4.4.3 Zwitterionic/amphoteric surfactants

Amphoteric or zwitterionic surfactants have two functional group, one anionic and one cationic. In most cases it is the pH which determines which the groups would dominate, by favoring one or the other ionization: anionic at alkaline pH and cationic at acid pH. Near the so-called isoelectric point, these surfactants display both charges and are truly amphoteric, often with a minimum of interfacial activity and a concomitant maximum of water solubility.

4.5 Micelles

Their hydrophilic group is a non-dissociating type and does not ionize in aqueous solutions. At low concentration of dissolved surfactants molecules are dispersed as monomers. When the surfactant concentration increased above a specific concentration known as critical micelle concentration (CMC) the surfactants tend to self-assemble into various aggregate shapes such as rodlike micelles, spherical (Figure 22). The orientation of monomers in aqueous solution exposes the hydrophilic head to water. In non-aqueous system the orientation of the monomers is reversed.

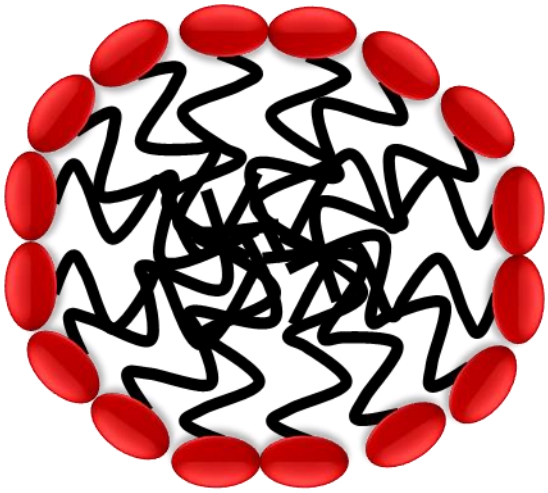

Figure 22: Schematic of surfactant structure (Spherical micelle)

The hydrophobic tails are covered by the hydrophilic head which will be in contact with the solvent. Each of them earns its characteristics depending on the way that the molecules ionize in the aqueous solution.

4.6 Rheology measurements

The properties of the viscoelastic materials were frequently measured by applying a sinusoidal input strain (Equation 4.1). Subsequently the shear stress produced will be recorded (Equation 4.2).

$$\gamma = \gamma_o \sin(\omega t) \tag{4.1}$$

$$\tau = \tau_0 \sin(\omega t + \delta) \tag{4.2}$$

In a rheometer. The linear viscoelastic region donated as (LVR) is the area in which the viscoelastic properties of the material were not dependent on the stress or strain. Experiments on colloidal dispersions have been conducted by number of researchers using two modes for the oscillatory measurement to study the properties of the VES (Ferry, 1980):

- Single frequency sweep for LVR identification:

The limit of the linear viscoelastic region can be determined by changing the amplitude of the input signal at constant frequency in a stress or strain sweep.

The limit of the LVR can be determined by measuring the critical sweep parameter. The stress or strain sweep performed by changing the amplitude of the input signal at constant frequency.

- Frequency sweep

The frequency sweep test is usually conducted and considered as a most prevalent type of oscillatory test, which shows the effect of the frequency on the viscoelastic behavior of the material.

4.7 Experimental work

4.7.1 Materials

In this study, zwitterionic surfactant class namely “erucamidopropyl hydroxypropyl used in this study. Brine solutions of Nacl and $CaCl_2$ with different concentrations were used to prepare VES solutions.

4.7.2 Sample Preparation

The rheological experiments were conducted with TA- instrument (DHR-3 Rheometer) with concentric cylinders. The temperature around the cylinder is maintained by a fluid circulating bath. The samples prepared by dissolving the required amount of salts in a deionized water. After that, VES was mixed with the aqueous solution for 10 minutes at 8000 rpm using ultra homogenizer. The foam produced as a result of the mixing process. The centrifuge was operated at 4000 rpm for 15 minutes to degas the foam. Most of the bubbles air had been removed after centrifuging and a clear solution with no turbidity was obtained. The solution was left for 24 hours for equilibrium. Finally, the sample was used for rheology measurement.

4.8 Results and discussion

A constant frequency was selected to perform the strain sweep test. To define the LVR, strain was changed, since the loss modulus and storage modulus are independent of strain. Then a strain in the linear viscosity range was utilized to perform the dynamic frequency

sweep tests. Apparent viscosity, shear, and loss modulus were measured by using 1 wt. % VES in 5, 10, 15, 20 wt. % $CaCl_2$ solution at 25°C. The same experiments were conducted with NaCl solution. A shear rate sweep (0.001 to 1000 S^{-1}) was performed for the NaCl and $CaCl_2$ solutions to analyze the effect of shear rate on the viscosity.

4.8.1 Effect of NaCl Concentration on VES Rheology

The effects of the salt on the viscosity of the VES system was investigated at different concentration. NaCl was dissolved in a distilled water at a concentration of 5, 10, 15 and 20 wt. % with a fixed concentration of 1 wt. % VES. Dynamic frequency sweep test was performed using a strain of 39 %.

Figure 23 shows that, as the frequency increased the viscosity decreased gradually. At low shear rate there was no visible change in the viscosity trend (behave as Newtonian fluid). As the shear rate increased the viscosity decreased gradually. This reduction in viscosity can be explained by the breaking of the viscoelastic micelle structures to small pieces (Nasr-El-Din et al., 2006). The higher viscosity corresponds to the low shear rate is due to the entanglement of the micelles of the surfactant. Figure 24 shows the shear stress versus shear rate (γ). At a low shear rate below the critical value ($\gamma < 0.1$), stress and shear rate are linearly proportional. These results are similar to Berret's chart. Berret named this shear rate as (γ_{In}) which reflect the start of the transition phase between the isotropic and the nematic (Berret, 1997). Above (γ_{In}), the stress changing independent of the shear rate and sometimes show unstable behavior. AS a result of that shear thinning behavior at high shear rates exhibit, which can be observed by optical birefringence in a Couette flow (Berret, 1997).

The storage modulus G′ represents the elasticity and the loss modulus G″ reflects the viscosity. Figures 25 and 26 show that as the concentration of NaCl increases the storage modulus and loss modulus increase gradually. As the concentration of NaCl increased in the solution the viscosity increased until a specific concentration then decreased. The decrease in viscosity after 15 wt. % NaCl can be explained by the decrease of the effective headgroup area that caused a shift toward a lamellar phase. Moreover, the electrostatic interactions of the wormlike micelles become screened. The drop in viscosity occurred because the repulsion generated by the charged surfaces of the micelles is no longer present.

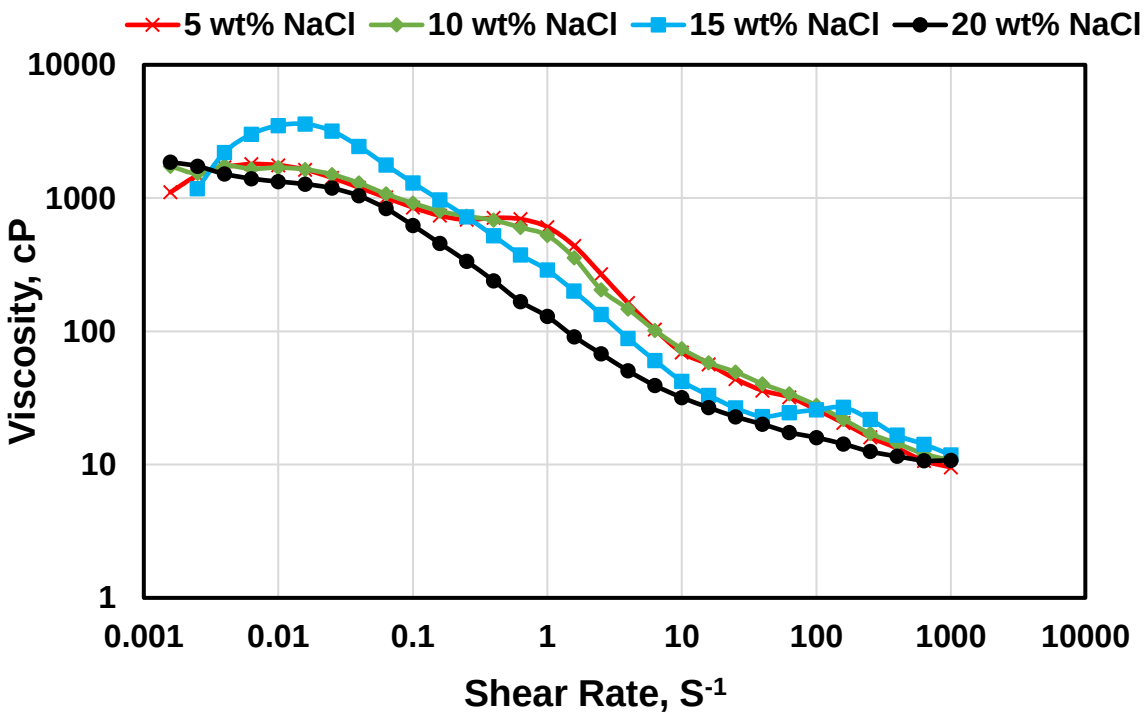

Figure 23: Effect of shear rate on apparent viscosity for different NaCl concentrations at a constant VES concentration of 1 wt% and at 25° C

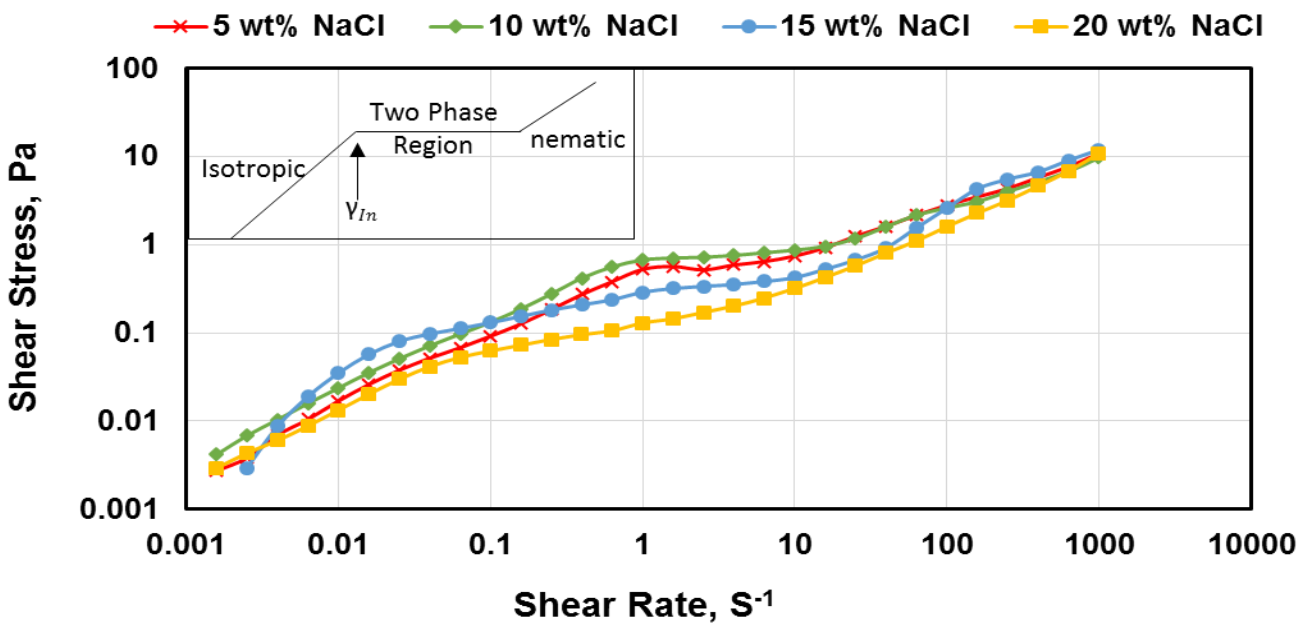

Figure 24: shear rate vs. shear stress for different NaCl concentrations at a constant VES concentration of 1 wt. % and at 25˚ C

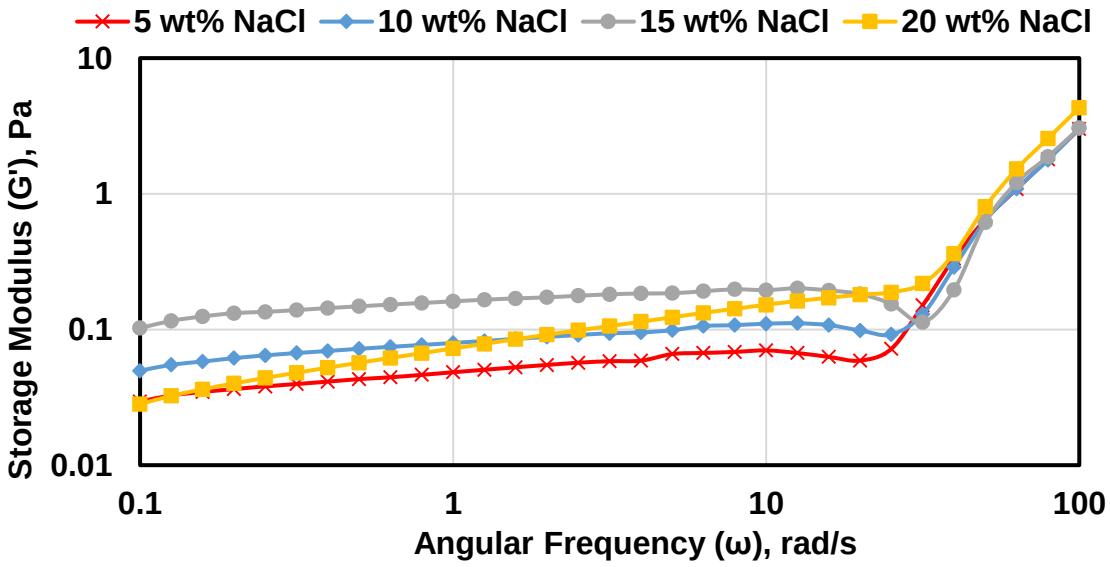

Figure 25 : Storage Modulus for different NaCl concentrations at a constant VES concentration of 1 wt. % and at 25˚ C

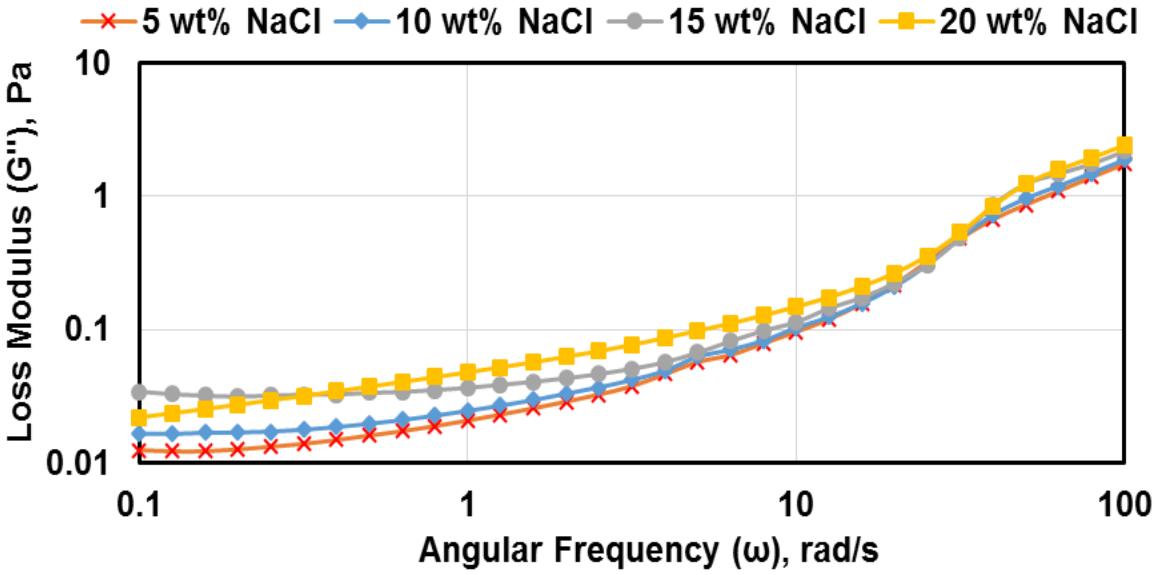

Figure 26: Loss Modulus for different NaCl concentrations at a constant VES concentration of 1 wt. % and at 25° C

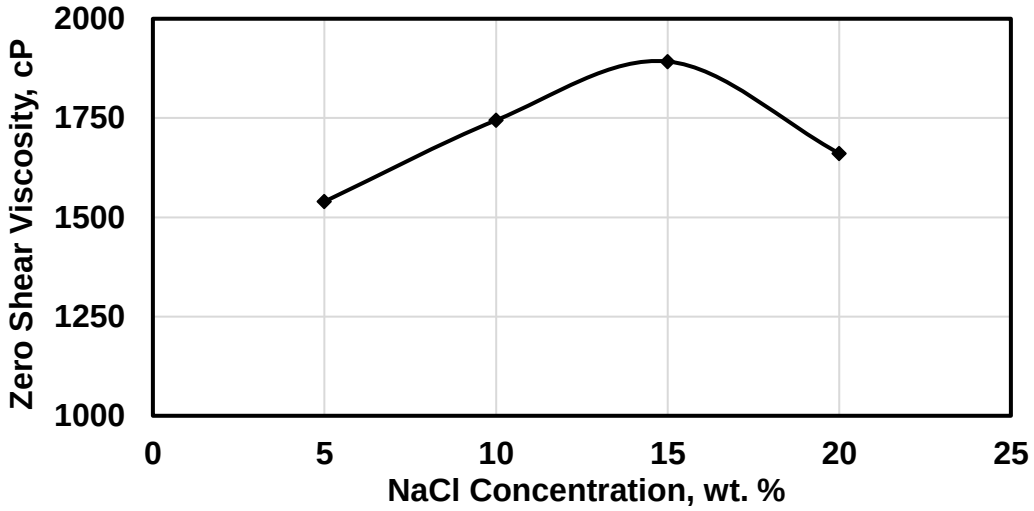

Figure 27: Zero Shear Viscosity for different NaCl concentrations at a constant VES concentration of 1 wt. % and at 25° C

Figure 27, on increasing the NaCl concentration with a fixed VES concentration of 1 wt. %, the viscosity increase sharply until a maximum of 1900 cP, and finally decrease dramatically. This behavior is expected. It is similar to the behavior obtained in several

aqueous surfactant/salt system (Ali, A. A., & Makhloufi, R., 1999) and explained by connections which result from the formation and breaking of wormlike micelles.

4.8.2 Effect of $CaCl_2$ Concentration on VES Rheology

As the shear rate increased the viscosity decreased gradually (Figure 28), which can be explained by the braking of the viscoelastic micelle structures into spherical micelles. The high viscosity values can be explained by the entanglement of the cylindrical micelles of the surfactant (Nasr-El-Din et al., 2006). Except at 20% $CaCl_2$ the viscosity decreased significantly.

Figure 29 show the shear stress versus shear rate (γ) for different $CaCl_2$ concentration. At a low shear rate, stress and shear rate are linearly proportional. These results are similar to Berret's chart. Berret named this shear rate as (γ_{In}) which reflect the start of the transition phase between the isotropic and the nematic (Berret, 1997). Above (γ_{In}), the stress changing independent of the shear rate and sometimes show unstable behavior. Figures 30 and 31 show the storage modulus and loss modulus changing as angular frequency change at different $CaCl_2$ concentration. Both moduli increase as the concentration increase, except the 20% concentration it exhibit low moduli values comparing with the general trend.

For the zero shear viscosity, as the concentration of $Cacl_2$ increased in the solution the viscosity increased until a specific concentration then decreased to a minimum value of 30 cP at a concentration of 20 wt% $Cacl_2$. The decrease in viscosity after 15 wt. % $CaCl_2$ can be explained by the decrease of the effective head group area that caused shift toward a lamellar phase (Ali, A. A., & Makhloufi, R., 1999).

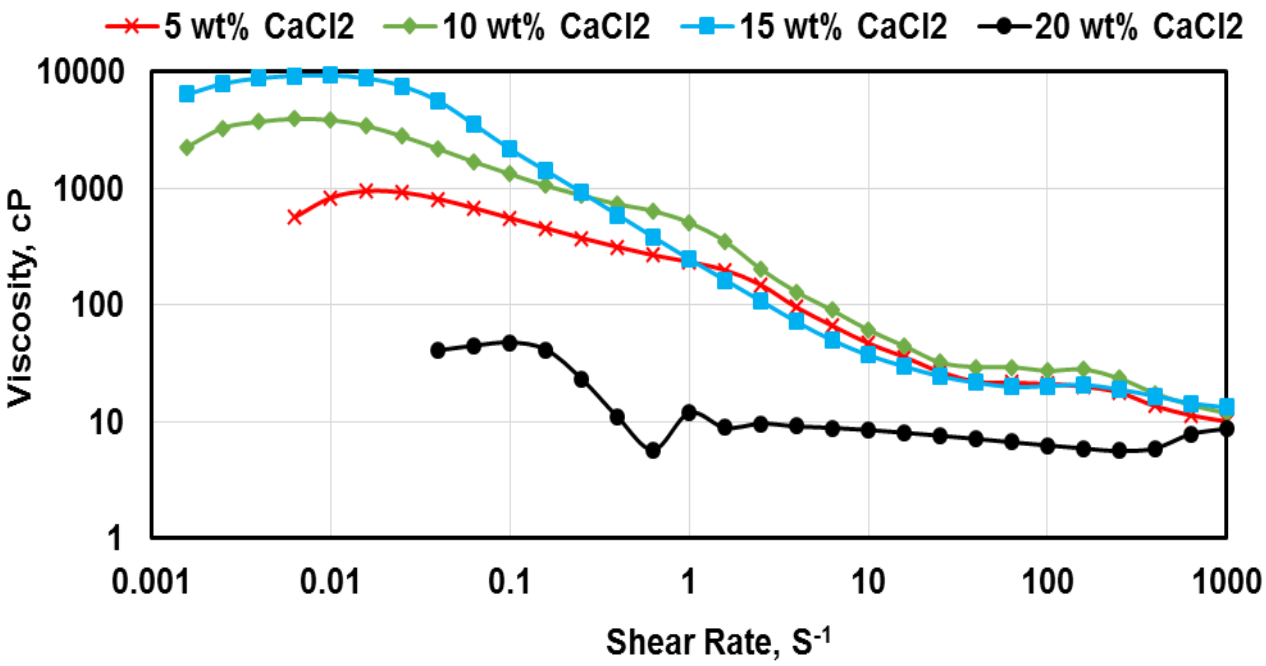

Figure 28: Effect of shear rate on apparent viscosity for different $CaCl_2$ concentrations at a constant VES concentration of 1 wt% and at 25° C

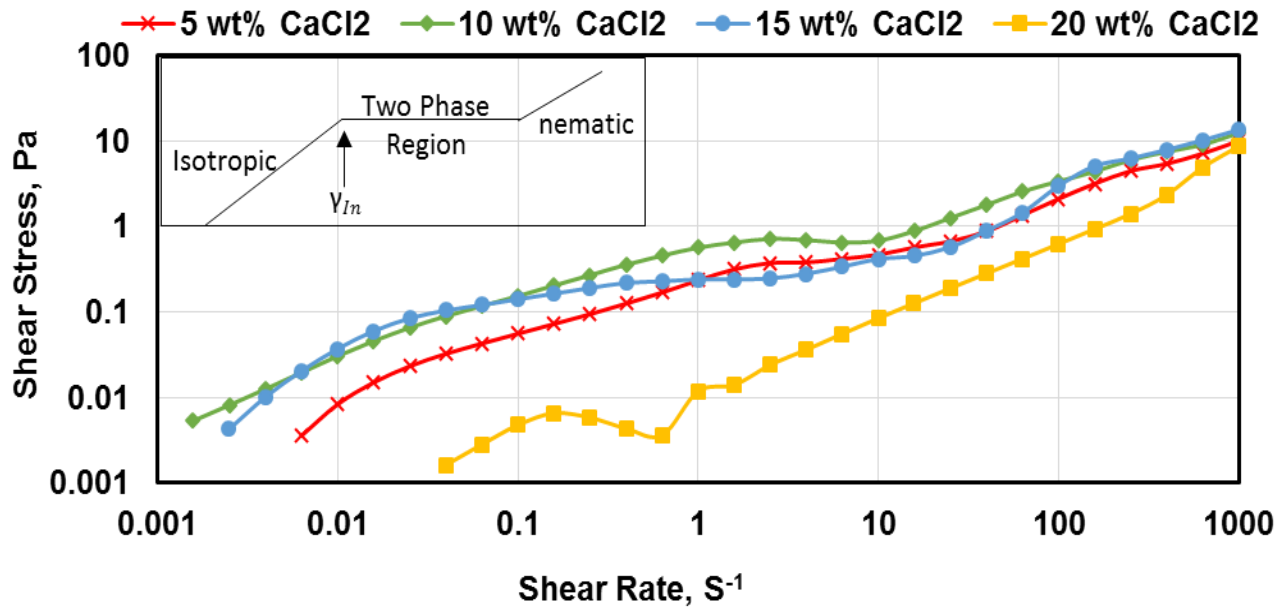

Figure 29: shear rate vs. shear stress for different $CaCl_2$ concentrations at a constant VES concentration of 1 wt. % and at 25° C

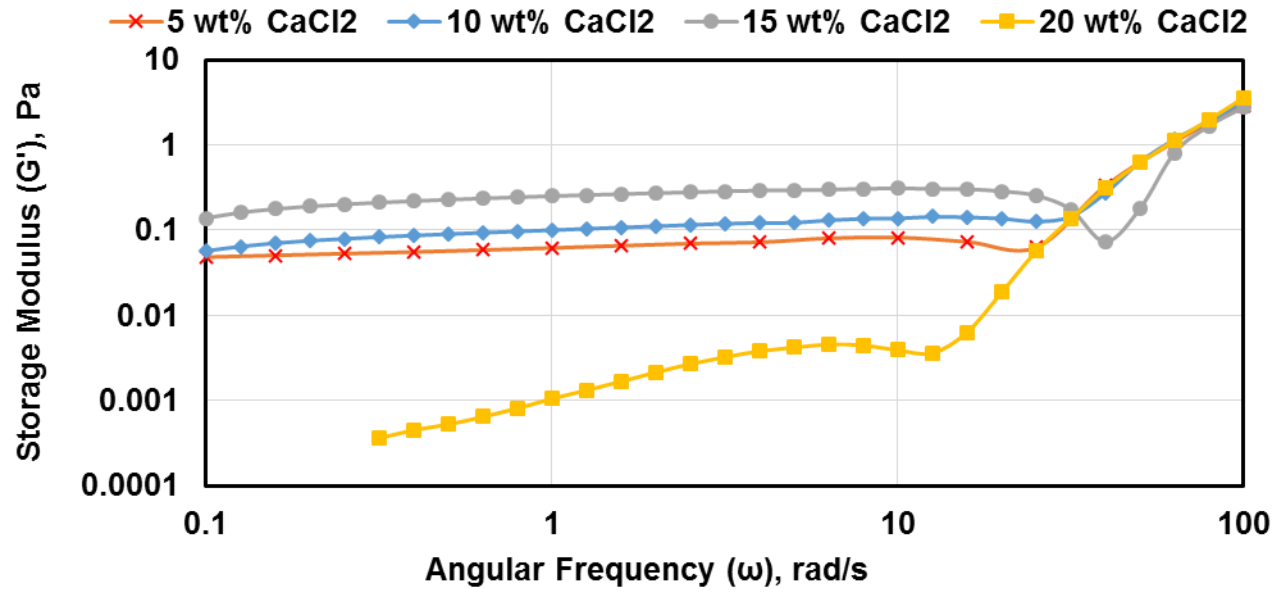

Figure 30: Storage Modulus for different $CaCl_2$ concentrations at a constant VES concentration of 1 wt. % and at 25° C

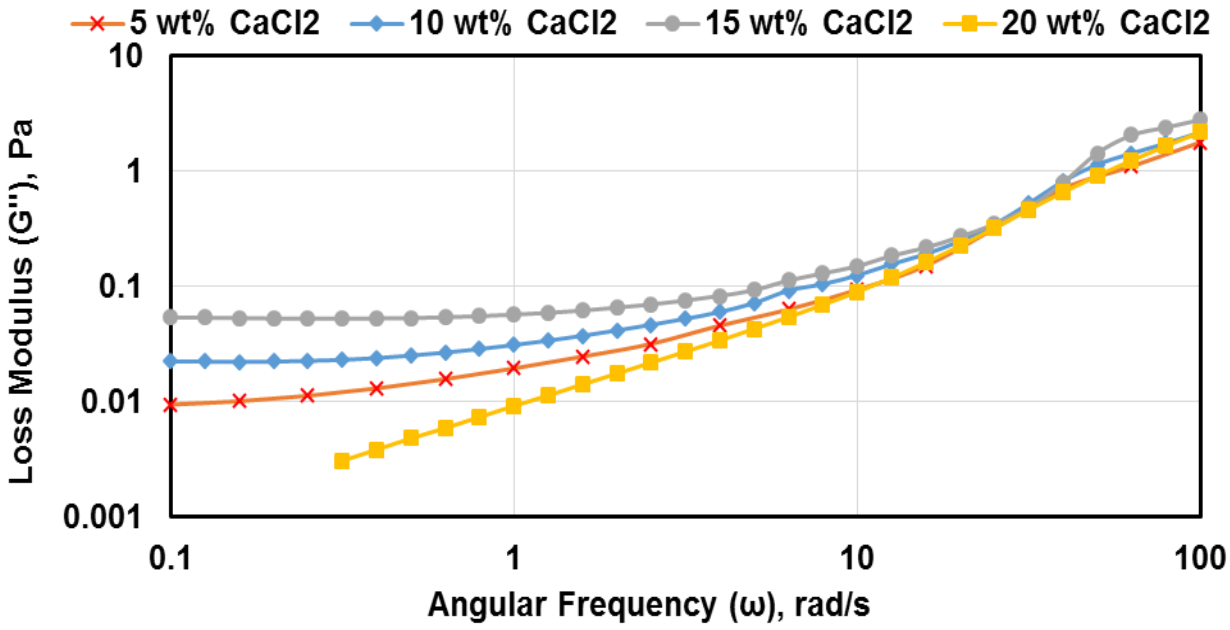

Figure 31: Loss Modulus for different $CaCl_2$ concentrations at a constant VES concentration of 1 wt. % and at 25° C

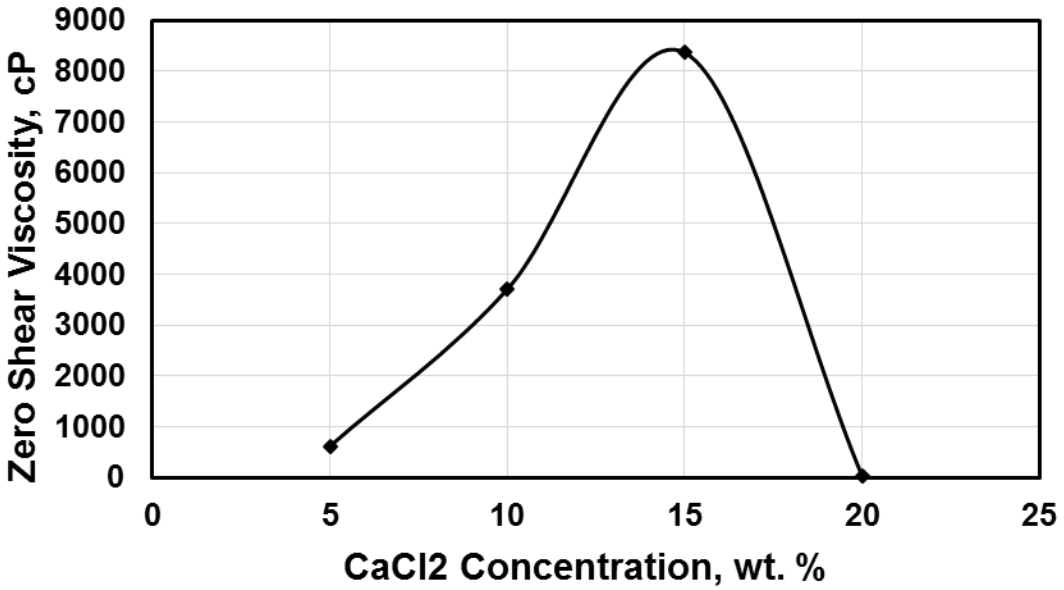

Figure 32: Zero Shear Viscosity for different $CaCl_2$ concentrations at a constant VES concentration of 1 wt. % and at 25° C

4.9 Conclusion

In this study, the effect of two type of salts on VES rheology were investigated: NaCl and $CaCl_2$. The salts were added at different concentration to study their effect on the viscosity, loss modulus and storage modulus. In addition, the samples investigated under different shear rate.

As a result, the viscosity with shear rate for both NaCl and $CaCl_2$ showing the same trend behavior. The viscosity decreased as the shear rate increased. The maximum viscosity was to found to be at zero shear rate.

The zero shear rate viscosity increased to a maximum of 1892.4 cP for the concentration of 15 wt. % NaCl and 8361.9 cP for the concentration of 15 wt. % $CaCl_2$. After this concentration the viscosity started to decreased with the concentration to reach a viscosity of 1661 and 30 cP for 15 wt. % NaCl and 15 wt. % $CaCl_2$, respectively.

CHAPTER 5

FORMATION DAMAGE IN SANDSTONE ROCKS

5.1 Introduction

The productivity of oil and gas wells depends on the effective permeability of reservoir rock to those fluids. The decrease in the permeability will reduce the rate of oil and gas production.

Generally, the sandstone formation contain swelling, non-swelling clays and interstitial water. Before any intervention caused to the oil fields, the clays considered at equilibrium state with the original water in the reservoir. As a result of intervention (production, drilling, any operation to produce the oil), external fluids will filtrated into the formation and cause incompatibility between the reservoir fluids and the introduced fluids. This incompatibility will disturb the clay equilibrium. Mostly there will be a salinity contrast between the original and the introduced fluids.

The water can cause damage to the sandstone formation due to clay swelling. The swelling may reduce or plug the pore throat opening which will reduce the flow and subsequently the production. The “water sensitive formation” is termed for the formation that could be damaged due to water interaction.

This chapter discusses the effect of injecting different fluid (DIW and HCl) on the permeability of Berea and Bandera sandstone. Moreover, to check the ability of NMR to detect the damage induced by deionized water and HCl.

5.2 Materials and Experimental work

5.2.1 Materials

The experiments conducted in this study on Bandera brown sandstone (porosity ∅ = 25.4%; brine permeability k = 14.9 md), Berea sandstone (porosity ∅ = 18.7%; brine permeability k = 100). The core plugs of dimensions 1.5'' in diameter and 3" in length.

Fluids used for these experiments were: 3 wt. % KCl and 5 wt. % KCl were used as a compatible fluid with the sandstone to measure the permeability. While, 15 wt. % HCl and fresh water were used as a damaging fluid since they affect the clay minerals in the sandstone. All the fluids solutions prepared in deionized water. The mineralogical composition of the different sandstone core are listed in Table 4.

Table 4 Mineralogy of Sandstone Cores (wt. %)

Mineral	Bandera Brown	Berea		Mineral	Bandera Brown	Berea
Quartz	68.6	87		Kaolinite	0.7	5.0
Dolomite	-	2.0		Illite	5.2	1.0
Calcite	-	2.0		Chlorite	7.4	2.0
Feldspar	-	3.0		Plagioclase	-	-

5.2.2 Experiment procedure for Formation damage Evaluation

The cores were saturated with (3 wt. % KCl for Berea and 5 wt. % KCl for Bandera Brown) at room temperature under pressure. Then the core was analyzed by NMR to measure the porosity and depict the baseline T_2 signal distribution. The initial permeability was measured using 3 wt. % KCl for Berea and 5 wt. % KCl for Bandera Brown (from the formation to the wellbore direction). After that, the core plug was flooded with damaging fluid (fresh water and HCl) at injection constant injection rate of 5 cm^3/min (from the wellbore to the formation direction).

The core was analyzed again by NMR to measure the alteration of the T_2 signal distribution and porosity. The cores were back flooded (from the formation to the wellbore direction) to measure the final permeability with the same fluids used for initial permeability measurement.

5.2.3 Core flooding Experiment

The Berea core plugs were flooded by 3 wt. % KCl and Bandera Brown flooded by 5 wt. % KCl at four different rates to measure the initial permeability. The pressure drop readings were recorded when the flow stabilized as shown in (Figures 33, 34 and 35). A back pressure regulator adjusted gradually up to 1000 psi and a confining pressure of 1700 psi was set.

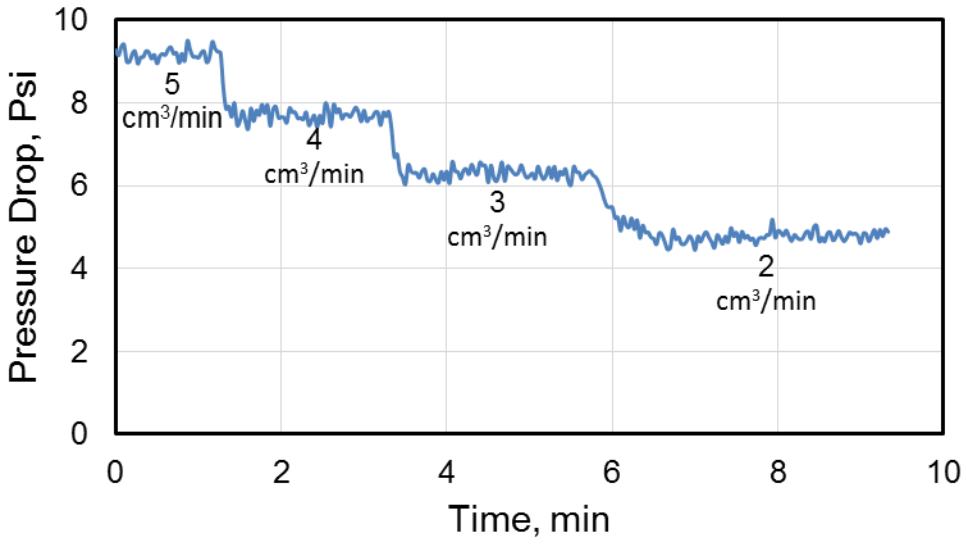

Figure 33: Pressure Drop vs. Time for initial permeability measurement of Berea Sandstone Core Sample flooded by 3 wt% KCl (Confining Pressure of 1700 psi, Backpressure of 1000 psi and at Room temperature), Sample BE3.

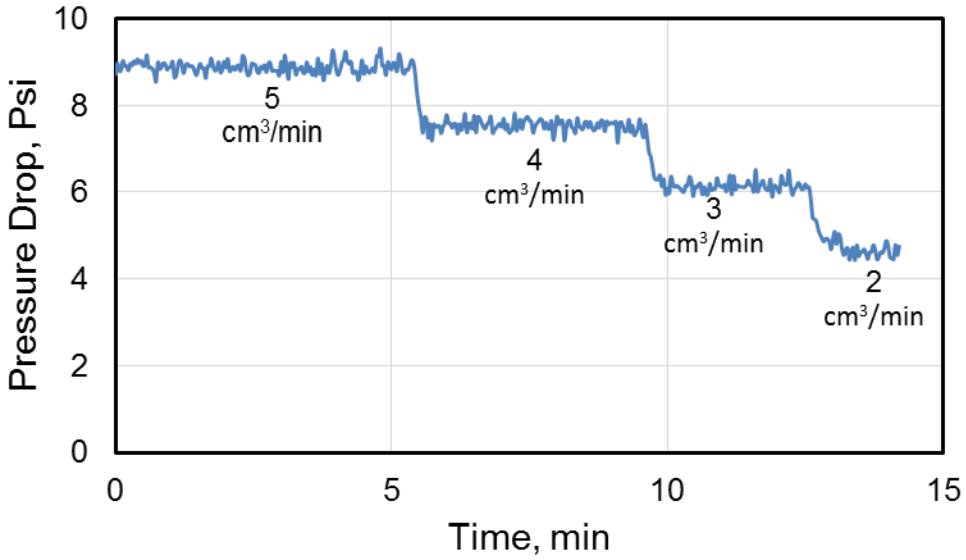

Figure 34: Pressure Drop vs. Time for initial permeability measurement of Berea Sandstone Core Sample flooded by 3 wt% KCl (Confining Pressure of 1700 psi, Backpressure of 1000 psi and at Room temperature), Sample BE4.

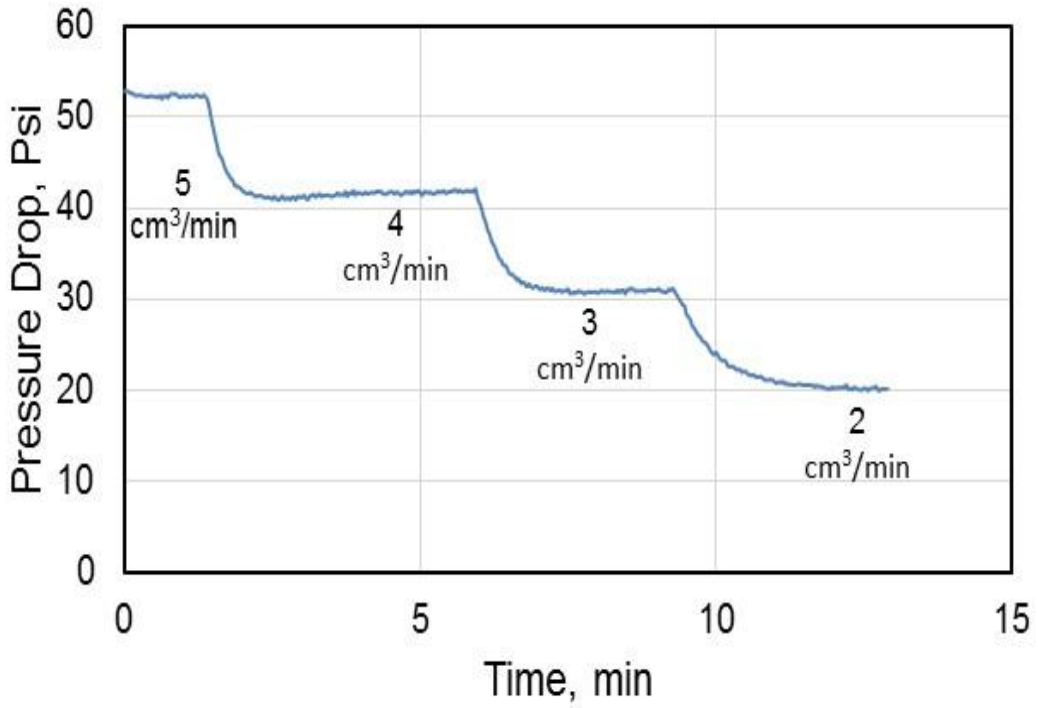

Figure 35: Pressure Drop vs. Time for initial permeability measurement of Bandera Brown Sandstone Core Sample flooded by 5 wt% KCl (Confining Pressure of 1700 psi, Backpressure of 1000 psi and at Room temperature), Sample BB4.

Figures 36, 37 and 38. Show the initial permeability measured by 3 wt. % KCl for samples BE3 and BE4 were 97.2 mD and 101.6 mD. Whereas, For BB4 the initial permeability measured by 5 wt. % KCl was 16.5 mD (from the formation to the wellbore direction), consequently sample BE3 flooded by fresh water, BE4 and BB4 flooded by 15 wt. % HCl (from the wellbore to the formation direction) to induce formation damage. The fresh water and 15 wt. % HCl were flooded at a rate of 5 cm^3/min. The pressure drop across the cores were recorded as 450, 15 and 100 psi for BE3, BE4 and BB4, respectively.

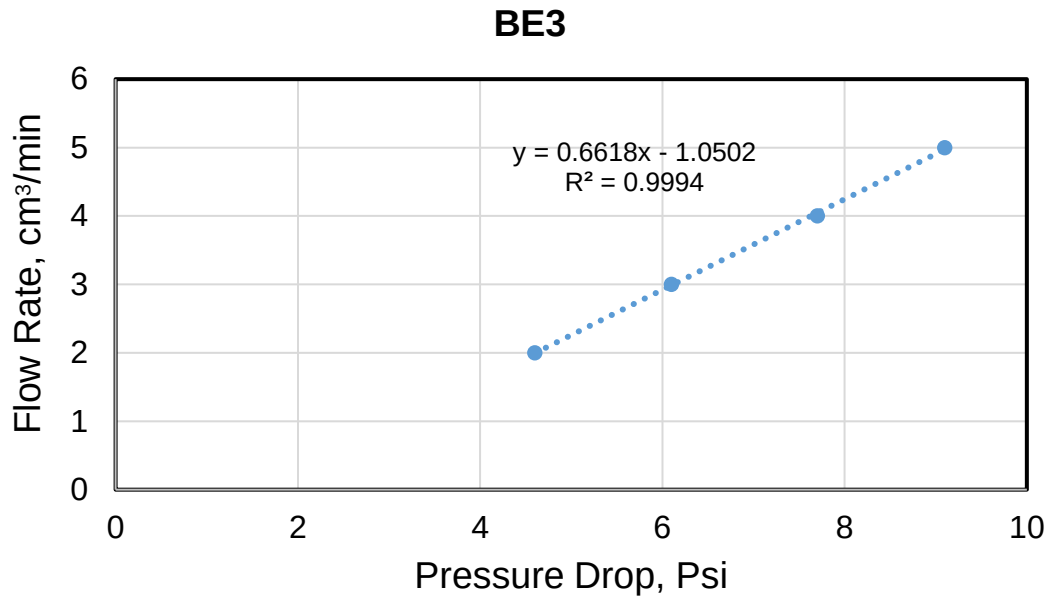

Figure 36: Initial permeability Measurement for Berea Sandstone using 3 wt % KCl at backpressure 1000 psi and Confining Pressure of 1700 psi

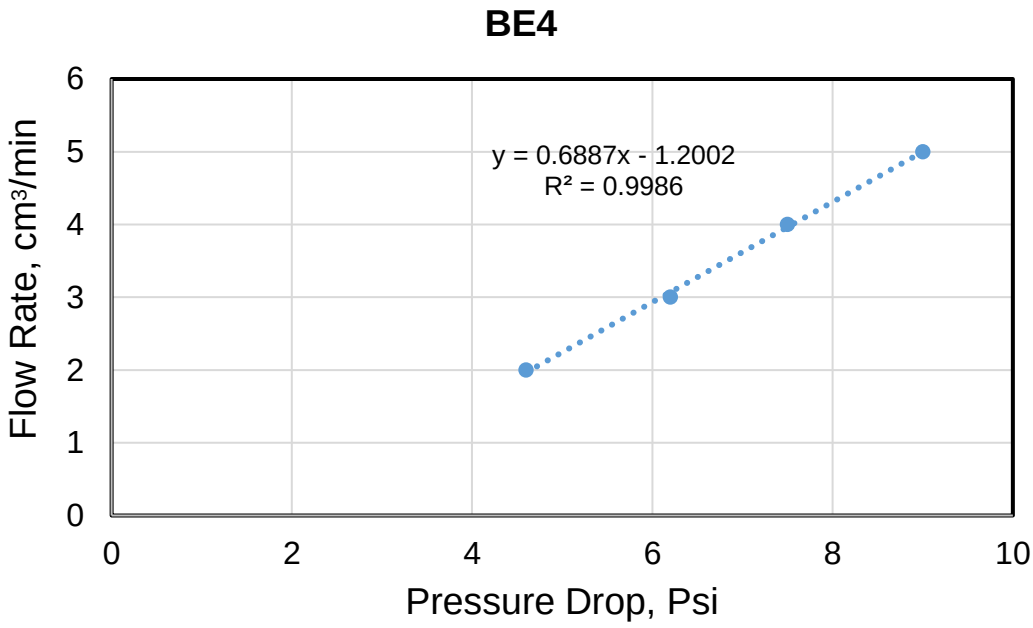

Figure 37: Initial permeability Measurement for Berea Sandstone using 3 wt % KCl at backpressure 1000 psi and Confining Pressure of 1700 psi

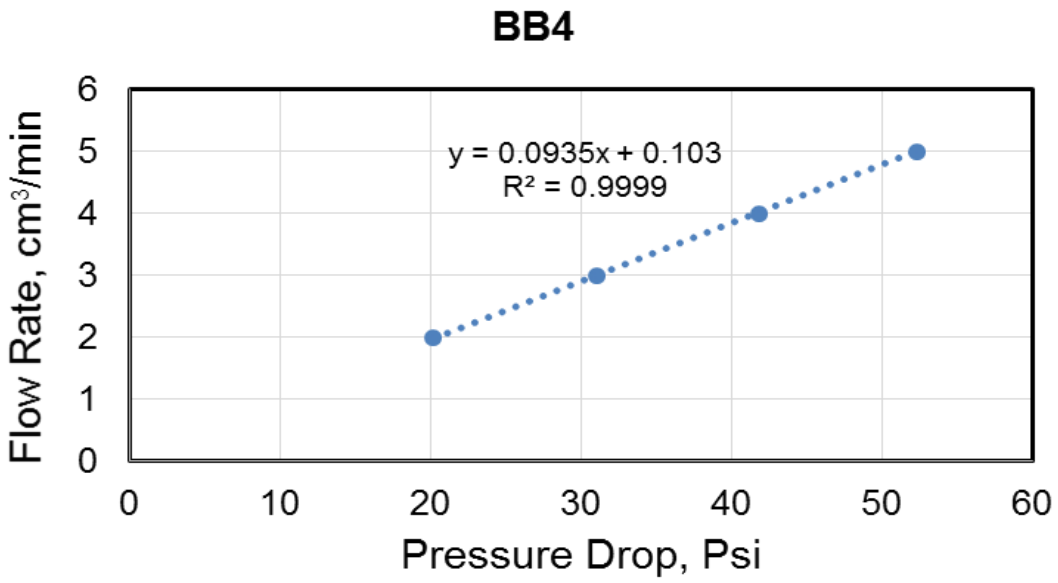

Figure 38: Initial permeability Measurement for Bandera Brown Sandstone using 3 wt % KCl at backpressure 1000 psi and Confining Pressure of 1700 psi

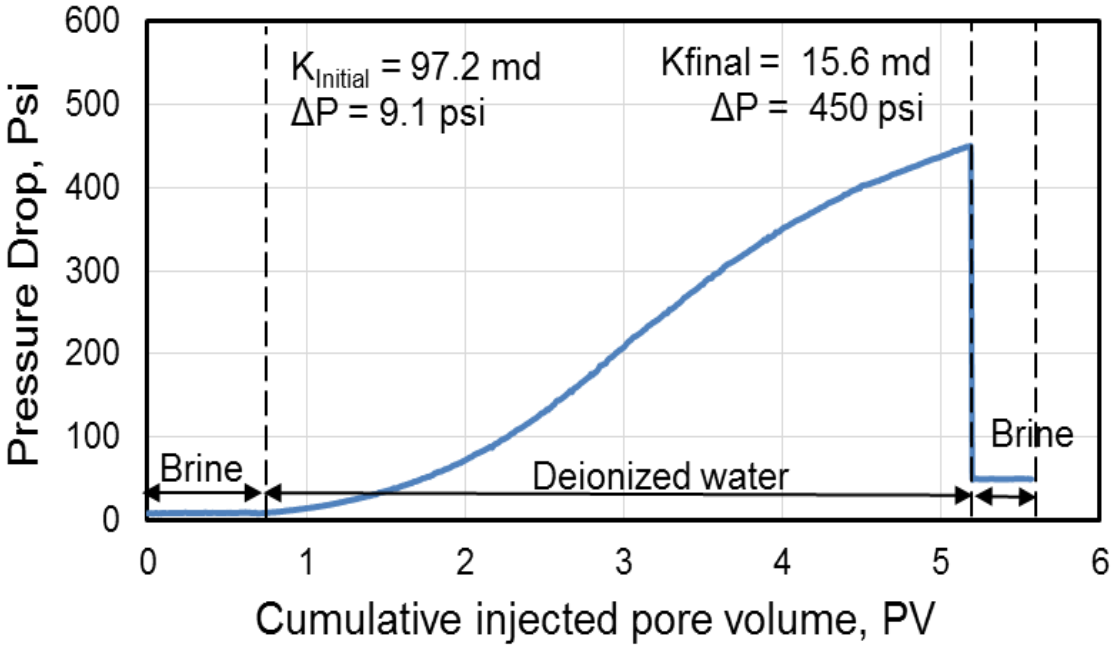

Figure 39: Pressure drop across the sample as the deionized water injected into the Berea sandstone core at 5 cm^3/min, backpressure of 1000 psi and confining pressure of 1700 psi

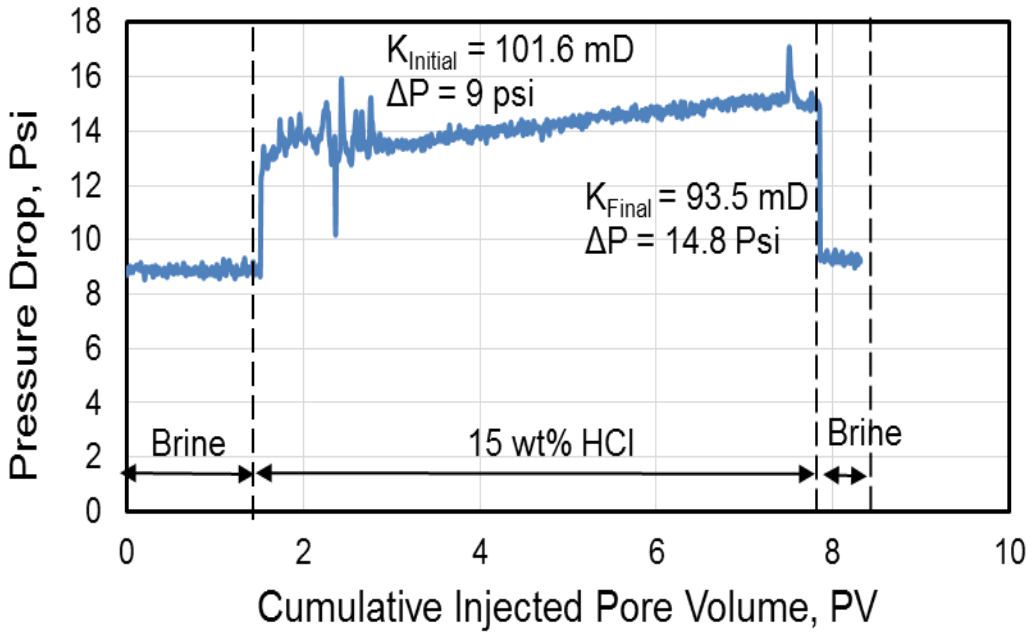

Figure 40: Pressure drop across the sample as 15 wt. % HCl injected into the Berea sandstone core at 5 cm^3/min, backpressure of 1000 psi and confining pressure of 1700 psi

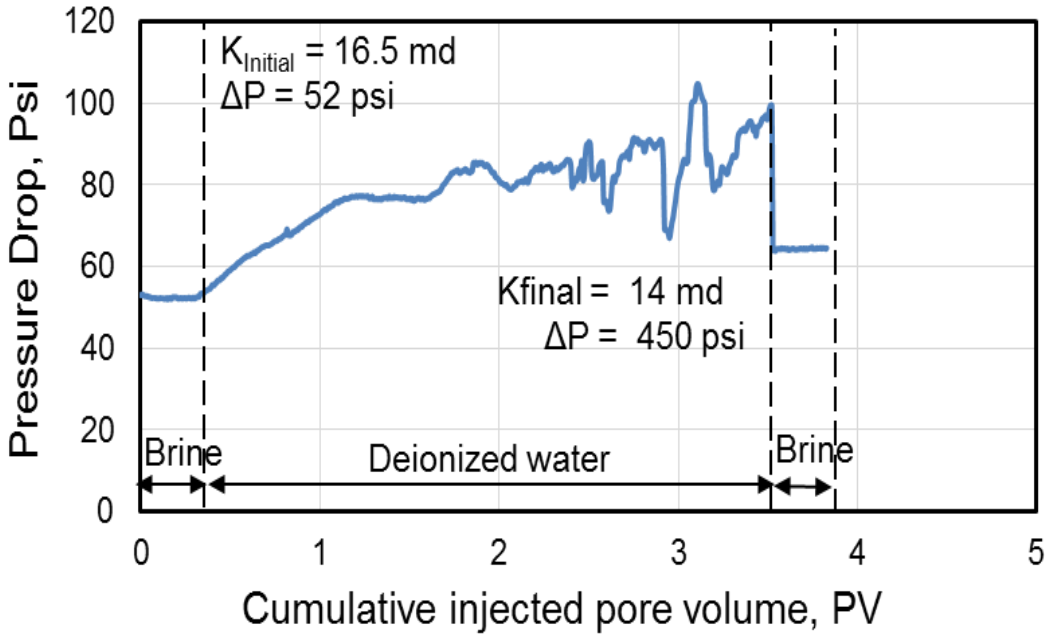

Figure 41: Pressure drop across the sample as the deionized water injected into the Bandera Brown sandstone core at 5 cm^3/min, backpressure of 1000 psi and confining pressure of 1700 psi

Figures 39, 40 and 41 show the pressure drop across the core as the deionized water was injected into the core. The pressure drop increased to 450 psi, 15 psi and 100 psi as a maximum for sample BE3, BE4 and BB4, respectively. The pressure drop increased in BE3 due to injection of fresh water attributed to the solid migration that resulted from the salinity contrast between the 3 wt. % KCl solution and fresh water. The Kaolinite is most expected mineral to be responsible from the migration since it attached to the pores, the damage mechanism can be attributed to swelling-induced migration. While, in Figure 42 there is no significant increase in the pressure drop which reflect there is no fine migration occurred. HCl is react mainly with chlorite and illite which caused formation of reaction product that may migrate and lead to increase of viscosity. The damage caused by 15 wt. % HCl in sample BB4 can be attributed to chlorite which contribute by 7.4 % of the total clay and secondary to illite that can migrate and plug the pores throat.

Figure 43, 44 and 45 show the changing rate with time for final permeability measurement. Since the rate stabilized the pressure difference recorded and the next rate applied.

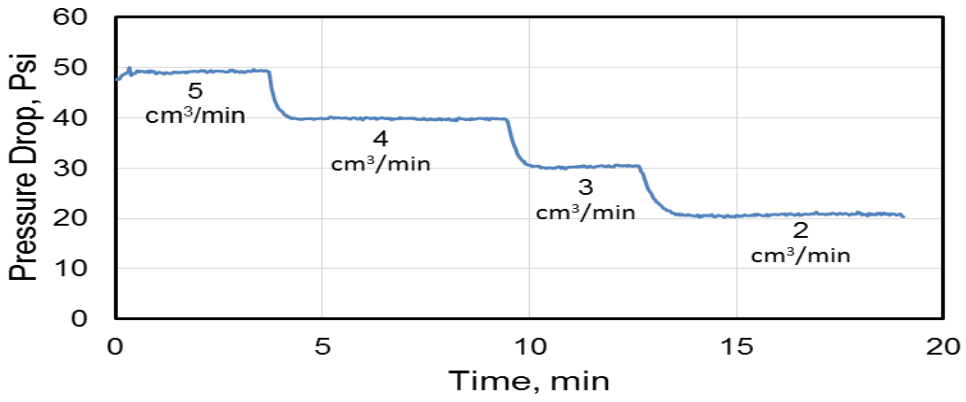

Figure 42: Pressure Drop vs. Time for final permeability measurement of Berea Sandstone Core Sample flooded by 3 wt% KCl (Confining Pressure of 1700 psi, Backpressure of 1000 psi and at Room temperature), Sample BE3.

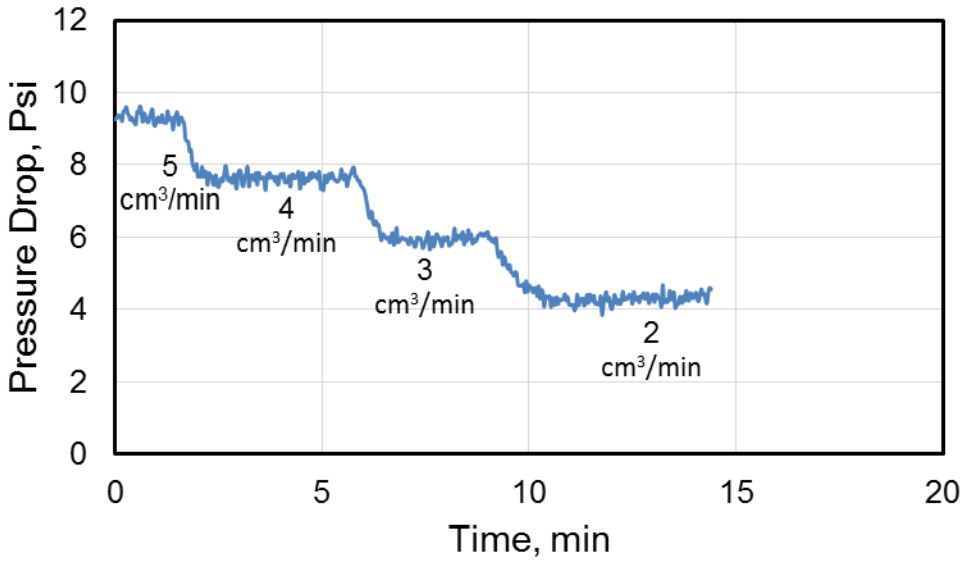

Figure 43: Pressure Drop vs. Time for final permeability measurement of Berea Sandstone Core Sample flooded by 3 wt% KCl (Confining Pressure of 1700 psi, Backpressure of 1000 psi and at Room temperature), Sample BE3.

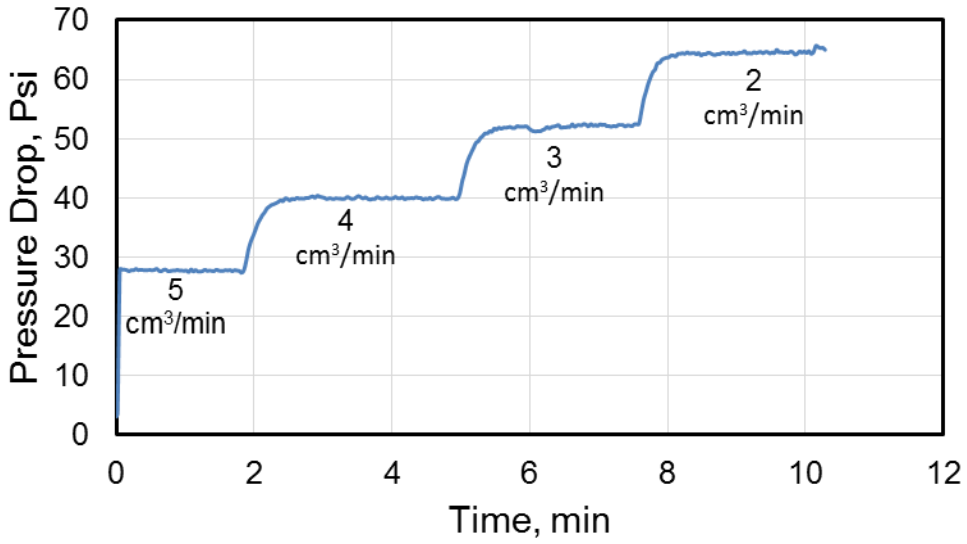

Figure 44: Pressure Drop vs. Time for final permeability measurement of Bandera Brown Sandstone Core Sample flooded by 5 wt% KCl (Confining Pressure of 1700 psi, Backpressure of 1000 psi and at Room temperature), Sample BE3.

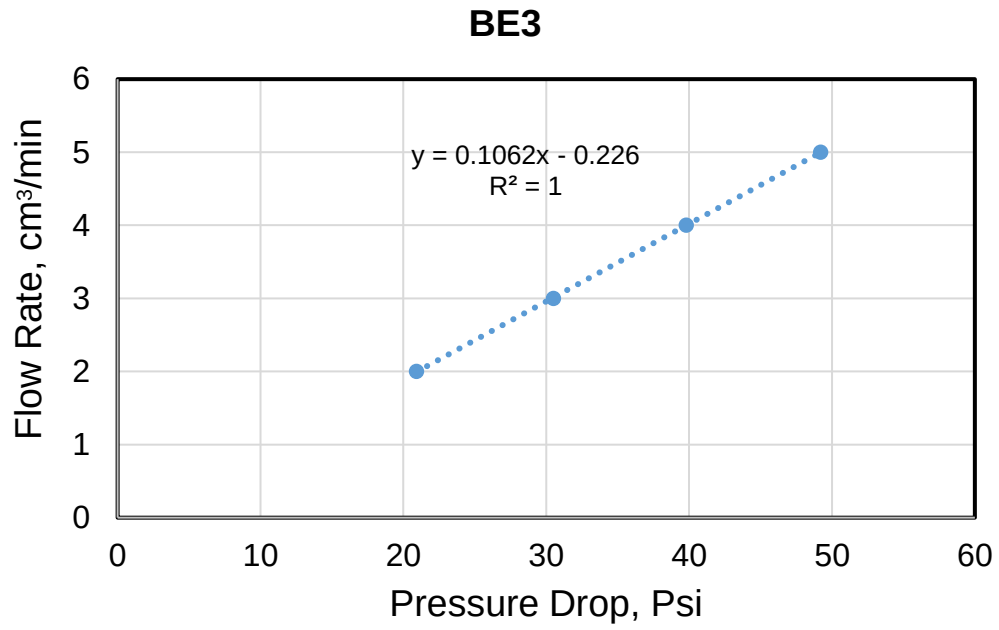

Figure 45: Final permeability Measurement for Berea Sandstone using 3 wt % KCl at backpressure 1000 psi and Confining Pressure of 1700 psi

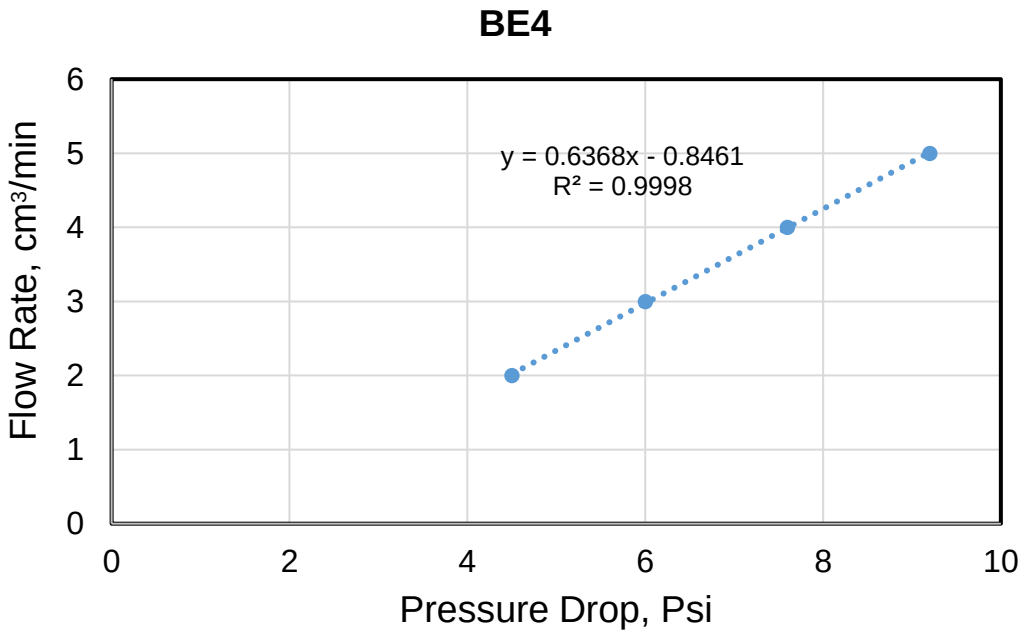

Figure 46: Final permeability Measurement for Berea Sandstone using 3 wt % KCl at backpressure 1000 psi and Confining Pressure of 1700 psi

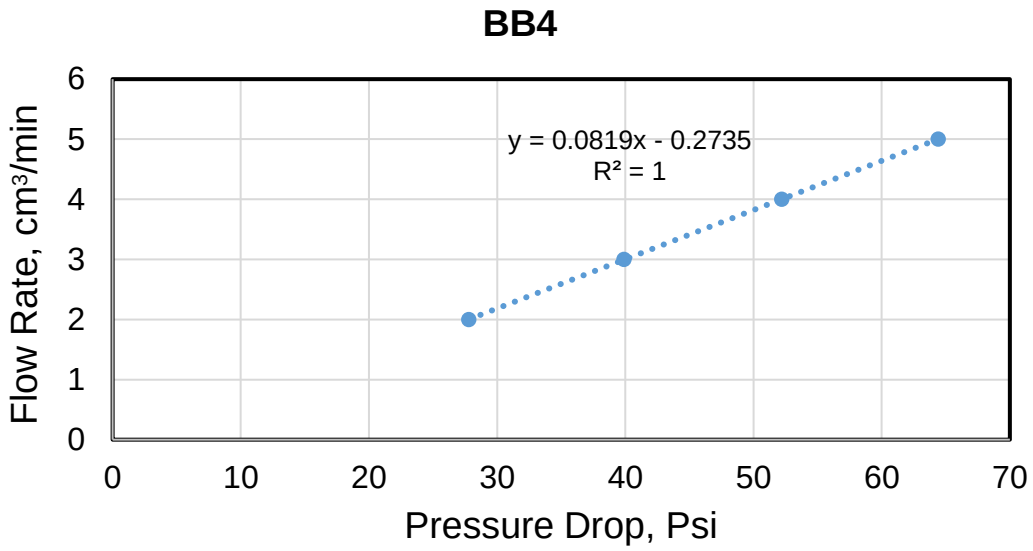

Figure 47: Final permeability Measurement for Bandera Brown Sandstone using 3 wt % KCl at backpressure 1000 psi and Confining Pressure of 1700 psi

The final stage was to measure the final permeability (Figure 45, 46 and 47) to evaluate the damage and how much the permeability reduced. Core samples BE3 and BE4 flooded with 3 wt. % KCl (from the formation to the wellbore direction) at a four different rates, the final permeability was measured to be 15.6 mD and 93.5 mD for BE3 and BE4, respectively.

5.2.4 NMR experiments

The NMR experiment conducted at three stages: after saturating the sample with 3 wt. % KCl or 5 wt. % KCl; after flooding the sample with fresh water or HCl; after flooding the sample with 3 wt. % KCl or 5 wt. % KCl at the final stage.

Figure 48, 49 and 50 show the pore distribution of the core sample BE3 after saturated with 3 wt. % KCl and for samples BE4 and BB4 after flooded by 5 wt. % KCl. The measured porosity was 18.5, 18.7 and 24% for samples BE3, BE4 and BB4, respectively.

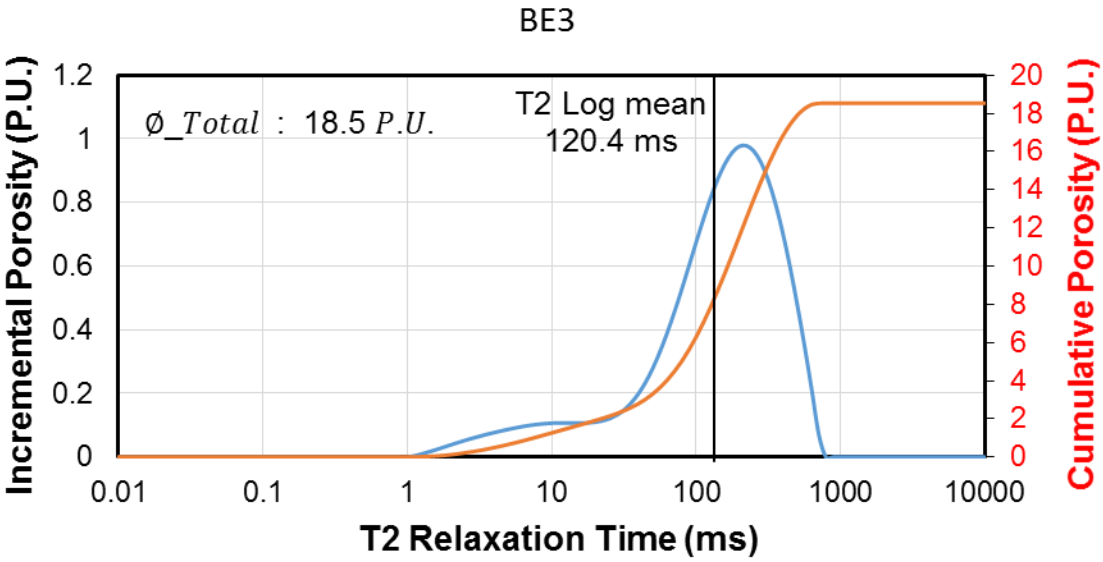

Figure 48: NMR T_2 response curve for Berea sandstone core after saturation with 3 wt. % KCl at 25˚C

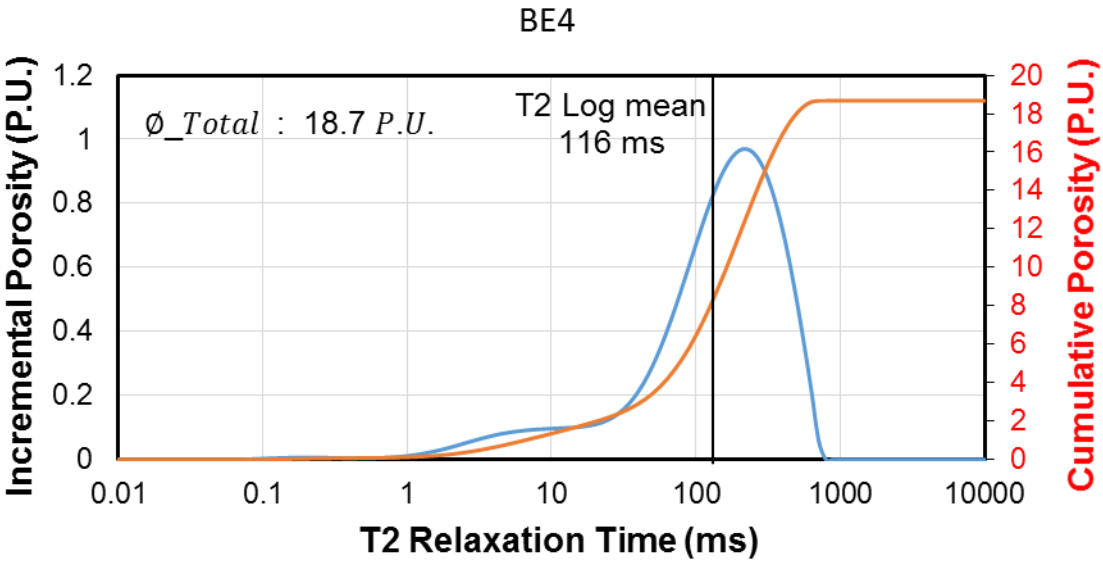

Figure 49: NMR T_2 response curve for Berea sandstone core after saturation with 3 wt. % KCl at 25˚C

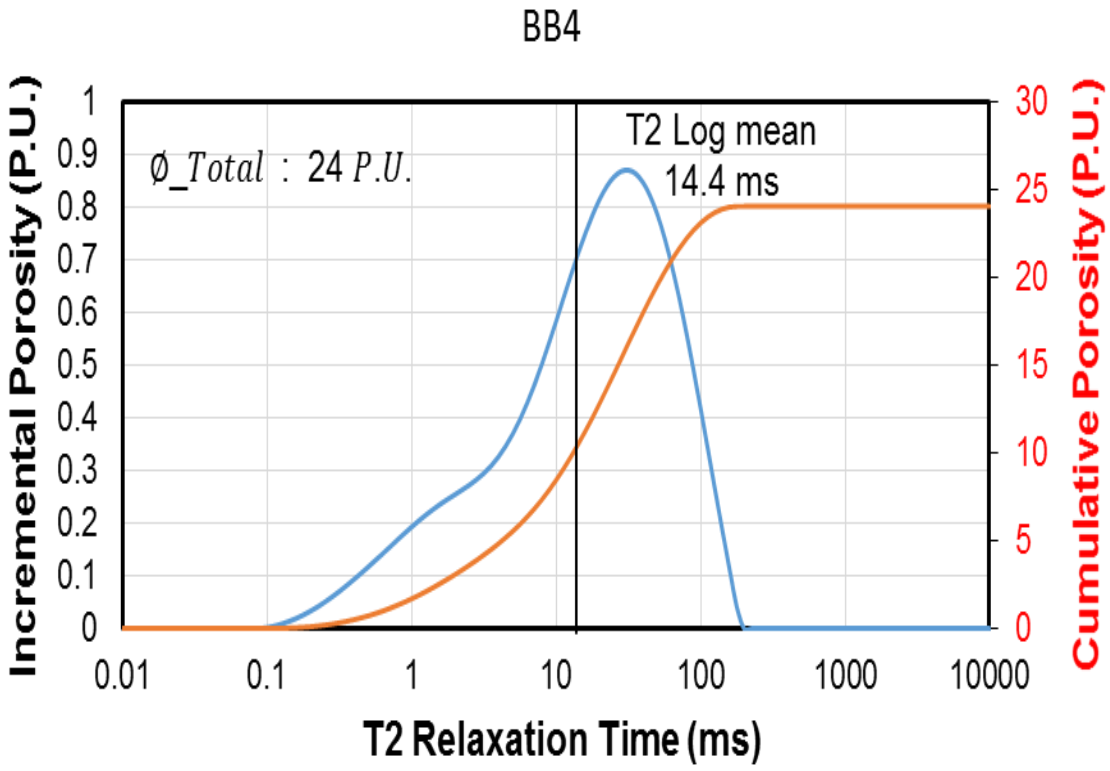

Figure 50: NMR T2 response curve for Bandera Brown sandstone core after saturation with 5 wt. % KCl at 25°C

All cores show bi-modal distribution consist of macro and micro pores. The macro pores (T_2 > 33 ms) represent the major contribution to the total porosity.

Figure 51 shows the T_2-distribution after flooding the sample BE3 with deionized water. There is slight increase in porosity to be 18.6 %.

Figure 52 and 53 show the T2-distribution for sample BE4 and BB4 after flooding by 15 wt. % HCl. The measured porosity were 12.6 and 25.4 % for sample BE4 and BB4, respectively.

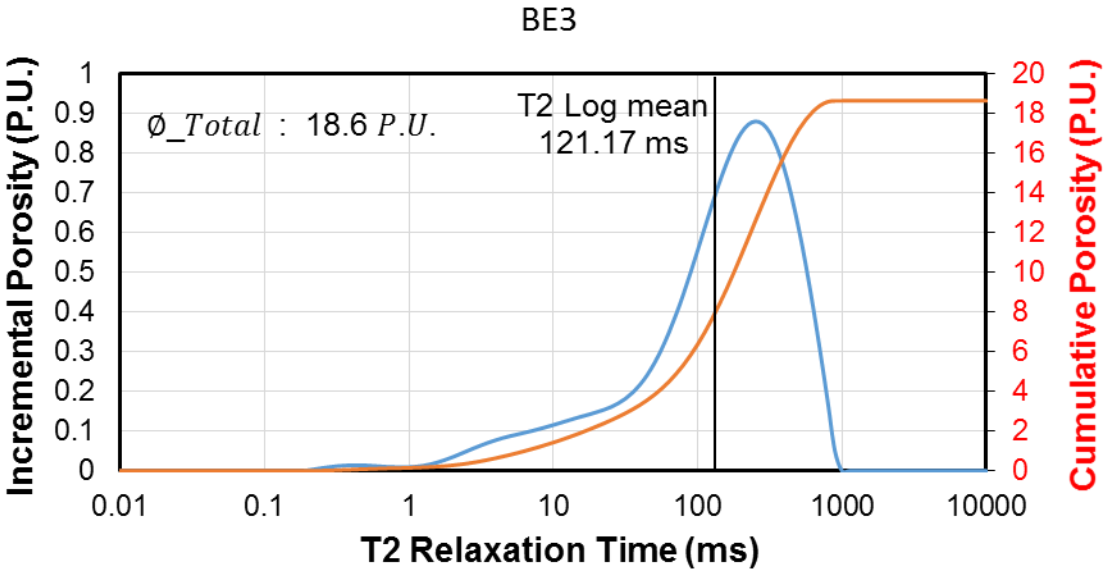

Figure 51: NMR T2 response curve for Berea sandstone core after flooded with deionized water (after damage) at 25°C

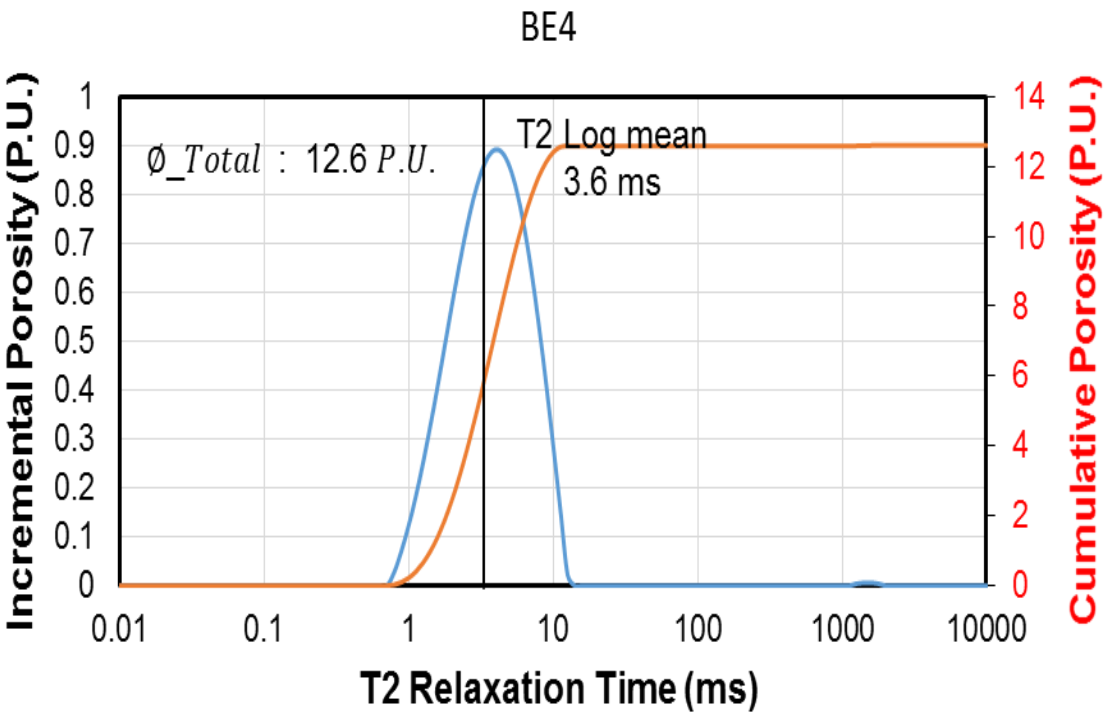

Figure 52: NMR T2 response curve for Berea sandstone core after flooded with 15 wt. % HCl (after damage) at 25°C

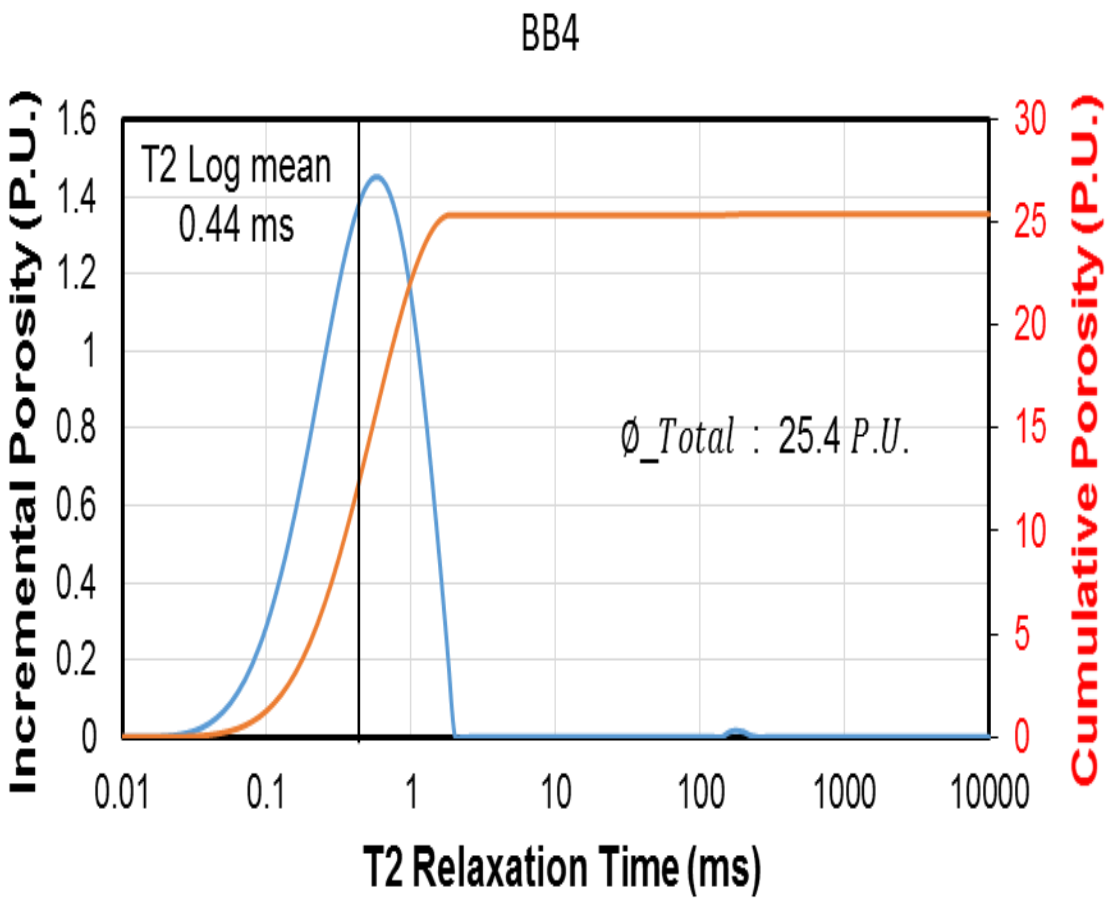

Figure 53: NMR T2 response curve for Bandera Brown sandstone core after flooded with 15 wt. % HCl (after damage) at 25˚C

After introduced the damaging fluid (fresh water, HCl) to the cores, the following observations were found:

- Berea core (BE3) damaged by fresh water: The spectra of the long peak (macro pores) shifted toward small relaxation time which indicate pore shrinkage (Figure 54). There is no noticeable change occurred on the spectra of the small peak (micro pores). We attribute that to the effect of the kaolinite which detected by the SEM-images. Some of the kaolinite partially block the macro pores. Hence, the shift of the long peak

spectra reflect the reduction of macro pores size. The slight addition in the amplitude of the long peak attributed to the detached and migrated kaolinite. This migration of kaolinite lead to the slight increase in porosity.

- Berea core (BE4) damaged by HCl: The bi-modal distribution become uni-modal distribution after flooded the sample by HCl (Figure 55). From the figure, the long peak (before damage) disappeared (after damage). This infer that the system become dominantly consist of micro pores ($1 < T_2 < 20$) ms. the amplitude of the small peak correspond to the micro pores increase significantly after damage. These change can be attributed to the migrated kaolinite that deposit at the surface of the micro pores and decreased their size to smaller pores.

- Bandera Brown (BB4) damaged by HCl: Figure 56 shows that the bi-modal system (before damage) which was dominantly consist of micro pores become a uni-modal system consist of micro pores ($0.01 < T2 < 20$) ms. this change in the porosity system combined with an increase in porosity. We attribute that to the reaction of the HCl with the clays attached to the rock surface. After reaction, a new porosity created and some clays migrated and deposit at the surface of the macro pores that lead to decrease the size of the macro pores (Talabi et al., 2009; Al-Yaseri et al., 2015). The additional porosity can be attributed to the dissolution of some clays by HCl.

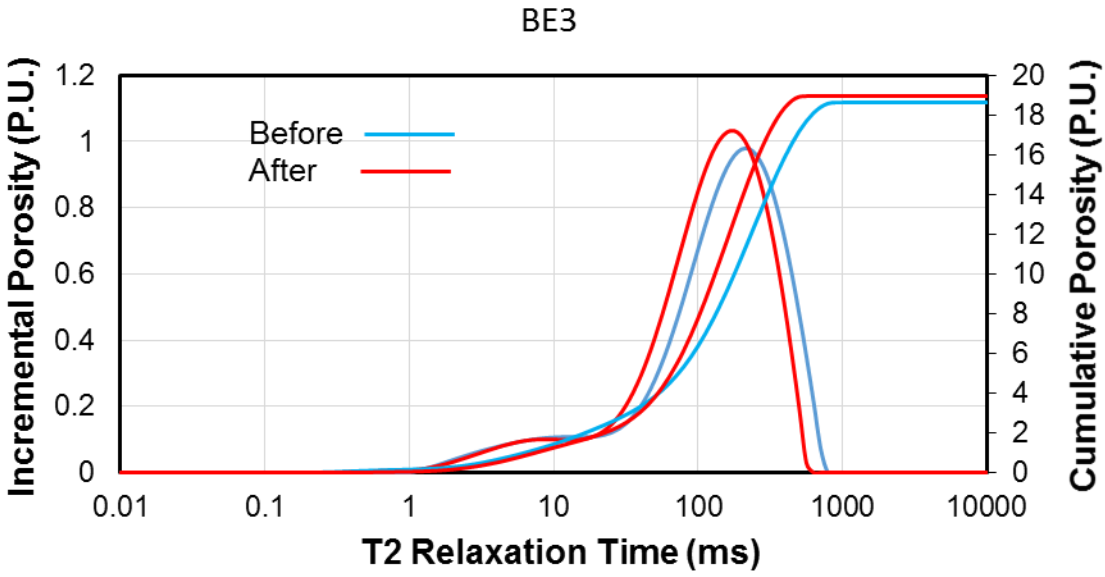

Figure 54: NMR T2 response curve for Berea sandstone core before and after damage at 25˚C

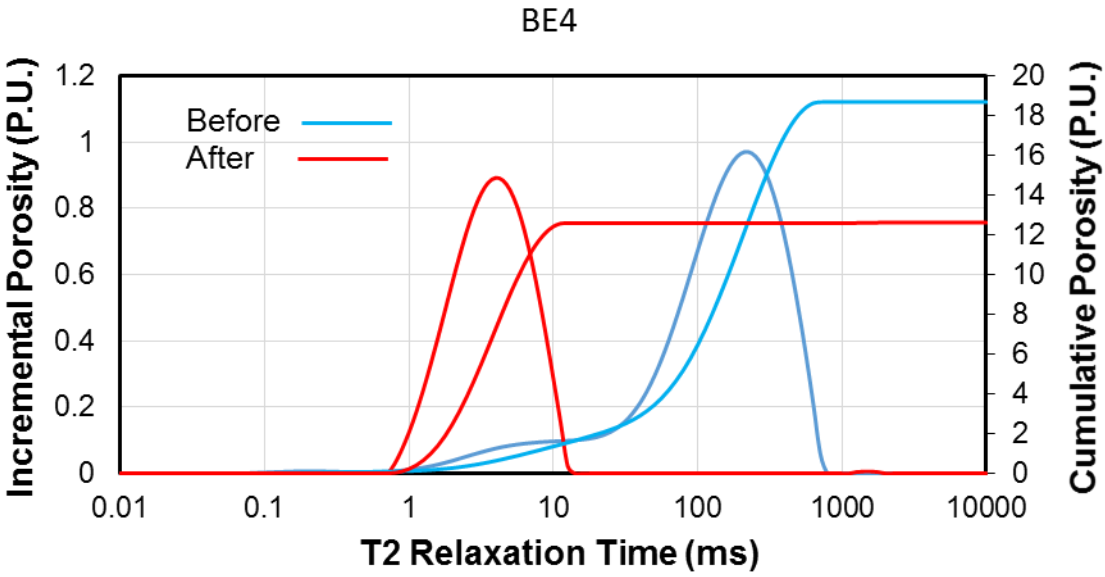

Figure 55: NMR T2 response curve for Berea sandstone core before and after damage at 25˚C

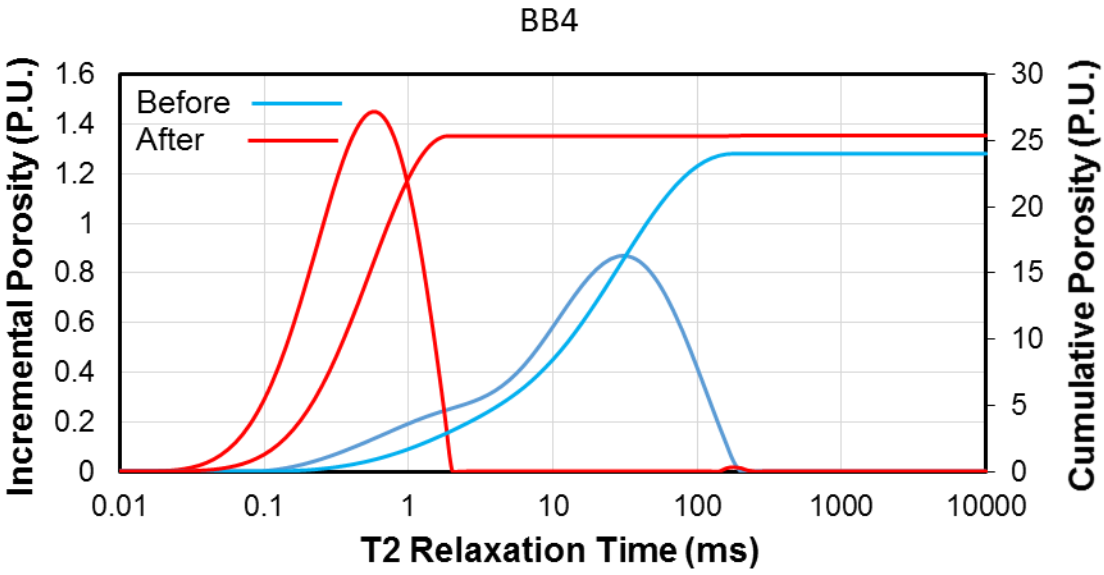

Figure 56: NMR T2 response curve for Bandera Brown sandstone core before and after damage at 25°C

The effect of the HCl affect mainly the macro pores in the case of the Berea sandstone. The clay migrated and mainly deposit at the surface of the macro pores with less deposit at the pore throat. In the other side, HCl affected Bandera brown porosity system. This change occurred mainly on the macro pores with a creation of new pores as a result of the reaction of HCl with clays.

5.2.5 SEM analysis

The SEM images showed the morphology of the carbonate and sandstone core samples before and after the damage. Also, the images showed the clay minerals present in the sandstone rock.

Figure 57, 58 showed the morphology of Berea sample (BE3) before damage. The figures showed the structure of the rock and the clays presence in the rock. The images shows a high amount of kaolinite with small amount of chlorite and Illite.

After the core was injected by fresh water, the clays detached from the rock surface, migrate and block the pore throat mainly. Some of the clays partially block the macro pores and lead to change the porosity system. This observation can be seen clearly on the cores that were damaged by HCl (Figures 60 and 61).

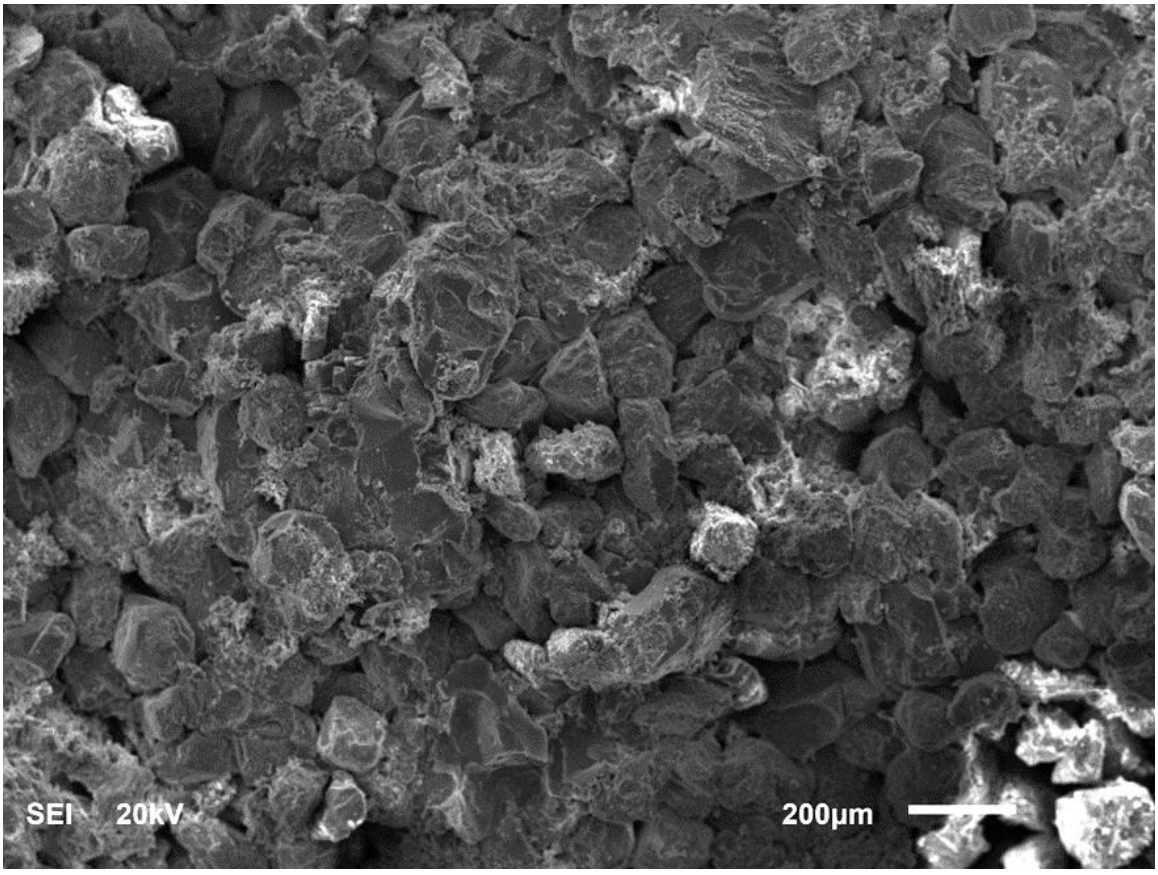

Figure 57: Morphology of Berea sandstone before damage

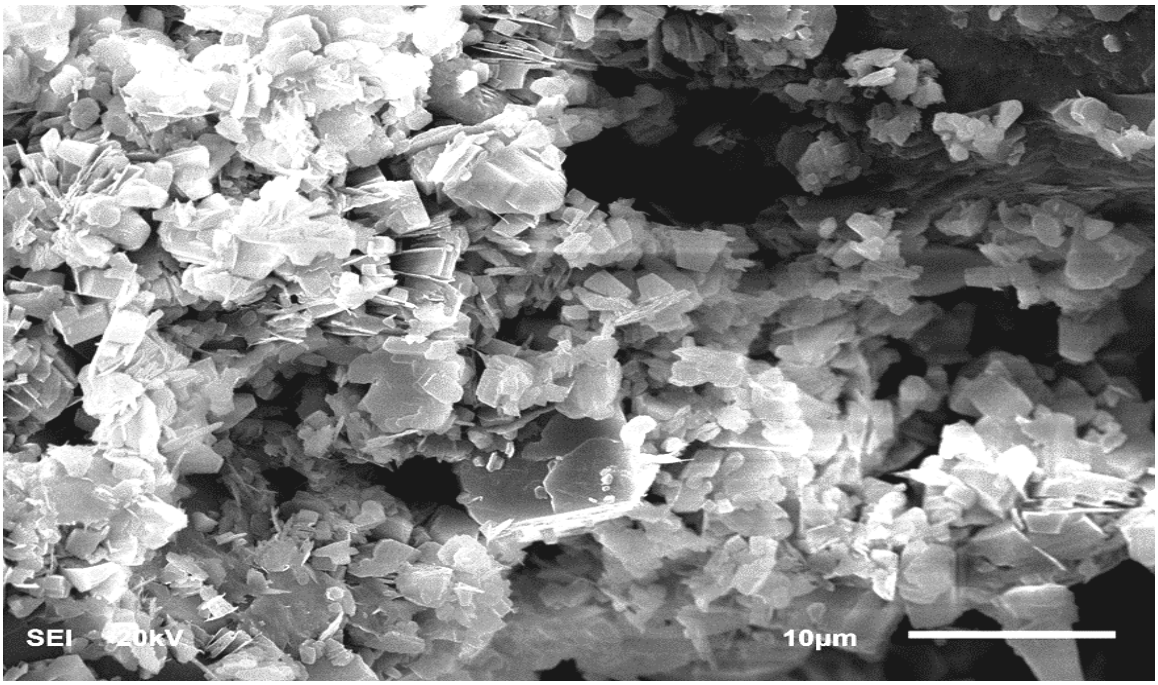

Figure 58: Clay minerals in Berea sandstone before damage

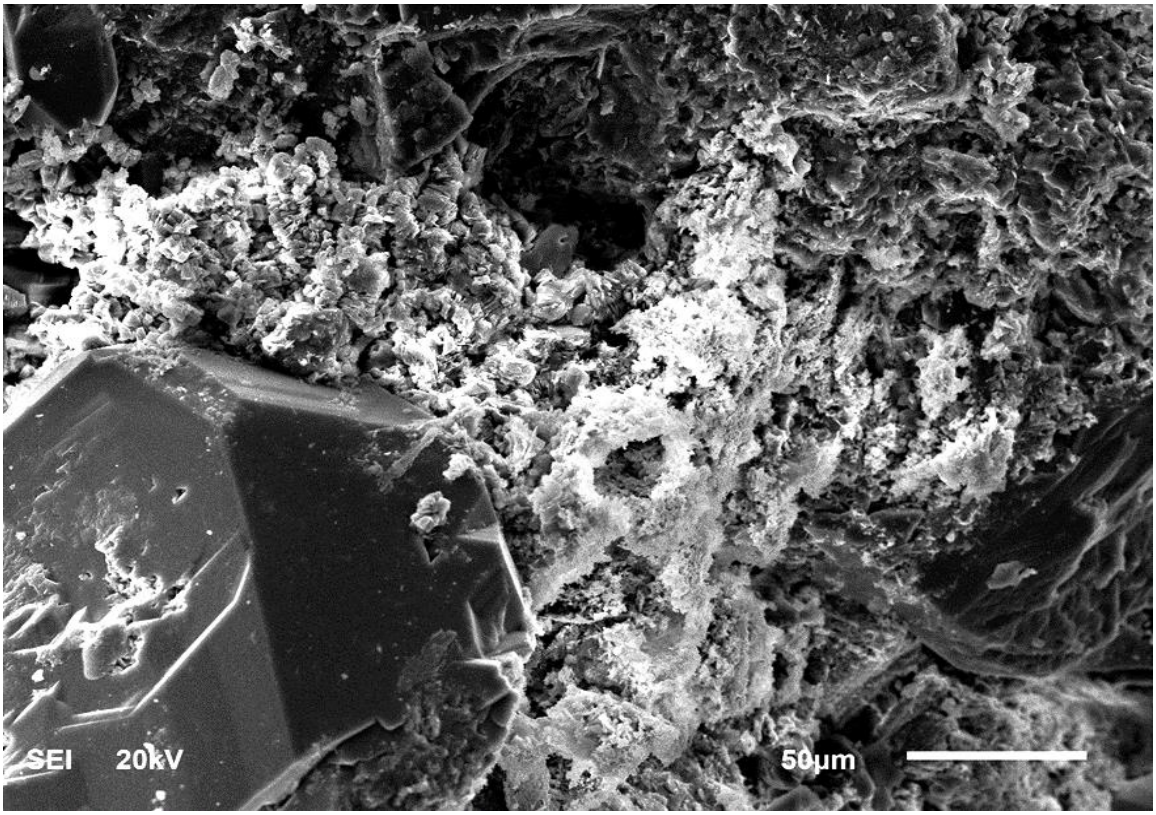

Figure 59: Effect of fresh water on clay mineral (Berea)

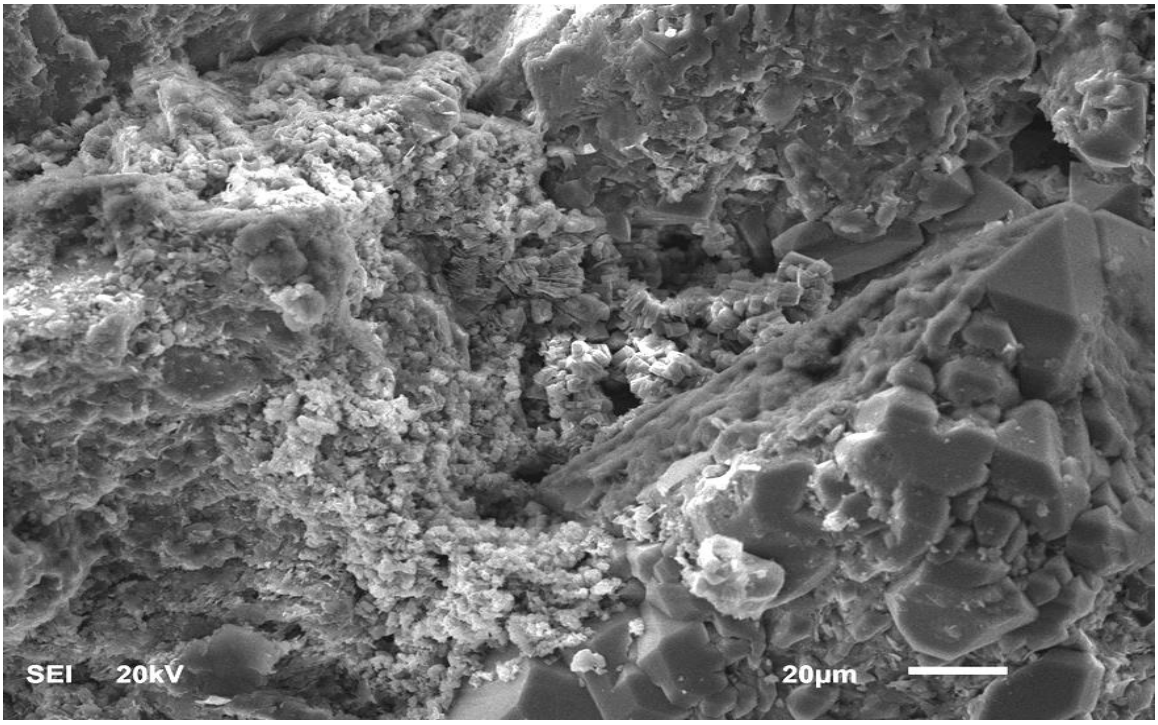

Figure 60: Effect of HCl on the clay mineral (Berea)

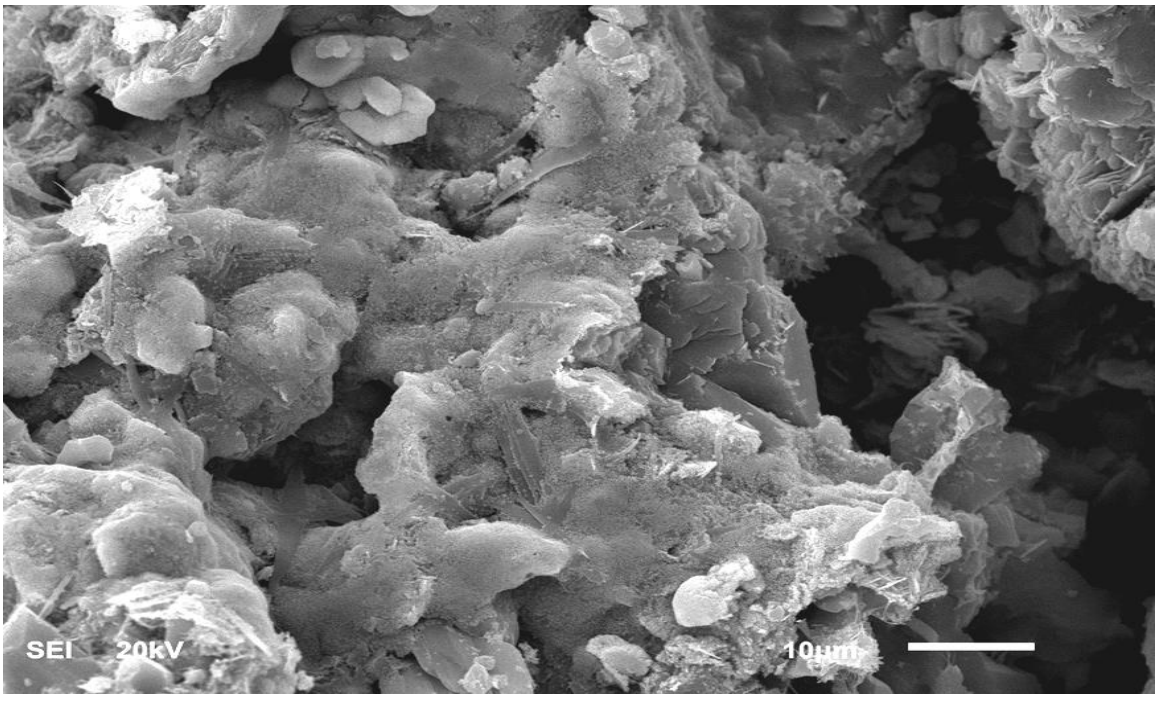

Figure 61: Effect of HCl on clays (Bandera Brown)

5.3 Conclusion

The T_2-NMR experiment were conducted on two types of samples: Bandera Brown and Berea sandstone. The samples were analyzed at two stages:

- Before damage: the samples were saturated with 3 wt. % KCl and 5 wt. % KCl for Berea and Bandera sandstone respectively.
- After damage: the samples were saturated with 15 wt. % HCl and fresh water.

The NMR results showed a clear change in the pore system after the injection of fresh water and HCl. The affection of the pore system depend mainly on the clay minerals presence in the sample and the way it will react with the injected fluid. The permeability measurement showed the reduction in permeability after the damage induced. The reduction in permeability varied by the variation of the sample and the injected fluid. The SEM images clarified the migration and the deposition of the clay minerals that affect the pore system and the permeability of the core samples.

CHAPTER 6

FORMATION DAMAGE BY VES ADSORPTION

6.1 Introduction

One of the most successful methods to enhance oil recovery is the chemical flooding. Surfactant flooding is an example of chemical flooding which is an injection of one or more liquid chemicals and surfactants. In this method, the injection effectively controls the phase behavior in the oil reservoir, thus the trapped crude oil by lowering IFT between the injected liquid and the oil. The liquid surfactant injected into the reservoir is often a complex chemical system, which creates a so-called micelle solution. During surfactant flooding it is important to be aware of the high loss of surfactant, occurring as a result of adsorption, retention and phase partitioning inside the reservoir. Due to the different minerology, most solid surfaces, including reservoir rocks, are charged. It is generally, believed that sandstone rocks are negatively charged and carbonate rocks are positively charged. Not all surfactant retention is caused by adsorption because some surfactant molecules, depending on their size and rheological characteristics, get trapped inside formation pores. Adsorption and retention can be defined as the interaction between the surfactant molecules and the porous medium which lead polymer to be retained or adsorbed. Surfactant retention consist of three main mechanisms: surfactant adsorption, mechanical entrapment and hydrodynamic retention.

6.2 Materials and Experimental work

6.2.1 Materials

The experiments conducted in this study on two types of rocks: (1) Pink desert limestone (porosity ranges from (25.4 – 27) %; brine permeability ranges from (27.9 - 47 md). (2) Bandera Grey sandstone (porosity ranges from (18 – 21) %; brine permeability in the range of 20 md. The core plugs of dimensions 1.5'' in diameter and 3" in length.

Fluids used for limestone cores in these experiments were: fresh water which used as a compatible fluid with the carbonate to measure the permeability. While, the blended of the surfactant fluid used as a damaging fluid. All the fluids solutions prepared in deionized water. The mineralogical composition of the Bandera Grey is listed in Table 5

Table 5 Minerology of Bnadera Grey sandstone

Mineral	Bandera Grey
Quartz	57
Dolomite	16
Calcite	-
Feldspar	-
Kaolinite	3.0
Illite	10
Chlorite	1.0
Plagioclase	12

For the sandstone cores, three fluids were used:

- 3 wt% KCl used to measure the permeability before and after the damage.
- 7 vol% VES mixed with 5 wt% $CaCl_2$
- 1 wt% VES mixed with 15 wt% $CaCl_2$

6.2.2 Experimental procedure for formation damage evaluation

The limestone cores were saturated with fresh water at room temperature under pressure. Then the core was analyzed by NMR to measure the porosity and depict the baseline T_2 signal distribution. The initial permeability was measured using fresh water (from the formation to the wellbore direction). After that, the core plug was flooded with damaging fluid (VES fluid) at injection constant injection rate of 1 cm^3/min (from the wellbore to the formation direction).

The core was analyzed again by NMR to measure the change in the T_2 signal distribution and porosity. The cores were back flooded (from the formation to the wellbore direction) to measure the final permeability with the same fluids used for initial permeability measurement.

The same procedures used for the sandstone core with only change in the fluid used for saturation and permeability measurement (3 wt% KCl used for saturation and permeability measurement).

6.2.3 Core Flooding Experiment

The limestone core plugs were flooded by fresh water at four different rates to measure the initial permeability. The pressure drop readings were recorded when the flow stabilized. A back pressure regulator adjusted gradually up to 1000 psi and a confining pressure of 1700 psi was set.

As shown in Figure 62, the pressure drop start to increase from a value of 3.7 psi as the VES fluid injected. The increase of the pressure drop increased due to the adsorption of the VES at the pore throat surface. After 0.8 PV, the pressure drop stabilized since there is no more surface area to accommodate more VES. As a result of the adsorption, the initial permeability reduced by more than 90%.

When the low viscosity VES fluid injected the pressure increased gradually. After 1.5 PV, the pressure drop is about to stabilize with a fluctuation. The rapid increase and decrease in the pressure drop after 1.5 PV (shown as a peaks) attributed to the effect of friction between the adsorbed VES and the injected VES fluid. After 4.8 PV, the pressure drop stabilized as shown in (Figure 63).

Two sandstone cores were used for the core flooding experiment. The cores were flooded by 3 wt% KCl to measure the initial permeability. Then the cores analyzed by NMR .Then the cores flooded with two different VES solution as following:

(1) Flood (BR3) with blend of 15 wt% $CaCl_2$ and 1 wt% VES
(2) Flood (BR4) with blend of 7 Vol% VES and 5 wt% $CaCl_2$

After the damage induced by VES solution, the final permeability measured by 3 wt% KCl. Finally the cores analyzed by NMR.

The effect of high VES concentration examined by flooding of 7 vol% VES. As the high VES concentration solution injected to the core, the pressure drop increased sharply from 8.8 psi and stabilized after 4.5 PV at 200 psi.

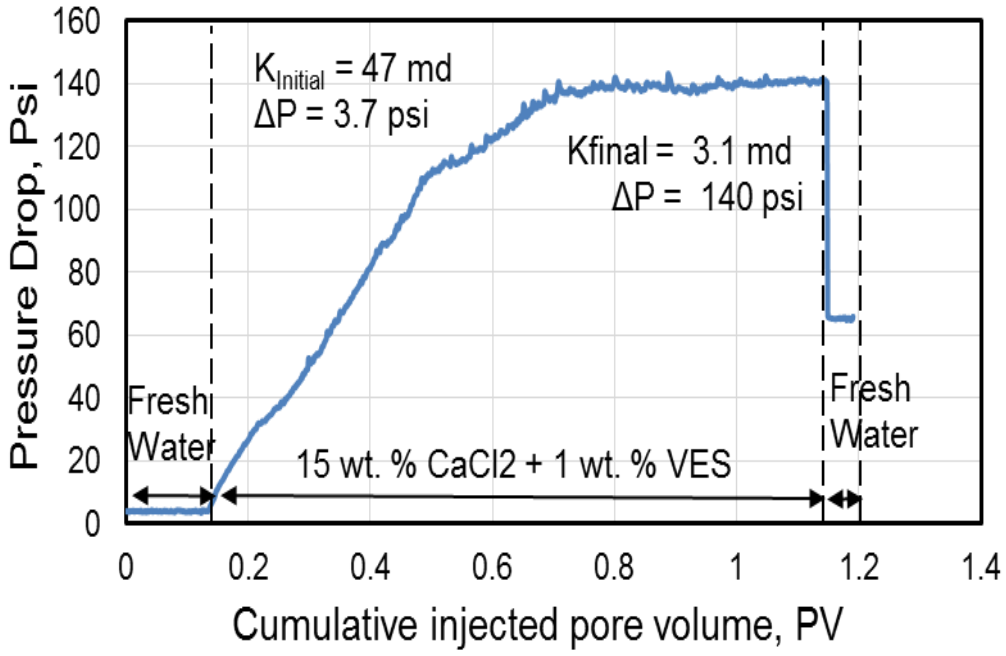

Figure 62: Pressure drop across the sample as the high viscosity VES blend injected into Pink Desert core at 1 cm3/min, backpressure of 1000 psi and confining pressure of 1700 psi

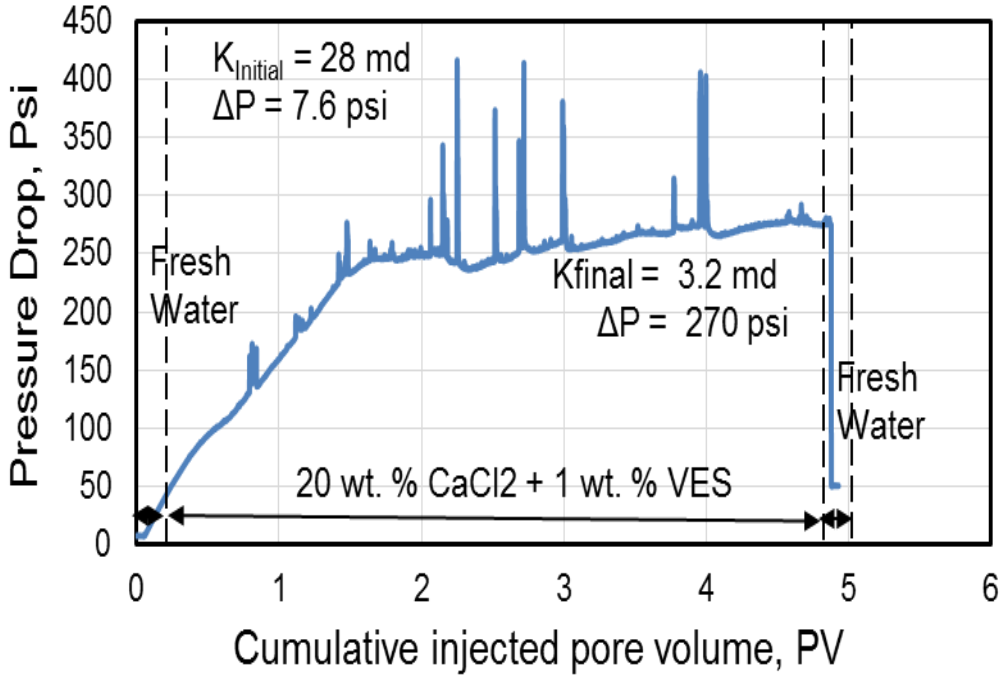

Figure 63: Pressure drop across the sample as the low viscosity VES blend injected into Pink Desert core at 1 cm3/min, backpressure of 1000 psi and confining pressure of 1700 psi

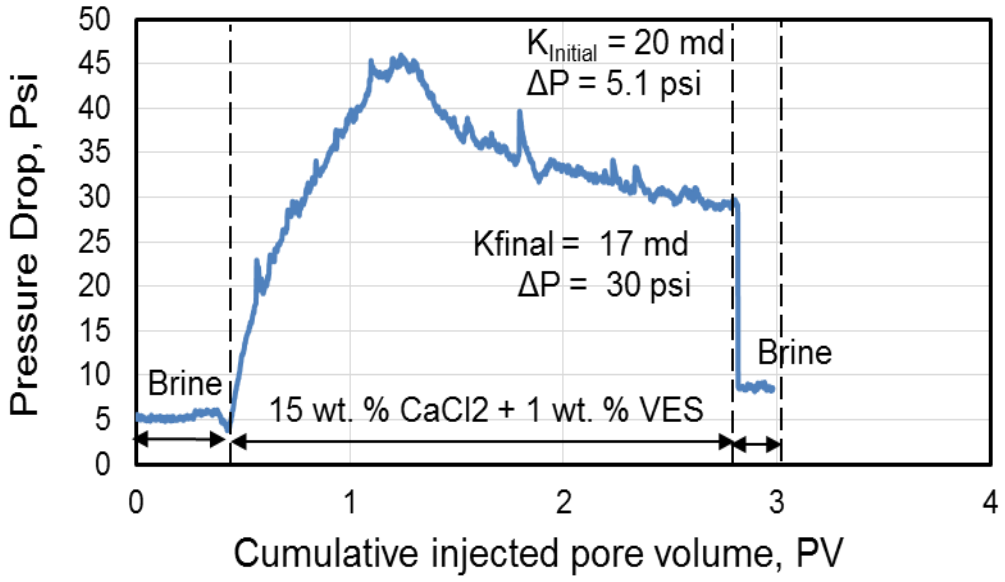

Figure 64: Pressure drop across the sample as the high viscosity VES blend injected into Bandera Grey sandstone core at 1 cm3/min, backpressure of 1000 psi and confining pressure of 1700 psi

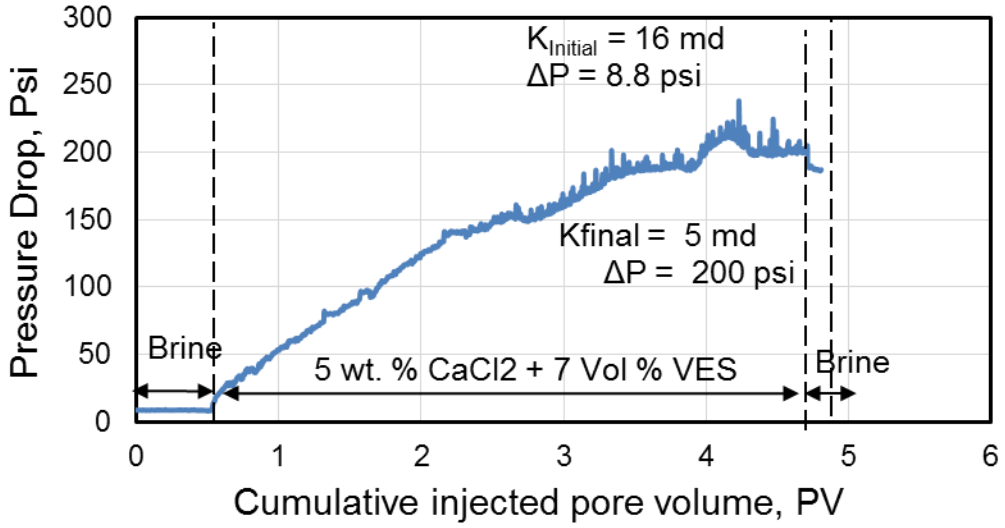

Figure 65: Pressure drop across the sample as high concentration of VES blend injected into Bandera Grey sandstone core at 1 cm3/min, backpressure of 1000 psi and confining pressure of 1700 psi

6.3 NMR Experiment

The NMR experiments performed on the core samples before and after the damage to analyze the effect of the VES fluid on the pore system. First, the samples analyzed by NMR

when it saturated with fresh water as a reference (before damage). After the VES fluid was injected the samples analyzed to compare the NMR spectra before and after the damage.

Figure 66 show the NMR spectra before and after the damage. The core shows bi-modal modal distribution. The major contribution of the porosity come from the macro pores. After the damage, the total porosity decreased slightly. The long peak that corresponds to the macro pores decreased, which confirm that the adsorption of the VES at the surface of the macro pores. Once the adsorption takes place at the macro pores, the contribution of the macro pores to the total porosity decreased. Thus, the amplitude of the long peak (macro pores) decreased, reflecting blockage of some macro pores.

In the other side, the effect of the low viscosity VES fluid affect the macro pores also. Almost the effect on the pore system resembles that caused by the high viscosity VES fluid as shown in Figure 67.

The NMR results for the sandstone cores are shown in (Figures 68 and 69). Figure 68 show the effect of 15 wt% $CaCl_2$ and 1 wt% VES on the core. The initial spectra show a system composed of dual modal. After the injection of the VES solution, the long peak corresponding to the macro pores decreased. The reduction in the macro pores referred to decrease of the contribution of the macro pores to the total porosity as a result of plugging. While the contribution of the micro pores increased due to the split of some of the macro pores to smaller pores. The same behavior observed when 5 wt% $CaCl_2$ and 7 vol% VES used.

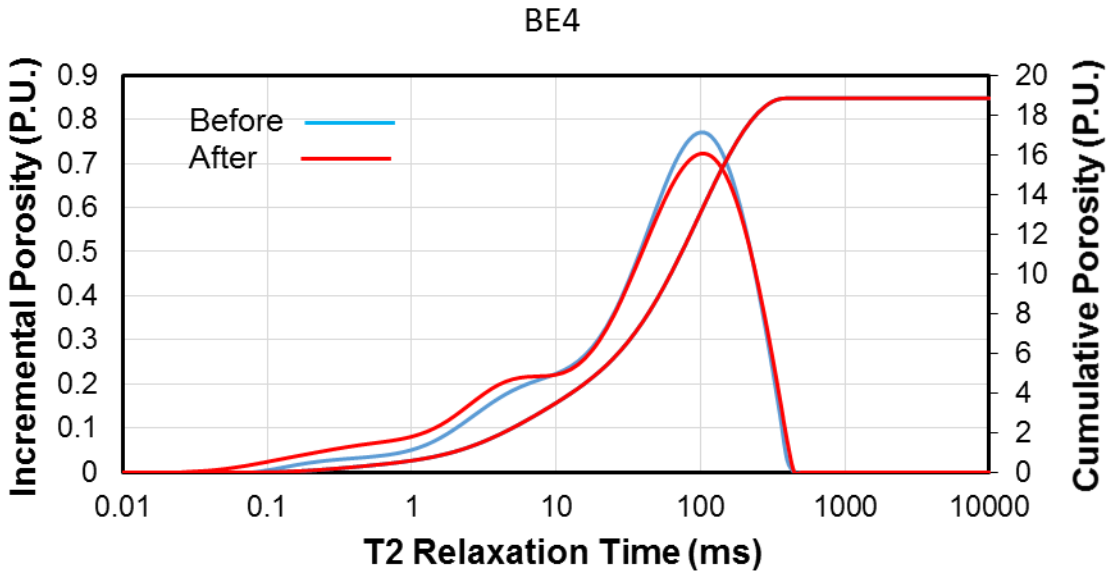

Figure 66: NMR T2 response curve for Berea sandstone core before and after damage at 25˚C

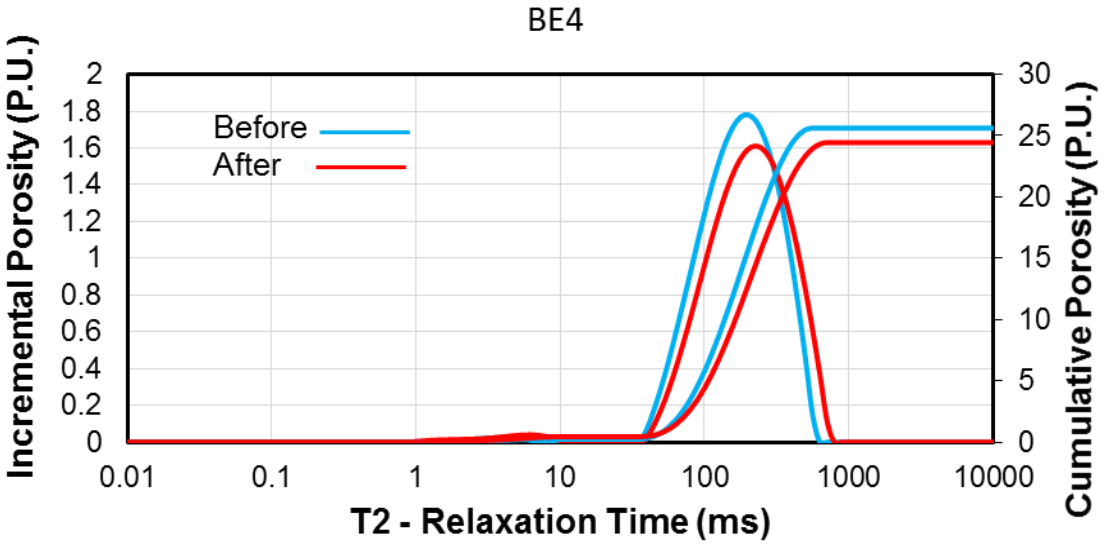

Figure 67: NMR T2 response curve for Berea sandstone core before and after damage at 25˚C

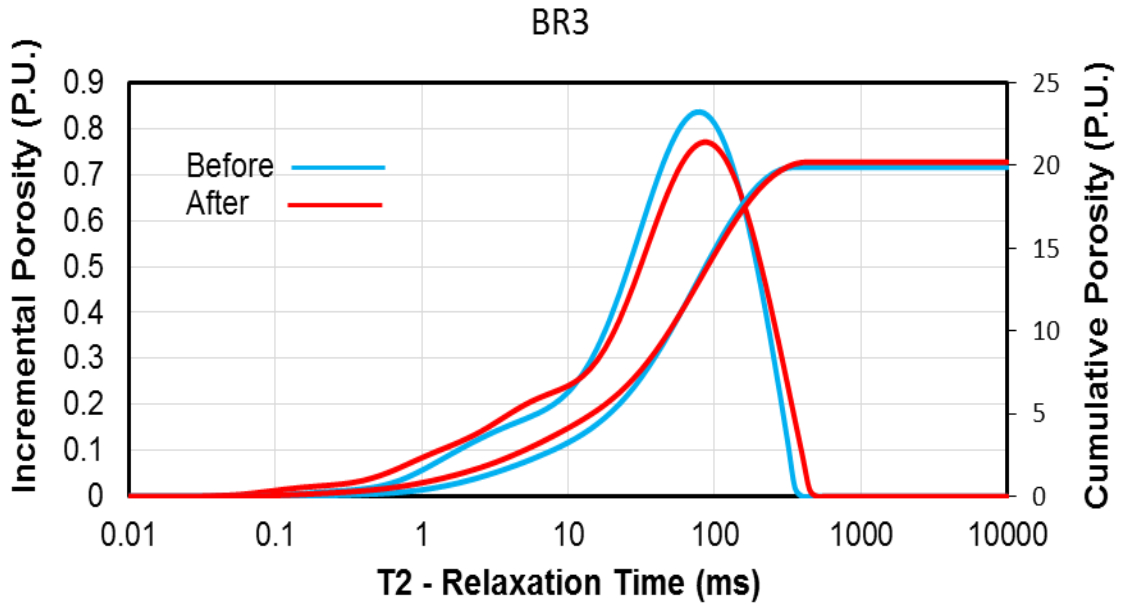

Figure 68: NMR T2 response curve for Bandera Brown sandstone core before and after damage at 25°C

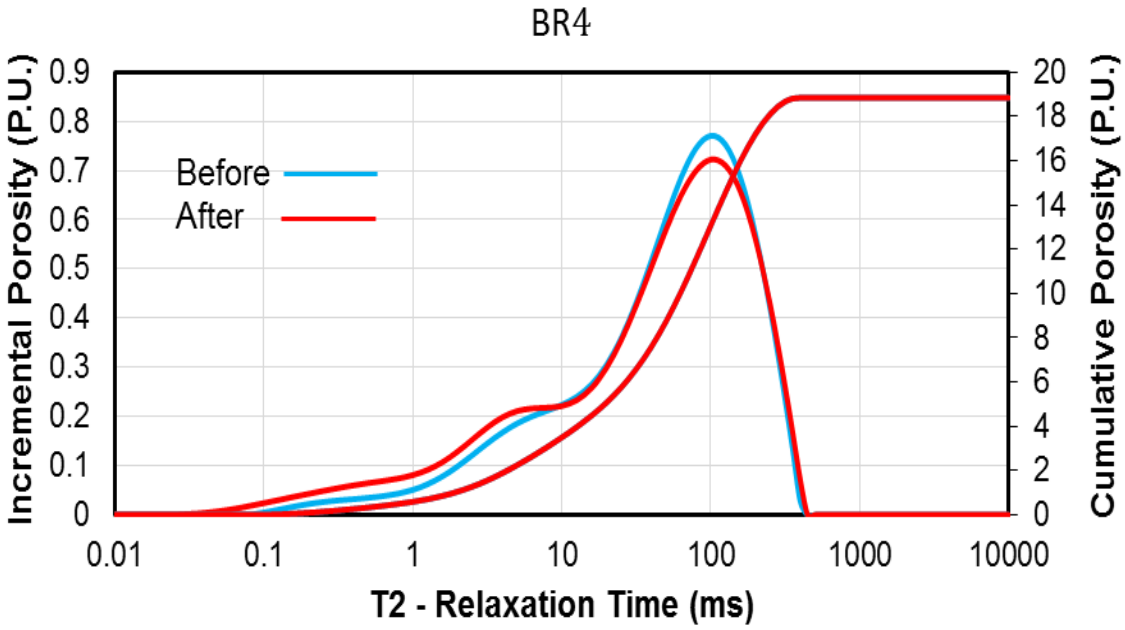

Figure 69: NMR T2 response curve for Bandera Brown sandstone core before and after damage at 25°C

6.4 SEM Analysis

The structure of the rock sample and the distribution of the pores at a micro scale analyzed by the SEM technique. The SEM images showed the structure of the rock sample before the damage. After the damage, the SEM images showed the presence of the VES particles which adsorbed on the pore system.

Figure 70 shows the structure of the pink desert core (before damage). The rock samples consist mainly from calcite. As shown in the figure, the small grains of calcite represent as majority beside the big grains of calcite.

After the injection of the high viscosity VES fluid, the VES particles adsorbed to the surface of the calcite grains. As shown in (figure 71), the small white grains represent the VES particles. The white particles of VES aggregated on the surface of the calcite grains.

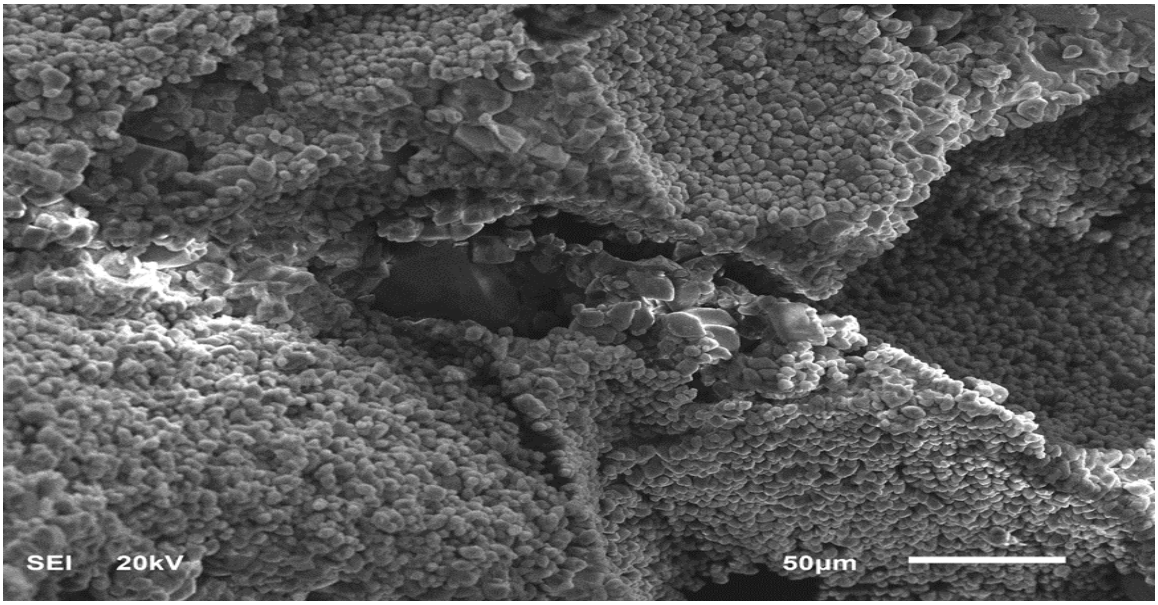

Figure 70: Structure of Pink Desert Core Sample (P1)

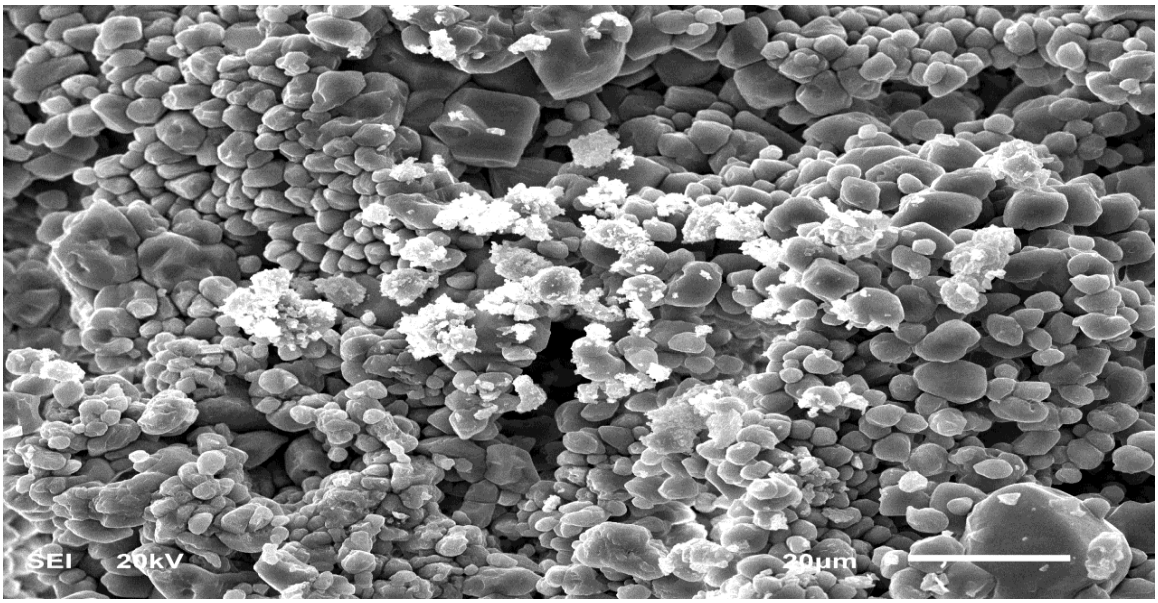

Figure 71: VES Particles adsorbed into the pore system (P1)

6.5 Conclusion

The used of VES as a chemical EOR fluid that contributes to increasing oil recovery could have the disadvantage that makes the EOR process economically unfeasible. The adsorption and retention of the VES into the pore system could be accounted as disadvantages.

This study confirms the adsorption of VES during the EOR process. The experiments which conducted using two VES fluid with different viscosity found that:

- The VES adsorbed into the pore throat caused a permeability reduction.
- A considerable amount of VES was adsorbed when a high VES fluid system was used.
- The VES adsorbed mainly into the pore throat and at the macro pores.

CHAPTER 7

CONCLUSION AND RECOMMENDATION

7.1 Conclusion

In this study, NMR techniques with the assistance of a core flooding system was used to quantify the formation damage in both carbonate and sandstone outcrop core samples and to identify the possible damaging mechanism responsible for formation damage. These mechanisms are fines migration in sandstone cores with high clay content, and viscoelastic surfactant (VES) adsorption on carbonate cores that are used in matrix stimulation and EOR process. In addition, we located the formation damage in carbonate cores due to VES adsorption during EOR processes that could be in the micro, meso, or macro pores. NMR profiles showed the region of damage.

For the sandstone cores, the HCl and fresh water showed a clear effect on the reduction of permeability. Core flooding system results showed a clear damage in sandstone rocks after they were flooded by DIW and HCl. The initial permeability was reduced by 84% and 7.9% when DIW and HCl was flooded. NMR results showed change in the pore size distribution after damage in sandstone and carbonate rocks. SEM images depict the damage induced by fine migration and VES adsorption in sandstone and carbonate rocks, respectively.

The adsorption of VES on both carbonate and sandstone cores was confirmed by the reduction of the permeability using the core flooding system and by the SEM-images. The reduction of permeability in carbonate rocks reached more than 80% of the initial permeability, while in the sandstone the initial permeability was reduced by around 65%.

7.2 Recommendation

It is recommended to extend this work to study the following aspects: to

1. The effect of the temperature on the VES adsorption.
2. Use the micro-CT scan to depict formation damage inside a pore throat.

References

Al-Aboudi, M. M., Ghofrani, R., & Sengupta, P. 1995. Damage Caused By Clay-based And Clay-free Inhibitive Fluids in Sandstone Formations. PETSOC J. **34** (1). http://dx.doi.org/ 10.2118/95-01-05

Al-Anzi, E., Al-Mutawa, M., Al-Habib, N., Al-Mumen, A., Nasr-El-Din, H., Alvarado, O., Brady, M., Davies, S., Fredd, C., Fu, D. and Lungwitz, B. 2003. Positive reactions in carbonate reservoir stimulation. Oilfield Rev, 15, 28-45.

Alle, T. O., & Worzel, H. C. 1956. Productivity method of evaluating gun perforating. Presented at the Spring Meeting of the Southwestern District, Division of Production, Fort Worth, Texas. March. API-56-112.

Ali, A. A., & Makhloufi, R. 1999. Effect of organic salts on micellar growth and structure studied by rheology. Colloid and Polymer Science, 277(2-3), 270-275.

Audibert, A., Argillier, J.-F., Ladva, H. K. J., Way, P. W., & Hove, A. O. 1999. Role of polymers on formation damage. Presented at the European formation damage conference. The Netherlands, 31 May -1 June. SPE-54767-MS. http://dx.doi.org/ 10.2118/54767-MS

Al-Yaseri, A., Lebedev, M., Vogt, S. J., Johns, M. L., Barifcani, A., & Iglauer, S. 2015. Pore-scale analysis of formation damage in Bentheimer sandstone with in-situ NMR and micro-computed tomography experiments. J. Pet. Sci & Eng. **129**(0): 48-57. http://dx.doi.org/ http://dx.doi.org/10.1016/j.petrol.2015.01.018.

Asghari, K., Kharrat, R., and Vossoughi, S. 1995. Alteration of Permeability by Fine Particle Movement - A Water Injectivity Problem. Presented at the SPE international Symposium on Oilfield Chemistry, USA, San Antonio, TX, USA, 14-17 February. SPE-29006-MS. http://dx.doi.org/10.2118/29006-MS.

Basan, P. 1985. Formation damage index number: a model for the evaluation of fluid sensitivity in shaly sandstones. Presented at the 60th Annual Technical Conference and Exhibition. NV, Las Vegas. 22-25 September. SPE-14317-MS. http://dx.doi.org/ 10.2118/14317-MS

Bishop, S. R. 1997. The Experimental Investigation of Formation Damage Due to the Induced Flocculation. Presented at the European Formation Damage Conference. The Hague, the Netherlands. 2-3 June. SPE 38156-MS. http://dx.doi.org/ 10.2118/38156-MS

Brown, R. J. S., & Gamson, B. W. 1960. Nuclear magnetism logging. Presented at the 34th Annual Fall Meeting. Dallas, USA. 4-7 October. SPE 1305-G.

Berret, J. F., Porte, G., & Decruppe, J. P. 1997. Inhomogeneous shear flows of wormlike micelles: mA master dynamic phase diagram. Physical Review E. **55**(2), 1668.

Blunt, M. J., Bijeljic, B., Dong, H., Gharbi, O., Iglauer, S., Mostaghimi, P., and Pentland, C. 2013. Pore-scale imaging and modelling, Advances in Water Resources Journal.**51**(0)197216.http://dx.doi.org/http://dx.doi.org/10.1016/j.advwatres.2012.03.003.

Byrne, M. T., Spark, I. S. C., Patey, I. T. M., and Twynam, A. J., 2000. A Laboratory Drilling Mud Overbalance Formation Damage Study Utilising Cryogenic SEM Techniques. Presented at the SPE International Symposium on Formation Damage Control, Lafayette, Louisiana, USA, 23–24 February. SPE-58738-MS. http://dx.doi.org/10.2118/58738-MS.

Coates, G. R., Xiao, L., & Prammer, M. G. 1999. NMR logging: principles and applications. Gulf Professional Publishing, Texas.

Curbelo, F. D., Santanna, V. C., Neto, E. L. B., Dutra, T. V., Dantas, T. N. C., Neto, A. A. D., & Garnica, A. I. 2007. Adsorption of nonionic surfactants in sandstones. Colloids and Surfaces A: Physicochemical and Engineering Aspects. **293**(1):14.http://dx.doi.org/http://dx.doi.org/10.1016/j.colsurfa.2006.06.038.

Economides, M.J. and Nolte, K.G. 2000. Reservoir stimulation. Chichester Wiley.

Edwards, J. C. 2003. "Principles of NMR." Process NMR Associates LLC, 87A Sand Pit Rd, Danbury CT 6810.

Ghofrani, R., Zhang, Y., & Bosch, V. 1996. New method in evaluating the formation damage in laboratorial investigations. Presented at the International Symposium on Formation Damage Control. Lafayette, Louisiana, USA. 14-15 February. SPE 35151-MS. http://dx.doi.org/10.2118/35151-MS

Green, J., Cameron, R., Patey, I., Nagassar, V., and Quine, M. 2013. Use of Micro-CT Scanning Visualisations to Improve Interpretation of Formation Damage Laboratory Tests Including a Case Study from the South Morecambe Field. Presented at the SPE European Formation Damage Conference, Noordwijk, The Netherlands, 5-7 June. SPE-165110-MS. http://dx.doi.org/doi:10.2118/165110-MS.

Hayatdavoudi, A., & Ghalambor, A. 1998. "Controlling Formation Damage Caused by Kaolinite Clay Minerals: Part II." Presented at the International Symposium on Formation Damage Control. Lafayette, Louisiana, USA. 14-15 February. SPE 39464-MS. http://dx.doi.org/10.2118/39464-MS.

Kenyon, B., Kleinberg, R., Straley, C., Gubelin, G., & Morriss, C., 1995. "Nuclear magnetic resonance imaging—technology for the 21st century." Oilfield Review **7**(3): 19-33.

Krueger, R. 1956. Joint Bullet and Jet Perforation Tests (Progress Report). Drilling and Production Practice, American Petroleum Institute.

Mahmoud, M. A., Nasr-El-Din, H. A., & De Wolf, C. A. 2015. High-Temperature Laboratory Testing of Illitic Sandstone Outcrop Cores with HCl-Alternative Fluids. SPE J. **30** (1): 43-51. SPE-147395-PA. http://dx.doi.org/ 10.2118/147395-PA.

Monaghan, P. H., Salathiel, R. A., Morgan, B. E., & Kaiser, A. D. 1959. Laboratory Studies of Formation Damage in Sands Containing Clays. Society of Petroleum Engineers. Presented at the Fall Meeting of Los Angeles Basin Section. Los Angeles, Calif., USA. 16-17 October. SPE 1162-G.

Monicard, R. P. 1980. Properties of reservoir rocks: core analysis, Editions OPHRYS.

Mu, J. H., & Li, G. Z. 2001. Rheology of viscoelastic anionic micellar solutions in the presence of a multivalent counterions. Colloid and Polymer Science, **279**(9): 872-878.

Muskat, M. 1981. "Physical principles of oil production."

Nadeau, P. H. 1998. "An experimental study of the effects of diagenetic clay minerals on reservoir sands." Clays and Clay Minerals **46**(1): 18-26.

Neasham, J. W. 1977. The Morphology Of Dispersed Clay In Sandstone Reservoirs And Its Effect On Sandstone Shaliness, Pore Space And Fluid Flow Properties. Presented at the 52nd Annual Fall Technical Conference and Exhibition. Denver, Colorado, USA. 9-12 October. SPE 6858-MS. http://dx.doi.org/10.2118/6858-MS.

Patzkó, Á., & Dékány, I. 1993. Ion exchange and molecular adsorption of a cationic surfactant on clay minerals. Colloids and Surfaces A: Physicochemical and Engineering Aspects. **71**(3):299-307. http://dx.doi.org/10.1016/0927-7757(93)80045-G.

Paria, S., & Khilar, K. C. 2004. A review on experimental studies of surfactant adsorption at the hydrophilic solid–water interface. Advances in colloid and interface science. **110**(3): 75-95. http://dx.doi.org/ 10.1016/j.cis.2004.03.001.

Priisholm, S., Nielsen, B. L., & Haslund, O. 1987. "Fines migration, blocking, and clay swelling of potential geothermal sandstone reservoirs, Denmark." SPE J. **2** (2): 168-178. SPE-15199-PA. http://dx.doi.org/10.2118/15199-PA.

Saraf, D. N., & Fatt, I. 1967. "Three-phase relative permeability measurement using a nuclear magnetic resonance technique for estimating fluid saturation. SPE J. **7** (3): 235-242. SPE-1760-PA. http://dx.doi.org/ doi:10.2118/1760-PA

Seevers, D. O. 1966. A Nuclear Magnetic Method For Determining The Permeability Of Sandstones. Paper presented at the SPWLA 7th Annual Logging Symposium, January.

ShamsiJazeyi, H., Verduzco, R., & Hirasaki, G. J. 2014. Reducing adsorption of anionic surfactant for enhanced oil recovery: Part I. Competitive adsorption mechanism. Colloids and Surfaces A: Physicochemical and Engineering Aspects, 453: 162-167. http://dx.doi.org/ 10.1016/j.colsurfa.2013.10.042.

Timur, A. 1969. "Producible porosity and permeability of sandstones investigated through nuclear magnetic resonance principles". The Log Analyst **10** (1): 3-11.

Tran, T. V., Civan, F., and Robb, I. D. 2010. Effect of Permeability Impairment By Suspended Particles On Invasion Of Drilling Fluids. Presented at the IADC/SPE Asia Pacific Drilling Technology Conference and Exhibition. Ho ChiMinh, Vitenam, November 1-3. SPE-133724. http://dx.doi.org/ 10.2118/133724-MS.

Van Everdingen, A. F., & Hurst, W. 1949. The application of the Laplace transformation to flow problems in reservoirs. Trans., AIME **186** (305): 97-104.

Wilson, L., Wilson, M. J., Green, J., & Patey, I. 2014. The influence of clay mineralogy on formation damage in North Sea reservoir sandstones: A review with illustrative examples. Earth-Science Reviews **134** (0): 70-80.

Yu, M., Mahmoud, M., & Nasr-El-Din, H. A. 2010. Propagation and Retention of Viscoelastic Surfactants Following Matrix Acidizing Treatments in Carbonate Cores. Presented at SPE International Symposium and Exhibition on Formation Damage Control Lafayette, Louisiana, USA, 10-12 February. SPE-128047. http://dx.doi.org/ 10.2118/128047-MS.

Vitae

Education

- **M.Sc. in Petroleum Engineering, May 2016**

King Fahd University of petroleum and minerals, Dhahran, Saudi Arabia

- Thesis title: Formation Damage Quantification by Nuclear Magnetic Resonance
- Description: The main objective of this work is to quantify the formation damage due to retention and adsorption of Viscoelastic Surfactant (VES) during stimulation and Enhanced Oil Recovery (EOR) process respectively using Nuclear Magnetic Resonance (NMR)
- Equipment were used during the experimental work and thesis
  - Core flooding system
  - NMR machine
  - Viscosity-meter
  - Density-meter
  - Centrifuge machine
  - DHR Rheometer

- **B.Sc. in Mining Engineering, August 2009**

University of Khartoum, Khartoum, Sudan

- Thesis title: Oil Shale Evaluation
- Description: This work aims to estimate the amount of the combustible material in the oil shale and study the effect of temperature and particles size that controlling the efficiency of the retorting process

Workshops & Trainings

- Training workshop in " Academic Laboratory Safety" organized by KFUPM Environment, Health and Safety Department, Dhahran, Saudi Arabia, January 2015
- Training in "Hydrogen Sulfide (H_2S) & Breathing Apparatus (BA)" organized by RUSS Technical Operations and Training Center, Dhahran, Saudi Arabia, October 2014
- Training in Lubricants Business Department & Aviation Department at Petronas Marketing Sudan Ltd., Khartoum, Sudan, 2010
- Field Training in underground mining at Advanced mining works co., South Ad-Damazin, Sudan, 2008
- Field Training in open pit mining at Ariab Mining Company, Ariab, Sudan, 2007
- Field Training in plan surveying by University of Khartoum at Sabaloga, Sudan, 2006

Work Experience

➢ **Mining Engineer**

Nub-Nubia Company for Mining, Khartoum, Sudan, Oct 2009 - May2010

➢ **Operations Supervisor**

AL-Terhab for Transport, Khartoum, Sudan, Sep 2010 – June 2012

Research & Publications

- Laboratory evaluation of Zwitterionic VES Rheology and quantification of related formation damage in carbonate cores – In progress
- Quantifying Viscoelastic Surfactant Adsorption in Carbonate Reservoir by Nuclear Magnetic Resonance– In progress

Personal Information

- Name : Mohamed Abdalsalam Hanfi Jad
- Nationality : Sudanese
- Date of Birth : May 1988
- Email : hanfi121@hotmail.com
- Address : Sudan- Khartoum- Bahri